
Fluctuation Effects in Chemical Reactions with Anomalous Diffusion

A Non Perturbative Renormalization Group Study far from Equilibrium

Ingo Homrighausen



München 2012

Fluctuation Effects in Chemical Reactions with Anomalous Diffusion

A Non Perturbative Renormalization Group Study far from Equilibrium

Ingo Homrighausen

Masterarbeit
an der Fakultät für Physik
der Ludwig-Maximilians-Universität
München

vorgelegt von
INGO HOMRIGHAUSEN
aus Siegen

München, den 15. März 2012

Erstgutachter: Prof. Dr. Erwin Frey
Zweitgutachter: Prof. Dr. Ulrich Schollwöck

Abstract

Reaction diffusion models provide a plethora of intensively studied non equilibrium many body systems. One of the simplest, yet nontrivial example, is the diffusion limited pair annihilation process $A + A \rightarrow 0$, where the particles diffuse in space and annihilate on contact. The system is known to be dominated by fluctuation effects below the critical dimension $d_c = 2$, whereas the fluctuations are not influential enough to change the law of mass action qualitatively above the critical dimension.

In this thesis we investigate the pair annihilation process for the case where the particles perform anomalous diffusion inside a cubic lattice. The anomalous diffusion is realized via Lévy flights that are characterized by long range jumps and lead to super diffusive behavior. As a consequence, the critical dimension depends continuously on the control parameter of the Lévy flight distribution. This instance is used to study the system close to the critical dimension by means of the non perturbative renormalization group theory. One crucial result will be that the law of mass action is corrected by additional non analytic terms above the critical dimension. We found that these corrections are universal functions of the non universal macroscopic reaction rate. As the number and influence of these corrections grows close to the critical dimension they are interpreted as a hallmark of the breakdown of the law of mass action. The results are confirmed by computer simulations.

We conclude with a discussion on the ternary annihilation process $3A \rightarrow 0$ and argue why corrections to the law of mass action are less important in this case.

Contents

1	Introduction	1
2	The Doi Peliti Formalism	5
2.1	The master equation and second quantization	5
2.2	Measuring observables	7
2.3	Coherent states and field theory	7
2.4	The partition function Z	10
2.5	The mean particle density for pair annihilation	11
2.6	Summary	11
3	Normal diffusion versus Lévy flights	13
3.1	The dispersion relation	15
3.2	Normal diffusion	17
3.3	Lévy flights	21
3.4	Summary	25
4	Non perturbative renormalization group (NPRG)	27
4.1	Macroscopic behavior emerging from a microscopic model	27
4.2	The idea of coarse graining	29
4.3	The derivation of the Wetterich flow equation	31
4.4	Proof of $\Gamma_\Lambda = S$	33
5	The local potential approximation (LPA)	35
5.1	The flow equation in LPA	36
5.2	Causality	38
5.3	The hierarchy of vertex functions	39
6	Corrections to the law of mass action in $d > d_c$	45
6.1	Macroscopic rate equation	45
6.2	The cutoff function	47
6.3	The leading term	50
6.4	Analytic and non analytic corrections	57
6.5	Further non analytic corrections	66
6.6	Comparison with simulations	71
6.7	Summary	76
7	The breakdown of the law of mass action in $d \leq d_c$	79
7.1	The continuum model	80
7.2	The IR stable fixed point	81
7.3	The density decay in $d < d_c$	83

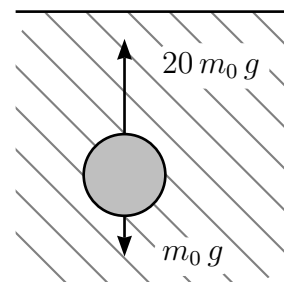
7.4	The density decay in $d = d_c$	85
7.5	Comparison with simulations	86
8	Trimolecular reaction kinetics	89
8.1	The problem of NPRG in $3A \rightarrow \emptyset$	89
8.2	The perturbative approach	91
8.3	Comparison with simulations	93
9	Conclusion	95
A	Fourier transform	97
B	Operators and Integral Kernels	101
	Bibliography	103

1 Introduction

Some of the most successful theories in physics of the last century are formulated in the mathematical language of (quantum) field theory (QFT). Field theories are suitable to describe many body problems and are thus predestinated for particle physics and statistical physics. Before we outline the *non perturbative* renormalization group (NPRG) treatment of (quantum) field theories, we follow the historical chronology and briefly sketch the *perturbative* treatment. After the description of perturbation theory, we will appreciate the advantages of NPRG even more.

A famous example for the perturbative treatment of QFT from the area of particle physics is quantum electrodynamics (QED). Perturbative QED predicts the anomalous magnetic moment of the electron up to an remarkably high precision of accuracy [1]. Despite its success, the concept of perturbative QFT was considered controversial due to the occurrence of ultra violet (UV) diverging integrals. To make sense out of these divergences, the theory is regularized¹ by the *artificial* UV cutoff Λ and the resulting divergences of the limit $\Lambda \rightarrow \infty$ are absorbed by counter terms. The cancelation of *each primitive* divergence is only defined up to a finite part. The remaining ambiguities are fixed by making physical measurements. This procedure goes under the name of *renormalization prescription*. Importantly, as every primitive divergence requires a physical measurement, the number of primitive divergences ought to be small (especially finite), in order for the QFT not to lose its predictivity. If the number of primitive divergences is finite, the theory is called *renormalizable*. Renormalizability is spoiled by the so called non renormalizable couplings. A byproduct of the renormalization procedure is the fact that the couplings become scale dependent, expressed by the perturbative renormalization group (RG) equation a.k.a. *Callan-Symanzik equation*.

A beautiful analogy of this scale dependence, which is not plagued by infinities, goes back to *Sidney Coleman* [2]. Imagine a light ping pong ball of volume V and mass m_0 which happens to be under water. Assume the ping pong ball's mass is equal to $m_0 = 1/20 \rho V$, where ρ is the water density. Besides the gravitational force $m_0 g$, the ping pong ball experiences the buoyant force of $20 m_0 g$ in the opposite direction. *Naively* using Newton's equation, the net effect is an *absurdly large* acceleration of $19 g$ (roughly speaking, this is the analog of the diverging integrals in QFT). The solution to this puzzle is the following hydrodynamical observation: When the spherical ping pong ball moves with velocity \mathbf{v} through water, parts of the fluid are forced to move along with the ball which contributes an additional momentum of $1/2 \rho V \mathbf{v} = 10 m_0 \mathbf{v}$ to Newton's equation [3]. The momentum of the *total* system (ball and fluid) is thus given by $11 m_0 \mathbf{v}$ and the ping pong ball is accelerated by $19/11 g$ and *not*



¹There are other regularization schemes, such as the dimensional regularization. For the sake of concreteness and due to the fact that the discussion is independent of the particular regularization scheme, we restrict to the UV-cutoff-regularization.

by $19g$. In the words of renormalization theory, the bare mass m_0 becomes renormalized to $m_R = 11m_0$ because of the interaction with the fluid.

In the simple ping pong ball toy model, one is able to *calculate* the renormalized mass, by making use of the underlying microscopic physics (i.e. Newton's law, hydrodynamics, the bare mass m_0 and the volume V of the *spherical* ping pong ball). The situation is more subtle in the case of the renormalizable QFT, as there is usually no additional deeper physical insight into the microscopic nature than the QFT itself. Speaking in terms of Coleman's ping pong ball analogy, QFT is not in the position to know about hydrodynamics or the spherical shape of the ping pong ball. The only way to determine the renormalized mass m_R in this case, is to measure the acceleration $a_{\text{experiment}} \approx 19/11g$ and conclude $m_R \approx 11m_0$. This is what the renormalization prescription in QFT does. Against this background, a renormalizable QFT should be viewed as a coarse grained, *phenomenological* theory, depending on a few phenomenological parameters that need to be fixed in experiments [4]. The number of those parameters is given by the number of primitive divergences.

The phenomenological character of perturbation theory is the result of the fact that all non renormalizable couplings were neglected right from the beginning, whereas true nature is not restricted to renormalizable couplings only. If non renormalizable couplings were included in perturbation theory, an infinite number of measurements would be needed for the renormalization prescription. Of course, since it is impossible to perform infinitely many measurements, it is impossible to go beyond phenomenology with any perturbative approach. The reason why e.g. QED is successful, in spite of neglecting all non renormalizable couplings, is that the non renormalizable contributions are not relevant for the description of the long distance physics [5]. Let us point out two related consequences of the phenomenological character of perturbation theory: **First**, there will be a microscopic length scale Λ^{-1} , where the coarse grained, phenomenological picture is too rough and new physics is observed in experiments². The divergences for $\Lambda \rightarrow \infty$ can be interpreted as the inaccessibility of the phenomenological perturbation theory for this new kind of physics. **Second**, the perturbation theory is only able to calculate *universal* quantities, i.e. quantities that do not depend on the (unknown) microscopic physics [6, 7].

Compared to perturbation theory, the non perturbative renormalization group (NPRG) is a rather recent development of the 1990s [8] which is inspired by Kadanoff's block spin transformation [9, 10]. The NPRG formalism is described in detail in chapter 4 of this thesis. One main difference, compared to perturbation theory, is that NPRG does not distinguish between renormalizable and non renormalizable couplings [5]. The idea is to start with a given model³ at some microscopic scale Λ . In contrast to perturbation theory, the scale Λ is taken seriously and the limit $\Lambda \rightarrow \infty$ is not an issue. This prevents the occurrence of divergences. The NPRG formalism prescribes how the microscopic theory looks on a coarse grained macroscopic scale by means of an *exact* flow equation. This flow equation is conceptually much easier than the analogous Callan-Symanzik equation in perturbation theory. As the NPRG flow equation is exact, the macroscopic theory goes beyond phenomenology and incorporates *non universal* properties depending on the microscopic model.

²For example, the new physics of quantum-gravity is expected to show up at the planck scale $\Lambda = 10^{19}\text{GeV}$.

³Finding an appropriate model for a certain physical purpose requires as always good intuition. There is no general recipe.

In this thesis, we investigate the chemical reaction between two identical particles denoted by the capital letter A . This type of problem has a long-standing tradition and theoretical considerations were started in 1917 by *Marian Smoluchowski* [11]. When it comes to the question of modeling, we have to face three interrelated questions:

1. What are the relevant intrinsic properties of the A particles?
2. How do we describe the dynamics of the A particles?
3. How do we model the reaction between two particles?

Without further physical or chemical justification, the answers to the questions are given in chronological order. We represent the A particles by idealized, *structureless point particles*. Nevertheless, to account for the spatial extend of real particles indirectly, we restrict the point particles' positions to the sites of a d dimensional lattice $a\mathbb{Z}^d$ with lattice spacing a . Hence, the purpose of the lattice is not to model the physical space, but rather to model the particle extension. Moreover, the lattice provides a natural UV cutoff. The A particles are assumed to jump randomly through the lattice. One possibility to specify this random movement is given by the *random walk* and leads to diffusive behavior. Instead, this thesis concentrates on *Lévy flights* which give rise to super diffusive behavior. The reason why Lévy flights are considered to be interesting is rather theoretical than practical: Compared to the diffusive case, Lévy flights lower the *critical dimension* d_c such that d_c becomes a manipulable parameter. This allows to investigate the system very close to the critical dimension. A precise definition of Lévy flights is given in chapter 3. If two point particles happen to be at the same lattice site, they react with a certain rate λ . After a reaction took place, both particles are taken out of the system. Schematically, this reads



and is called the *pair annihilation process* for obvious reasons.

Whether or not this model is in agreement with a real physical system, it phrases the interesting theoretical question how the particle density $\rho(t)$ decays in time. Known results for diffusion ($d_c = 2$) are

$$\rho(t) \xrightarrow{t \rightarrow \infty} \begin{cases} (8\pi)^{-1/2} t^{-1/2} & \text{for } d = 1 < d_c & [12] \\ (8\pi)^{-1} t^{-1} \log t & \text{for } d = 2 = d_c & [13] \\ \mathcal{A}_{d > d_c} t^{-1} & \text{for } d \geq 3 > d_c & [13]. \end{cases}$$

In the case of Lévy flights with Lévy flight exponent $0 < \mu < 2$, we have ($d_c = \mu$)

$$\rho(t) \xrightarrow{t \rightarrow \infty} \begin{cases} \mathcal{A}_{d < d_c} t^{-d/\mu} & \text{for } d > d_c & [14] \\ \mathcal{A}_{d = d_c} t^{-1} \log t & \text{for } d = d_c & [15] \\ \mathcal{A}_{d > d_c} t^{-1} & \text{for } d > d_c & [15]. \end{cases}$$

The dimension $d = d_c$ has a critical character: Below the critical dimension fluctuations are dominant and wash out the underlying microscopic lattice structure. As a consequence, the decay amplitude $\mathcal{A}_{d < d_c}$ is *universal* and can be determined by perturbation theory. To the authors knowledge, no attempt has been made to determine the amplitude $\mathcal{A}_{d > d_c}$ above the critical dimension. The reason is supposed to be twofold:

1. Above the critical dimension the density decay can be predicted qualitatively by a simple mean field approach. This is the reason why the case $d \leq d_c$ where mean field is not applicable, is considered to be more interesting.
2. The amplitude $\mathcal{A}_{d>d_c}$ is *non universal*. Hence, $\mathcal{A}_{d>d_c}$ depends on the details⁴ of the underlying microscopic model and *cannot* be calculated by a perturbative field theory. We will use NPRG to determine $\mathcal{A}_{d>d_c}$ in chapter 6.

As the non universal quantities depend on the chosen microscopic model, it is expected to be difficult to measure them in real experiments. Instead, we will simulate the model on a computational device to test the theoretical predictions. Interestingly, the behavior of $A + A \rightarrow \emptyset$ above the critical dimension is not ‘completely non universal’: We will determine correction terms which are *universal functions* of the *non universal* amplitude $\mathcal{A}_{d>d_c}$. The focus is set on the behavior close to the critical dimension d_c where the corrections are important as they hallmark the critical change below the critical dimension.

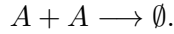
This thesis is structured as follows. After using the Doi Peliti formalism to map the pair annihilation process to a field theory in chapter 2, we compare the Lévy flights to the ordinary diffusion in chapter 3. Chapter 4 introduces the NPRG formalism and the non perturbative flow equation a.k.a. *Wetterich equation* is derived. The consequences of this flow equation for the pair annihilation process is described in chapter 5. Subsequently, the density decay in $A + A \rightarrow \emptyset$ is investigated for $d > d_c$ and $d \leq d_c$ in chapters 6 and 7, respectively. In the last chapter we briefly explain why the ternary annihilation $3A \rightarrow \emptyset$ cannot be described by NPRG in the same way as the pair annihilation. We propose an alternative method inspired by perturbation theory.

⁴such as the lattice structure or the particle shape

2 The Doi Peliti Formalism

In order to apply renormalization techniques to a reaction diffusion process, the problem has to be mapped onto a (classical) field theory. The essential advantage of non perturbative studies is the possibility to calculate non universal properties and thereby, to go beyond any phenomenological approach. To achieve this advantage, the field theory should incorporate all important microscopic details of the model. This rules out the possibility to use phenomenological methods such as the Martin-Siggia-Rose approach [16] for the mapping. Instead, the right starting point for the construction has to be the very microscopic level defined by the master equation.

In this chapter, the mechanism to arrive from a master equation to the field theory according to Masao Doi [17, 18] and Luca Peliti [19], is reviewed for the pair annihilation process



Although this is used as an example, the art of reasoning is generic enough to be used for other processes such as $kA \rightarrow lA$ [20] or the branching and annihilating random walk [21] straightforwardly. For pedagogical reviews see [22, 23].

2.1 The master equation and second quantization

Let L denote a set of N points in the space \mathbb{R}^d . L should be thought of being a lattice representing the physical space. The canonical choice is a regular cubic lattice $L = a\mathbb{Z}^d$ with lattice constant a . This example suggests that N may also be countably infinite. The elements of L are called lattice sites and are usually denoted by $\mathbf{x}_1, \mathbf{x}_2, \dots \in L$. Once the positions of the indistinguishable A particles are confined to the sites of the lattice, the state of the system is described by a tuple of non-negative integers $\mathbf{n} = (n_{\mathbf{x}_1}, n_{\mathbf{x}_2}, \dots) \in \mathbb{N}^N$. The notation means that there are $n_{\mathbf{x}_1}$ particles at the lattice site \mathbf{x}_1 , $n_{\mathbf{x}_2}$ particles at the lattice site \mathbf{x}_2 and so on. For a probabilistic treatment $P(\mathbf{n}, t)$ is defined as the probability that the system is in the state \mathbf{n} at time t , normalized such that $\sum_{\mathbf{n}} P(\mathbf{n}, t) = 1$.

Assuming that particles can jump from lattice site $\mathbf{x} \in L$ to $\mathbf{y} \in L$ with probability $p(\mathbf{x}, \mathbf{y})$, the master equation for the pair annihilation reads

$$\begin{aligned} \partial_t P(\mathbf{n}, t) = & \frac{1}{\tau} \sum_{\mathbf{x}, \mathbf{y} \in L} p(\mathbf{x}, \mathbf{y}) [(n_{\mathbf{x}} + 1) P(\{\dots, n_{\mathbf{x}} + 1, n_{\mathbf{y}} - 1, \dots\}, t) - n_{\mathbf{x}} P(\mathbf{n}, t)] + \\ & \lambda \sum_{\mathbf{x} \in L} [(n_{\mathbf{x}} + 2)(n_{\mathbf{x}} + 1) P(\{\dots, n_{\mathbf{x}} + 2, \dots\}, t) - n_{\mathbf{x}}(n_{\mathbf{x}} - 1) P(\mathbf{n}, t)]. \end{aligned} \quad (2.1)$$

The first line of (2.1) describes the particle jumping with respect to the probability distribution $p(\mathbf{x}, \mathbf{y})$ by means of gain and loss terms. The constant τ has the dimension $[\tau] = \text{time}$ and renders the equation to be dimensionally correct. The constant's precise interpretation will become clear in chapter 3. It turns out to be the characteristic, microscopic time scale

between two consecutive jumps. The second line of (2.1) is responsible for the particle reaction $A + A \rightarrow \emptyset$ and couples sectors with different particle numbers. This coupling makes the problem a nontrivial essential many particle problem. λ is the microscopic reaction rate with the dimension $[\lambda] = \text{time}^{-1}$. The numerical factors composed out of occupation numbers in front of each gain and loss term, are the combinatorial numbers of ways how a particular reaction can happen.

The suitable formalism to treat many body problems is *second quantization*. The profit of second quantization is to organize the couplings between the sectors in a more efficient way with less bookkeeping. Starting from the normalized vacuum state $|0\rangle$ corresponding to the empty lattice, the fock space is built up by using the bosonic creation and annihilation operators $a_{\mathbf{x}}^{\dagger}$ and $a_{\mathbf{x}}$ at each lattice site $\mathbf{x} \in L$. The ladder operators fulfill the usual canonical commutation relations

$$\left[a_{\mathbf{x}}, a_{\mathbf{y}}^{\dagger} \right] = \delta_{\mathbf{x},\mathbf{y}}, \quad \left[a_{\mathbf{x}}, a_{\mathbf{y}} \right] = \left[a_{\mathbf{x}}^{\dagger}, a_{\mathbf{y}}^{\dagger} \right] = 0 \quad \text{and} \quad a_{\mathbf{x}}|0\rangle = 0. \quad (2.2)$$

In this manner, the vector

$$|\mathbf{n}\rangle \equiv |n_{\mathbf{x}_1}, n_{\mathbf{x}_2}, \dots\rangle \equiv \prod_{\mathbf{x} \in L} a_{\mathbf{x}}^{\dagger n_{\mathbf{x}}} |0\rangle \quad (2.3)$$

represents the state $\mathbf{n} = (n_{\mathbf{x}_1}, n_{\mathbf{x}_2}, \dots)$. Using (2.2), the scalarproduct between two different states $|\mathbf{m}\rangle$ and $|\mathbf{n}\rangle$ is calculated:

$$\langle \mathbf{m} | \mathbf{n} \rangle = \prod_{\mathbf{x} \in L} n_{\mathbf{x}}! \delta_{n_{\mathbf{x}}, m_{\mathbf{x}}}. \quad (2.4)$$

Let $|\Psi(t)\rangle \equiv \sum_{\mathbf{n}} P(\mathbf{n}, t) |\mathbf{n}\rangle$ be the ‘generating function’ for the probabilities $P(\mathbf{n}, t)$. With this definition, the master equation (2.1) can be rewritten in the disguise of second quantization as

$$\begin{aligned} \partial_t |\Psi(t)\rangle &= -\widehat{H} |\Psi(t)\rangle \\ \widehat{H} &= \underbrace{\frac{1}{\tau} \sum_{\mathbf{x}, \mathbf{y} \in L} p(\mathbf{x}, \mathbf{y}) (a_{\mathbf{x}}^{\dagger} a_{\mathbf{x}} - a_{\mathbf{x}}^{\dagger} a_{\mathbf{y}})}_{\text{‘jumping’ part}} + \underbrace{\lambda \sum_{\mathbf{x} \in L} (1 - a_{\mathbf{x}}^{\dagger 2}) a_{\mathbf{x}}^2}_{\text{reaction part}} \end{aligned} \quad (2.5)$$

The simplicity of this ‘wick-rotated Schrödinger equation’ compared to (2.1) is convincing. Despite the correspondence to quantum mechanics, the ‘hamiltonian’ \widehat{H} does not need to be hermitian¹. Consequently $\langle \Psi(t) | \Psi(t) \rangle = \|\Psi(t)\|^2$ is not conserved in the case of pair annihilation. Given some initial condition $|\Psi(t=0)\rangle = |\Psi_0\rangle$, the master equation (2.5) is formally solved by

$$|\Psi(t)\rangle = \exp\left(-t \widehat{H}\right) |\Psi_0\rangle. \quad (2.6)$$

Once solved, the probabilities $P(\mathbf{n}, t) = (\prod_i n_i!)^{-1} \langle \mathbf{n} | \Psi(t) \rangle$ are recovered by making use of the orthogonality relation (2.4) (the product of factorials accounts for the fact that the particles are indistinguishable).

¹Hermiticity would be an indicator for detailed balance [24], which is not the case for the non equilibrium process $A + A \rightarrow \emptyset$.

2.2 Measuring observables

The following question arises: How does the mean value of an observable $A: \mathbb{N}^N \rightarrow \mathbb{R}$ evolve in time? I.e., we are looking for a way to compute the quantity $\langle A(t) \rangle \equiv \sum_{\mathbf{n}} A(\mathbf{n}) P(\mathbf{n}, t)$. To rephrase the question in the framework of second quantization, the vector

$$|\text{sum}\rangle \equiv \exp\left(\sum_i a_i^\dagger\right) |0\rangle$$

is defined. The vector has the property $\langle \text{sum} | (\sum_{\mathbf{n}} c_{\mathbf{n}} |\mathbf{n}\rangle) = \sum_{\mathbf{n}} c_{\mathbf{n}}$, which explains the choice of naming. Using this property of $|\text{sum}\rangle$, yields

$$\langle A(t) \rangle = \langle \text{sum} | \hat{A} | \Psi(t) \rangle \stackrel{(2.6)}{=} \langle \text{sum} | \hat{A} \exp(-t \hat{H}) | \Psi_0 \rangle, \quad (2.7)$$

where \hat{A} is obtained from $A(\mathbf{n})$ via replacing $n_{\mathbf{x}} \rightarrow \hat{n}_{\mathbf{x}} \equiv a_{\mathbf{x}}^\dagger a_{\mathbf{x}}$, i.e. $\hat{A} = A(a_{\mathbf{x}_1}^\dagger a_{\mathbf{x}_1}, a_{\mathbf{x}_2}^\dagger a_{\mathbf{x}_2}, \dots)$. Moreover, without loss of generality, it is assumed that the operator \hat{A} is given in normal ordered form, which means that all creation operators $a_{\mathbf{x}}^\dagger$ are commuted to the left. Note that the ‘hamiltonian’ \hat{H} (2.5) is normal ordered. The time dependence of the physical observable (2.7) appears indirectly through the time dependence of the time evolved state $|\Psi(t)\rangle$. This is structurally similar to the fact that the temperature dependence of any thermodynamic quantity sneaks in through the Boltzmann factor in equilibrium statistical physics.

As mentioned above, the time evolution (2.6) does not preserve the norm $\langle \Psi(t) | \Psi(t) \rangle$. However, it conserves the total probability $\langle \text{sum} | \Psi(t) \rangle = \sum_{\mathbf{n}} P(\mathbf{n}, t) = 1$, which can be verified by calculating $\langle \text{sum} | \partial_t \Psi \rangle = 0$ using (2.5) and $\langle \text{sum} | a_{\mathbf{x}}^\dagger = \langle \text{sum} |$ for all $\mathbf{x} \in L$.

2.3 Coherent states and field theory

The similarity of (2.6) and (2.7) to quantum mechanics allows to calculate $\langle A(t) \rangle$ by means of coherent state path-integral, analog to quantum mechanics [25]. This paragraph sketches the path integral formalism.

Let $\Phi \in \mathbb{C}^N$. The idea is that every lattice site $\mathbf{x} \in L$ gets attached a particular component $\Phi_{\mathbf{x}}$ of Φ . In this way Φ can be viewed as a map $\Phi: L \rightarrow \mathbb{C}$, $\mathbf{x} \mapsto \Phi_{\mathbf{x}} \equiv \Phi(\mathbf{x})$. The coherent state

$$|\Phi\rangle \equiv |\Phi(\mathbf{x})\rangle \equiv \exp\left(-\frac{1}{2} \sum_{\mathbf{x} \in L} |\Phi_{\mathbf{x}}|^2\right) \cdot \exp\left(\sum_{\mathbf{x} \in L} \Phi_{\mathbf{x}} a_{\mathbf{x}}^\dagger\right) |0\rangle \quad (2.8)$$

is the normalized eigenvector for the annihilation operator $a_{\mathbf{x}}$ with eigenvalue $\Phi(\mathbf{x})$, i.e.

$$a_{\mathbf{x}} |\Phi(\mathbf{x})\rangle = \Phi(\mathbf{x}) |\Phi(\mathbf{x})\rangle \quad \text{for all } \mathbf{x} \in L.$$

The dual statement reads $\langle \Phi(\mathbf{x}) | a_{\mathbf{x}}^\dagger = \langle \Phi(\mathbf{x}) | \Phi(\mathbf{x})^*$, where the star indicates complex conjugation. These coherent states form a resolution of unity

$$\hat{1} = \sum_{\mathbf{n}} \frac{1}{\prod_i n_i!} |\mathbf{n}\rangle \langle \mathbf{n}| = \int_{\mathbb{C}^N} \frac{d^N \Phi}{\pi^N} |\Phi\rangle \langle \Phi| \quad (2.9)$$

(abusing the notation slightly in the sense that $|\mathbf{n}\rangle$ means the state defined in (2.3), while $|\Phi\rangle$ denotes the coherent state), as can be checked by performing the integral for each lattice site in polar coordinates.

Let us make first use of the coherent states by specifying the initial condition $|\Psi_0\rangle = |\Psi(t=0)\rangle$ in (2.6). At $t=0$, the particles are assumed to be evenly distributed inside the lattice L with mean occupation number n_0 for every lattice site. Therefore, the initial state $|\Psi_0\rangle = \sum_{\mathbf{n}} P(\mathbf{n}, 0) |\mathbf{n}\rangle$ has to fulfill the two conditions

$$\langle \text{sum} | \Psi_0 \rangle = 1 \quad \text{and} \quad \langle \text{sum} | a_{\mathbf{x}} | \Psi_0 \rangle = n_0 \quad \text{for all } \mathbf{x} \in L.$$

Both conditions do not define the state $|\Psi_0\rangle$ completely. The remaining freedom is conveniently fixed by choosing $|\Psi_0\rangle$ to be proportional to a coherent state (2.8). In particular

$$|\Psi_0\rangle \equiv |n_0\rangle = \exp\left(-\sum_{\mathbf{x} \in L} n_0\right) \cdot \exp\left(\sum_{\mathbf{x} \in L} n_0 a_{\mathbf{x}}^\dagger\right) |0\rangle. \quad (2.10)$$

For this choice the probability $P(\mathbf{n}, 0)$ is given by the product of Poisson distributions $P(\mathbf{n}, 0) = \prod_{\mathbf{x} \in L} \exp(-n_0) \cdot n_0^{n_{\mathbf{x}}} / n_{\mathbf{x}}!$.

Starting with the initial state $|n_0\rangle$ (2.10), the idea to calculate $|\Psi(t)\rangle$, is to perform many infinitesimal time steps Δt . This idea is carried out by using the *Trotter product formula* [26]:

$$|\Psi(t)\rangle = \exp(-t \hat{H}) |n_0\rangle = \exp(-\Delta t \hat{H})^{t/\Delta t} |n_0\rangle.$$

Inserting the unities (2.9) for each time slice at $\tau = 0, \Delta t, 2\Delta t, \dots, t$, yields

$$\langle A(t) \rangle = \lim_{\Delta t \rightarrow 0} \int_{\mathbb{C}^N} \left(\prod_{\tau} \frac{d^N \Phi_{\tau}}{\pi^N} \right) \langle \text{sum} | \hat{A} | \Phi_t \rangle \left[\prod_{\tau=\Delta t}^t \langle \Phi_{\tau} | \exp(-\Delta t \hat{H}) | \Phi_{\tau-\Delta t} \rangle \right] \langle \Phi_0 | n_0 \rangle \quad (2.11)$$

for the mean value $\langle A(t) \rangle$. The benefit of introducing the coherent state identity operators is the relation [26]

$$\langle \Phi_{\tau} | \exp(-\Delta t \hat{H}) | \Phi_{\tau-\Delta t} \rangle \approx \langle \Phi_{\tau} | \Phi_{\tau-\Delta t} \rangle \exp[-\Delta t H(\Phi_{\tau}^*, \Phi_{\tau-\Delta t})] + \mathcal{O}(\Delta t^2). \quad (2.12)$$

The H on the right hand side of (2.12) denotes the matrix element $H(\mathbf{X}^*, \Phi) = \langle \mathbf{X} | \hat{H} | \Phi \rangle / \langle \mathbf{X} | \Phi \rangle$.

Using this approximation *cum grano salis*² in (2.11), gives (for details see [22])

$$\begin{aligned} \langle A(t) \rangle &= \lim_{\Delta t \rightarrow 0} \int_{\mathbb{C}^N} \left(\prod_{\tau} \frac{d^N \Phi_{\tau}}{\pi^N} \right) A(\Phi_t) \\ &\exp \left[- \sum_{\mathbf{x} \in L} \Delta t \sum_{\tau=\Delta t}^t \Phi_{\tau}(\mathbf{x})^* \frac{\Phi_{\tau}(\mathbf{x}) - \Phi_{\tau-\Delta t}(\mathbf{x})}{\Delta t} - \Delta t \sum_{\tau=\Delta t}^t H(\Phi_{\tau}^*, \Phi_{\tau-\Delta t}) \right] \\ &\exp \left[\sum_{\mathbf{x} \in L} \Phi_t(\mathbf{x})(1 - \Phi_t(\mathbf{x})^*) + \sum_{\mathbf{x} \in L} \Phi_0(\mathbf{x})^*(n_0 - \Phi_0(\mathbf{x})) \right]. \end{aligned} \quad (2.13)$$

The last line of this equation can be interpreted as setting up the initial and final constraint $\Phi_0(\mathbf{x}) = n_0$ and $\Phi_t(\mathbf{x})^* = 1$, respectively. The $A(\Phi_t)$ is obtained by replacing $a_{\mathbf{x}} \rightarrow \Phi_t(\mathbf{x})$ and $a_{\mathbf{x}}^{\dagger} \rightarrow 1$ in the normal ordered operator \hat{A} .

In the limit $\Delta t \rightarrow 0$, the time index τ labeling the time slices becomes the continuous argument $\tau \in \mathbb{R}$ of the field $\Phi: \mathbb{R} \times L \rightarrow \mathbb{C}$, $(\tau, \mathbf{x}) \mapsto \Phi(\tau, \mathbf{x})$. Moreover, the limit leads to

$$\Delta t \sum_{\tau} \rightarrow \int_0^t d\tau, \quad \int_{\mathbb{C}^N} \left(\prod_{\tau} \frac{d^N \Phi_{\tau}}{\pi^N} \right) \rightarrow \int \mathcal{D}\Phi \quad \text{and} \quad \frac{\Phi_{\tau}(\mathbf{x}) - \Phi_{\tau-\Delta t}(\mathbf{x})}{\Delta t} \rightarrow \partial_{\tau} \Phi(\tau, \mathbf{x}).$$

The time difference of the fields in H will be blurred $H(\Phi_{\tau}^*, \Phi_{\tau-\Delta t}) \rightarrow H(\Phi_{\tau}^*, \Phi_{\tau})$ with the requirement that the Φ^* field is understood to be slightly later in time than the Φ field (this continuous time ambiguity is discussed in detail in [27]). The infinitesimal time difference in the Φ^* and Φ field will be crucial for the diagrammatic treatment in chapter 5.

It is convenient to treat $\Phi(\mathbf{x})^* \in \mathbb{R}$ and $\Phi(\mathbf{x}) \in \mathbb{R}$ as two independent real degrees of freedom, instead of taking $\Phi(\mathbf{x}) \in \mathbb{C}$ as one complex degree of freedom. Additionally, performing the Doi shift $\bar{\Phi}(\mathbf{x}) \equiv \Phi(\mathbf{x})^* - 1$ while keeping $\Phi(\mathbf{x})$ unchanged, has the advantage that the field is expanded around its final value $\Phi_t(\mathbf{x})^* = 1$. Neglecting the initial and final condition (i.e. omitting the last line in (2.13)), gives

$$\langle A(t) \rangle \propto \int_{\bar{\Phi}_t=0} \mathcal{D}\Phi \mathcal{D}\bar{\Phi} A(\Phi_t) \exp \left[- \sum_{\mathbf{x} \in L} \int_0^t d\tau \bar{\Phi}(\tau, \mathbf{x}) \partial_{\tau} \Phi(\tau, \mathbf{x}) - \int_0^t d\tau H(\bar{\Phi}(\tau) + 1, \Phi(\tau)) \right] \quad (2.14)$$

²To use the approximation (2.12) in (2.11), sums are commuted implicitly with the integrals arising from the resolution of unity [22]:

$$\begin{aligned} &\left(\int \frac{d^N X}{\pi^N} |\mathbf{X}\rangle \langle \mathbf{X}| \right) \exp(-\Delta t \hat{H}) \left(\int \frac{d^N \Phi}{\pi^N} |\Phi\rangle \langle \Phi| \right) = \left(\int \frac{d^N X}{\pi^N} |\mathbf{X}\rangle \langle \mathbf{X}| \right) \sum_n \frac{1}{n!} (-\Delta t \hat{H})^n \left(\int \frac{d^N \Phi}{\pi^N} |\Phi\rangle \langle \Phi| \right) \\ &\approx \left(\int \frac{d^N X}{\pi^N} |\mathbf{X}\rangle \langle \mathbf{X}| \right) (1 - \Delta t \hat{H}) \left(\int \frac{d^N \Phi}{\pi^N} |\Phi\rangle \langle \Phi| \right) = \int \frac{d^N X}{\pi^N} \int \frac{d^N \Phi}{\pi^N} |\mathbf{X}\rangle \langle \mathbf{X}| (1 - \Delta t H(\mathbf{X}^*, \Phi)) |\Phi\rangle \langle \Phi| \\ &\approx \int \frac{d^N X}{\pi^N} \int \frac{d^N \Phi}{\pi^N} |\mathbf{X}\rangle \langle \mathbf{X}| \langle \mathbf{X} | \Phi \rangle \exp(-\Delta t H(\mathbf{X}^*, \Phi)). \end{aligned}$$

In general, this is not allowed. In a perturbative treatment however, this causes no harm. In a non perturbative approach, this may lead to serious problems, e.g. for $3A \rightarrow \emptyset$ (see chapter 8). For the pair annihilation process $A + A \rightarrow \emptyset$, the approximation turns out to be valid even for non perturbative purposes (see section 8.1).

for the mean value of the observable A in the continuous time path integral representation after the Doi shift³. Note that the space is still discrete, viz. the argument $\mathbf{x} \in L$ enumerates the lattice sites. Performing also the spatial continuous limit and thereby, neglecting the lattice, is an approximation which is postponed to chapter 7.

2.4 The partition function Z

In principle, equation (2.14) can be used to compute the expectation value for any observable A . A more skillful way, known from quantum field theory (QFT) [28], is to define the functional

$$Z[\bar{J}, J] \equiv \int \mathcal{D}\Phi \mathcal{D}\bar{\Phi} \exp \left[-S[\bar{\Phi}, \Phi] + \sum_{\mathbf{x} \in L} \int_{\mathbb{R}} d\tau \Phi(\tau, \mathbf{x}) J(\tau, \mathbf{x}) + \sum_{\mathbf{x} \in L} \int_{\mathbb{R}} d\tau \bar{\Phi}(\tau, \mathbf{x}) \bar{J}(\tau, \mathbf{x}) \right],$$

where $S[\bar{\Phi}, \Phi] = \sum_{\mathbf{x} \in L} \int_{\mathbb{R}} d\tau \bar{\Phi}(\tau, \mathbf{x}) \partial_{\tau} \Phi(\tau, \mathbf{x}) + \int_{\mathbb{R}} d\tau H(\bar{\Phi}(\tau) + 1, \Phi(\tau)).$

To abbreviate the notations, we introduce the vector $x \equiv (\tau, \mathbf{x}) \in \mathbb{R} \times L$ inspired by the notation of special relativity, and write $\int_x \equiv \sum_{\mathbf{x} \in L} \int_{\mathbb{R}} d\tau$ (see appendix A). With this notation the last formula condenses to

$$Z[\bar{J}, J] \equiv \int \mathcal{D}\Phi \mathcal{D}\bar{\Phi} \exp \left[-S[\bar{\Phi}, \Phi] + \int_x \Phi(x) J(x) + \int_x \bar{\Phi}(x) \bar{J}(x) \right], \quad (2.15)$$

where $S[\bar{\Phi}, \Phi] = \int_x \bar{\Phi}(x) \partial_{\tau} \Phi(x) + \int_{\mathbb{R}} d\tau H(\bar{\Phi}(\tau) + 1, \Phi(\tau)).$

According to particle physics, S is called the ‘action’ for this field theory. Once the functional Z is computed, all observables can be determined by simple differentiation with respect to the *current* J :

$$\langle A(t) \rangle = \frac{1}{Z[\bar{J}, J]} A \left(\frac{\delta}{\delta J(t, \mathbf{x})} \right) Z[\bar{J}, J] \Big|_{\bar{J}=0, J=0}. \quad (2.16)$$

This is the reason, why the object Z deserves the name *partition function*. While the current \bar{J} has a simple physical interpretation in terms of particle input⁴, the current J has no obvious meaning and therefore, should be regarded as an auxiliary current to be used in (2.16).

³Observe that the observable $A(\Phi_t)$ remains untouched by the field shift, because any observable is independent of $\bar{\Phi}$, if it is given in normal order form.

⁴Consider the master equation for the particle input $\emptyset \rightarrow A$ with rate $\bar{J}_{\mathbf{x}}$ at lattice site $\mathbf{x} \in L$

$$\partial_t P(\mathbf{n}, t) = \sum_{\mathbf{x} \in L} \bar{J}(\mathbf{x}) \Theta(n_{\mathbf{x}} \geq 1) P(\{\dots, n_{\mathbf{x}} - 1, \dots\}, t) - \bar{J}(\mathbf{x}) P(\mathbf{n}, t).$$

In the formalism of second quantization (see above) this reads:

$$\partial_t |\Psi(t)\rangle = - \sum_{\mathbf{x} \in L} \bar{J}(\mathbf{x}) (a_{\mathbf{x}}^{\dagger} - 1) |\Psi\rangle.$$

Performing the Doi shift, this constitutes the term $\sum_{\mathbf{x} \in L} \bar{J}(\mathbf{x}) \cdot \bar{\Phi}(\mathbf{x})$ in the partition function (2.15).

2.5 The mean particle density for pair annihilation

To put more flesh to the previous discussion, consider the particle density ρ as an example of one of the simplest nontrivial observable $\rho: \mathbb{N}^N \rightarrow \mathbb{R}, \mathbf{n} \mapsto \frac{1}{N} \sum_{\mathbf{x}} n_{\mathbf{x}}$. The corresponding second quantized operator $\hat{\rho} = \frac{1}{N} \sum_{\mathbf{x} \in L} a_{\mathbf{x}}^\dagger a_{\mathbf{x}}$ is already normal ordered. Using (2.16) to calculate the mean particle density at time t , gives

$$\langle \rho(t) \rangle = \frac{1}{N Z [0, 0]} \sum_{\mathbf{x} \in L} \frac{\delta}{\delta J(t, \mathbf{x})} Z [\bar{J}, J] \Big|_{\bar{J}=0, J=0}.$$

Assuming an infinitely large lattice $N \rightarrow \infty$ inducing translational symmetry, and defining $W [\bar{J}, J] \equiv \ln Z [\bar{J}, J]$, the latter equation becomes

$$\langle \rho(t) \rangle = \frac{\delta W [\bar{J}, J]}{\delta J(t, \mathbf{x}_0)} \Big|_{\bar{J}=0, J=0}.$$

The derivative was taken with respect to the current $J(t, \mathbf{x}_0)$ at site \mathbf{x}_0 . It also could have been taken with respect to any other site $\mathbf{x} \in L$, since translational invariance ensures that no site is singled out. In this way $\langle \rho(t) \rangle = \langle \Phi(t, \mathbf{x}_0) \rangle \equiv \frac{\delta W [\bar{J}, J]}{\delta J(t, \mathbf{x}_0)} \Big|_{\bar{J}=0, J=0}$ or just

$$\langle \rho(t) \rangle = \langle \Phi(t) \rangle. \quad (2.17)$$

In words: the expected particle density $\langle \rho(t) \rangle$ for the pair annihilation process $A + A \rightarrow \emptyset$ at time t is equal to the *one point function* $\langle \Phi(t) \rangle$ of the field theory (2.15).

Let us draw attention to an important subtlety. As explained in section 2.3, the Φ^* field fulfills $\Phi_t^* = 1$ at the final time t of observation, due to the last line of (2.13). Consequently, the shifted field $\bar{\Phi} = \Phi^* - 1$ has to vanish at time t . We conclude

$$\langle \bar{\Phi}(t) \rangle = \frac{1}{Z} \frac{\delta Z [\bar{J}, J]}{\delta J(t, \mathbf{x})} = 0. \quad (2.18)$$

This crucial result does not follow from the definition of $Z [\bar{J}, J]$ in (2.15) and has to be implemented ‘by hand’. The reason is that the initial and final constraints on the Φ and $\bar{\Phi}$ field are neglected in the definition of the partition function Z .

2.6 Summary

One of the thesis’ main aspects is to compute the mean particle density behavior $\rho(t)$ in $A + A \rightarrow \emptyset$ for late times t . In principle this question would be answered if one could solve the master equation (2.1) for this process (actually, any devisable question would be answered if one had solved the master equation). Solving (2.1) is way too hard. The Doi Peliti formalism comes as a rescue and maps the master equation onto a field theory given by the partition function (2.15). Once phrased in the language of field theory, the problem to determine $\rho(t)$ becomes amenable to renormalization group investigations. In particular, we will use the non perturbative renormalization group (NPRG) approach, described in chapter 4. NPRG has been proven to be a promising tool of describing a non equilibrium (critical) phenomena [29, 30, 31]. Therefore, NPRG also seems to be the right concept to gain more insight into the pair annihilation process. Moreover, as the Doi Peliti prescription is non phenomenological, we can use the field theory (2.15) to calculate *non universal* properties.

3 Normal diffusion versus Lévy flights

This chapter is organized as follows. In the first section 3.1 the general approach to include the random dynamics of the particles in the second quantization formalism (see section 2.1) is described. A comparison to hamiltonian dynamics is enlightening and gives rise to the dispersion relation ϵ . Sections 3.2 and 3.3 discuss the two concrete examples of the random walk and the Lévy flight, respectively. Finally, the important results are summarized in section 3.4.

Before we proceed in this way, we give some historical remarks to motivate the normal diffusion and subsequently the Lévy flights.

The theory of normal diffusion started its breakthrough in 1827, when Robert Brown observed the erratic motion of suspended pollen with a microscope [32]. To his honor, the random movement of small suspended particles is called *Brownian motion*. The first idea, that this phenomenon originates from life, contradicts the observation that the erratic motion can also be observed for small pieces of lifeless rocks.

The ingenious insight of Einstein was needed to explain *Brownian motion* based on the molecular-kinetic theory of heat in one of his famous *Annus Mirabilis papers* [33]. Intuitively speaking, a pollen is bombarded by a huge number of randomly moving, light water molecules and consequently, performs the *Brownian motion*. The random movement of the water molecules itself is a prediction of the molecular-kinetic theory of heat. In 1905, when Einstein published his paper, this atomistic theory was strongly debated and the existence of atoms was not universally accepted. With his paper, Einstein did not only explain *Brownian motion*, but also gave crucial evidence for the existence and smallness of atoms. Moreover, Einstein derived a theoretical prescription to measure the number of atoms. The key idea behind Einstein's prescription is to realize that the coarse grained movement of many Brownian particles can be described by a diffusion equation¹ with diffusion constant D , see also [34, 35]. The diffusion constant, as well as the particle's radius r , the viscosity η and temperature T of the liquid, can be measured on macroscopic and mesoscopic scales under a microscope. The *Einstein-Smoluchowski relation*

$$D = \frac{RT}{N_A} \frac{1}{6\pi\eta r}$$

allows to connect the mesoscopic measurements to the microscopic, atomistic physics; thereby, it goes beyond the scope of any microscope. It allows to determine the number of atoms N_A . In 1909, Perrin's experiments [36] brilliantly confirmed Einstein's thoughts.

The upshot of this historical sketch is that diffusion can be viewed most naturally as a collective, macroscopic phenomenon on the grounds of a microscopic theory of atoms.

In contrast to diffusion, the history of Lévy flights may be less impressive, but its applications are vast. Unlike the diffusive scaling $\text{space}^2 \sim \text{time}$, nature often exhibits different

¹In mathematical terms this is the central limit theorem as described in 3.2.

scalings between space and time. Those phenomena usually lead to anomalous diffusion. Extensive review on anomalous diffusion (either super- or subdiffusion) is given in [37, 38]. There are two mathematically motivated ways to circumvent the central limit theorem and obtain *anomalous diffusion* [39]:

Fractional Brownian motion extends the waiting time between two random particle steps. Specifically, the expectation of the waiting time has to diverge. Thus, particles can get stuck at some point in position space and the resulting dynamics is called *subdiffusive*. The scaling relation reads $\text{space}^2 \sim \text{time}^\alpha$ for some parameter $0 < \alpha < 1$.

Lévy stable process extends the step size of the random movement in such a way that the variance of the step size distribution diverges. The particles explore space more efficiently than in the normal diffusion case, since they can travel large distances from time to time [40]. Consequently, the dynamics is *superdiffusive* with $\text{space}^\mu \sim \text{time}$ for $0 < \mu < 2$. We will refer to the Lévy stable process simply as *Lévy flight*, a term coined by Benoit Mandelbrot [41]. We call the parameter μ the *Lévy flight exponent*.

The crucial difference between both approaches is that the former spoils the Markovity of the dynamics, whereas the latter does not. More precisely the diverging waiting time forces the process to be non Markovian. In a Markovian process, the future state of the system depends on the past only indirect through the present state. This property is tacitly assumed in the master equation (2.1): The master equation describes the change in the probabilities $\partial_t P(\mathbf{n}, t)$ at time t by means of the probabilities $P(\mathbf{m}, t)$ at the *same* time t . Obviously, a waiting time spoils this feature and the master equation approach becomes clumsy. This is the reason why the focus is set on superdiffusion, i.e. Lévy flights, in this thesis².

Lévy flights have found to be useful in describing the foraging of different animals [40, 43]. But Lévy flights also appear in the context of lifeless matter, like the energy of a single molecule inside a solid [44] or the movement of an ion embedded in an optical lattice [45]. The usage of Lévy flights in the pair annihilation process is mainly to reduce the critical dimension from $d_c = 2$ (normal diffusion) to $d_c = \mu$. Since the Lévy exponent $0 < \mu < 2$ is a free parameter, the critical dimension can be tuned by varying the particle's dynamics. This is an important new feature compared to the ordinary Brownian dynamics.

Figure 3.1 provides an intuitive picture of the difference between an ordinary random walk and a Lévy flight.

²In [42] Lévy flights with waiting time were investigated by the phenomenological Martin-Siggia-Rose approach [16]. As we use the non phenomenological Doi Peliti formalism on the basis of a master equation, the methods of [42] are not applicable.

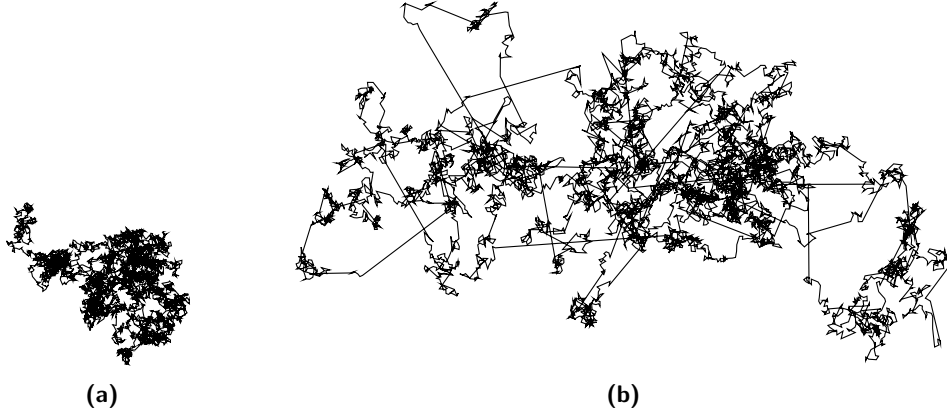


Figure 3.1: The trajectory of a Brownian random walker (a) is compared to the trajectory of a Lévy flight with $\mu = 1.5$ (b). In both cases the first 7000 steps are shown. The picture is borrowed from [38].

3.1 The dispersion relation

Recall the form of the second quantized ‘hamiltonian’ (2.5),

$$\hat{H} = \underbrace{\frac{1}{\tau} \sum_{\mathbf{x}, \mathbf{y} \in L} p(\mathbf{x}, \mathbf{y}) (a_{\mathbf{x}}^\dagger a_{\mathbf{x}} - a_{\mathbf{x}}^\dagger a_{\mathbf{y}})}_{\text{‘jumping’ part } \hat{H}_{\text{kin}}} + \underbrace{\lambda \sum_i (1 - a_{\mathbf{x}}^{\dagger 2}) a_{\mathbf{x}}^2}_{\text{reaction part } \hat{H}_{\text{pot}}},$$

derived in section 2.1. The constant τ is a microscopical time scale to set the dimensions right. Both of the two terms have qualitatively different meanings. The first comes from the fact that particles can jump from lattice site $\mathbf{x} \in L$ to $\mathbf{y} \in L$ with probability $p(\mathbf{x}, \mathbf{y})$, whereas the second term includes the possibility that particles at the same site react with rate λ . In hamiltonian language, the first part is called the *kinetic* term, being responsible for the force free dynamics. Likewise, the second part constitutes the *potential* term of the hamiltonian. In the following, the focus is set on the kinetic part in order to derive the *dispersion relation*.

For concreteness, we restrict to the case, where the jumping takes place in a regular, cubic and translational invariant lattice

$$L \equiv a \mathbb{Z}^d$$

with lattice spacing a in d dimensions. The fourier transform of functions $f: L \rightarrow \mathbb{C}$ on this lattice L takes the simple form (see appendix A)

$$\begin{aligned} \hat{f}: \left[-\frac{\pi}{a}, \frac{\pi}{a}\right]^d \rightarrow \mathbb{C}, \quad \mathbf{p} &\mapsto \sum_{\mathbf{x} \in L} f(\mathbf{x}) e^{-i\mathbf{x} \cdot \mathbf{p}} \equiv \int_{\mathbf{x}} f(\mathbf{x}) e^{-i\mathbf{x} \cdot \mathbf{p}}, \\ f: L \rightarrow \mathbb{C}, \quad \mathbf{x} &\mapsto \int_{\left[-\frac{\pi}{a}, \frac{\pi}{a}\right]^d} \frac{d^d p}{(2\pi/a)^d} \hat{f}(\mathbf{p}) e^{i\mathbf{x} \cdot \mathbf{p}} \equiv \int_{\mathbf{p}} \hat{f}(\mathbf{p}) e^{i\mathbf{x} \cdot \mathbf{p}}. \end{aligned}$$

Prior to specifying the concrete form of the jump length probability distribution $p: L \times L \rightarrow \mathbb{R}_+$, some general physically motivated properties are listed.

- **Normalization:**

$$\sum_{\mathbf{y} \in L} p(\mathbf{x}, \mathbf{y}) = 1. \quad (3.1)$$

The probability to jump from site \mathbf{x} to any other site, sums to one.

- **Symmetry:** $p(\mathbf{x}, \mathbf{y}) = p(\mathbf{y}, \mathbf{x})$.
- **Translational invariance:**

$$p(\mathbf{x}, \mathbf{y}) = p(\mathbf{x} - \mathbf{a}, \mathbf{y} - \mathbf{a}) \quad \text{for } \mathbf{a} \in L. \quad (3.2)$$

- **Isotropy:** $p(\mathbf{x}, \mathbf{y}) = p(R\mathbf{x}, R\mathbf{y})$ for $R \in O(L)$.

In the spirit of the Doi Peliti formalism, \hat{H} is only of interest when it is sandwiched in between coherent states $\langle \Psi | \hat{H} | \Phi \rangle$. The sandwiched kinetic term reads

$$\begin{aligned} \langle \Psi | \hat{H}_{kin} | \Phi \rangle &= \frac{1}{\tau} \sum_{\mathbf{x}, \mathbf{y} \in L} p(\mathbf{x}, \mathbf{y}) (\Psi^*(\mathbf{x}) \Phi(\mathbf{x}) - \Psi^*(\mathbf{x}) \Phi(\mathbf{y})) \\ &\stackrel{(3.1)}{=} \frac{1}{\tau} \sum_{\mathbf{x}, \mathbf{y} \in L} \Psi^*(\mathbf{x}) (\delta_{\mathbf{x}, \mathbf{y}} - p(\mathbf{x}, \mathbf{y})) \Phi(\mathbf{y}) \\ &= \frac{1}{\tau} \int_{\mathbf{p}, \mathbf{q}} \hat{\Psi}^*(\mathbf{p}) (\hat{\delta}(\mathbf{p} - \mathbf{q}) - \hat{p}(\mathbf{p}, -\mathbf{q})) \hat{\Phi}(\mathbf{q}) \equiv \frac{1}{\tau} (\hat{\Psi}, \epsilon \hat{\Phi}). \end{aligned}$$

A simple way to obtain the momentum representation in the last line, is to view the double sum as the quadratic form $(\Psi, \text{Op} \Phi)$ with the operator $K(\text{Op})(x, y) = \delta_{\mathbf{x}, \mathbf{y}} - p(\mathbf{x}, \mathbf{y})$, and to use equation (B.1). In momentum space, this operator is called the dispersion relation with integral kernel $K(\epsilon)(\mathbf{p}, \mathbf{q}) = \hat{\delta}(\mathbf{p} - \mathbf{q}) - \hat{p}(\mathbf{p}, -\mathbf{q})$.

The dispersion becomes diagonal for translational invariant systems: By a slight abuse of notation, the translation invariance (3.2) can be expressed through

$$\begin{aligned} p(\mathbf{x}, \mathbf{y}) &= p(\mathbf{x} - \mathbf{y}) \quad \text{and in momentum space} \\ \hat{p}(\mathbf{p}, \mathbf{q}) &= \hat{p}(\mathbf{p}) \hat{\delta}(\mathbf{p} + \mathbf{q}). \end{aligned}$$

This leads to

$$K(\epsilon)(\mathbf{p}, \mathbf{q}) = \hat{\delta}(\mathbf{p} - \mathbf{q}) - \hat{p}(\mathbf{p}, -\mathbf{q}) = \underbrace{(1 - \hat{p}(\mathbf{p}))}_{\equiv \epsilon(\mathbf{p})} \hat{\delta}(\mathbf{p} - \mathbf{q})$$

with the dispersion function $\epsilon(\mathbf{p})$. Hence, the kinetic term becomes

$$\langle \Psi | \hat{H}_{kin} | \Phi \rangle = \frac{1}{\tau} \int_{\mathbf{p}} \hat{\Psi}^*(\mathbf{p}) \epsilon(\mathbf{p}) \hat{\Phi}(\mathbf{p}) = \frac{1}{\tau} \int_{\mathbf{x}} \Psi^*(\mathbf{x}) (\mathcal{F}^{-1} \epsilon \mathcal{F}) \Phi(\mathbf{x}). \quad (3.3)$$

Phrased in words: modes with momentum \mathbf{p} contribute to the kinetic energy by $\epsilon(\mathbf{p})$. This justifies the convention of calling ϵ the dispersion relation. Note that despite this interpretation, the dispersion ϵ is dimensionless.

The normalization condition (3.1) for the probability $p(\mathbf{x} - \mathbf{y})$ induces two important properties for the dispersion function $\epsilon(\mathbf{p})$:

- Long range modes require no energy: $\epsilon(0) = 1 - \widehat{p}(0) = 0$.
- **Positivity:**

$$\epsilon(\mathbf{p}) = 1 - \sum_{\mathbf{x}} p(\mathbf{x}) e^{-i\mathbf{x}\cdot\mathbf{p}} \geq 1 - \left| \sum_{\mathbf{x}} p(\mathbf{x}) e^{-i\mathbf{x}\cdot\mathbf{p}} \right| \geq 1 - \sum_{\mathbf{x}} p(\mathbf{x}) = 0. \quad (3.4)$$

The energetic contribution for any mode \mathbf{p} is positive. Expressed in mathematical terms, the dispersion relation is a positive operator. The positivity will be used in sections 3.2 and 3.3 in the computation of the propagators.

Using the finding (3.3) in the action (2.15), yields

$$S[\bar{\Phi}, \Phi] = \underbrace{\int_x \bar{\Phi}(x) \left(\partial_t + \frac{1}{\tau} \mathcal{F}^{-1} \epsilon \mathcal{F} \right) \Phi(x)}_{=S_0[\bar{\Phi}, \Phi]} + \underbrace{\int_x \lambda \cdot (\bar{\Psi}^2 + 2\bar{\Psi}) \Psi^2}_{\text{reaction } A+A \rightarrow \emptyset}. \quad (3.5)$$

The *free action* S_0 includes a time derivative, rooted in the coherent state path integral prescription, and the kinetic part of the hamiltonian. It accounts for the free dynamics of the particles inside the lattice. This will be demonstrated in the following sections for the two cases of normal diffusion and Lévy flights. The second part of (3.5) stems from the potential and is responsible for the particle reactions, in this particular case $A + A \rightarrow \emptyset$.

3.2 Normal diffusion

The most prominent choice for the jump length probability distribution $p(\mathbf{x} - \mathbf{y})$ is that of a random walker, which can only jump to its neighboring sites

$$p(\mathbf{x} - \mathbf{y}) = \begin{cases} \frac{1}{2d} & , \text{ for } |\mathbf{x} - \mathbf{y}| = a \\ 0 & , \text{ else.} \end{cases} \quad (3.6)$$

The dispersion function is

$$\epsilon(\mathbf{p}) = 1 - \widehat{p}(\mathbf{p}) = 1 - \frac{1}{d} \sum_{i=1}^d \cos(a p_i) \quad (3.7)$$

in this case [46]. Figure 3.2 shows the plot of the dispersion function for two dimensions $d = 2$. The corresponding multiplication operator ϵ acts on functions $\Psi: L \rightarrow \mathbb{C}$ as

$$(\mathcal{F}^{-1} \epsilon \mathcal{F}) \Psi(\mathbf{x}) = \int_{\mathbf{p}} \left(1 - \frac{1}{d} \sum_{i=1}^d \cos(a p_i) \right) \widehat{\Psi}(\mathbf{p}) e^{i\mathbf{x}\cdot\mathbf{p}} = \Psi(\mathbf{x}) - \frac{1}{2d} \sum_{|\mathbf{y}|=a} \Psi(\mathbf{x} + \mathbf{y}).$$

The right hand side is proportional to the discrete version of the Laplace operator on the lattice $L = a \mathbb{Z}^d$, namely

$$-\nabla^2 \Psi(\mathbf{x}) \equiv \frac{1}{a^2} \cdot \left(2d \Psi(\mathbf{x}) - \sum_{|\mathbf{y}|=a} \Psi(\mathbf{x} + \mathbf{y}) \right)$$

(note that $[\nabla^2] = \text{length}^{-2}$), and thus,

$$(\mathcal{F}^{-1} \epsilon \mathcal{F}) \Psi(\mathbf{x}) = -\frac{a^2}{2d} \nabla^2 \Psi(\mathbf{x}). \quad (3.8)$$

This connection between the dispersion relation of a random walker and the discrete Laplacian is no coincidence. Roughly speaking, on a diffusive scale, the random walker becomes the Wiener process (central limit theorem), which is generated by the continuous Laplace operator.

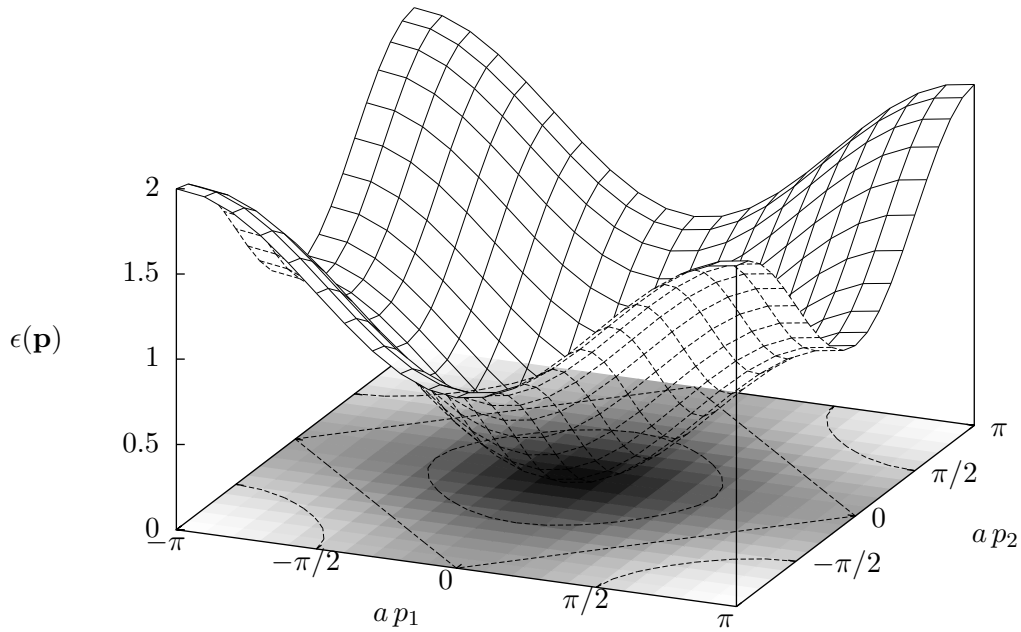


Figure 3.2: The dispersion relation $\epsilon(\mathbf{p}) = 1 - 1/2 [\cos(a p_1) + \cos(a p_2)]$ for the two dimensional lattice $a\mathbb{Z}^2$ is plotted on the first Brillouin zone $\mathbf{p} \in [-\pi/a, \pi/a]^2$.

In the neighborhood around $\mathbf{p} = 0$ the dispersion relation is spherically symmetric: $\epsilon(\mathbf{p}) \approx \frac{1}{2d} (a\mathbf{p})^2$ for $p \ll 1/a$. The spherical symmetry results from the fact that the distribution of lattice sites becomes isotropic for large distances.

On the other hand, as depicted by the contour lines, the isotropy is lost for larger momenta \mathbf{p} . It is the consequence of the anisotropy of the square lattice visible at short distances. The dispersion relation is sensitive for the underlying lattice structure for not too small \mathbf{p} . Indeed, different lattice types lead to different dispersion relations by altering the Fourier transform (see appendix A). However, the invariance of $\epsilon(\mathbf{p})$ under rotation by $\pi/2$ will be valid for all \mathbf{p} , as long as the lattice respects this symmetry.

In the proof of the central limit theorem the lattice shrinks and gives birth to the isotropic continuum \mathbb{R}^d . As a result, the dispersion has to be isotropic for all momenta $\mathbf{p} \in \mathbb{R}^d$ in this limit and becomes the continuous Laplacian $\epsilon(\mathbf{p})/\tau \xrightarrow{\text{CLT}} D \mathbf{p}^2$.

Central Limit Theorem

To be more precise, one random walker on $L = a\mathbb{Z}^d$ is considered to start its walk at the origin. Due to the jump length distribution (3.6), the random walker can only jump to one of its $2d$ neighboring sites every time step τ . Each jump is independent of any previous jump (figure 3.1(a) shows one possible trajectory). The process is modeled by a family of independent, identically distributed jump length random variables $\{\mathbf{v}_i\}_{i=0,\tau,2\tau,\dots}$ with $\mathbf{v}_i \in L$. Since the \mathbf{v}_i 's are distributed according to (3.6), they have vanishing mean $\langle \mathbf{v}_i \rangle = 0$ and finite variance $\langle \mathbf{v}_i^2 \rangle \equiv \sigma^2 = a^2$.

The random walker is restricted to the microscopic world defined by the microscopic time scale τ and the microscopic lattice spacing a . We are interested in leaving the microscopic scale and tell how the particle position is distributed on a macroscopic time scale t after an (almost) infinite number t/τ of random steps were performed. For this purpose the scale separation parameter $\epsilon \ll 1$ is introduced [47]. The diffusive scale is obtained by shrinking the microscopic time scale τ and the lattice spacing a according to

$$\tau \mapsto \epsilon \cdot \tau \quad \text{and} \quad a \mapsto \sqrt{\epsilon} \cdot a, \quad (3.9)$$

while leaving the macroscopic time t of order one. The different treatment of space and time in (3.9) is characteristic for diffusion and leads to the celebrated *central limit theorem* (CLT). The CLT states that the probability density function (PDF) of the random variable

$$\mathbf{X}_t^\epsilon \equiv \sqrt{\epsilon} \sum_{i=0}^{t/\epsilon\tau} \mathbf{v}_i \in \sqrt{\epsilon} L$$

converges to the universal Gaussian distribution³ [48]

$$\text{PDF}(\mathbf{X}_t^\epsilon)(\mathbf{x}, t) \xrightarrow{\epsilon \rightarrow 0} (4\pi D t)^{-d/2} \exp\left(-\frac{x^2}{4D \cdot t}\right), \quad \mathbf{x} \in \mathbb{R}^d, \quad (3.10)$$

where

$$D \equiv \frac{1}{2d} \cdot \frac{a^2}{\tau} \quad \text{with} \quad [D] = \text{length}^2 \cdot \text{time}^{-1} \quad (3.11)$$

denotes the *diffusion constant*. The random walker, living in the microscopic realm, peeks into the macroscopic world through the diffusion constant D (note that D is invariant under the diffusive scaling (3.9)). Equation (3.10) fulfills the famous diffusion equation

$$\partial_t \Phi(t, \mathbf{x}) = D \nabla^2 \Phi(t, \mathbf{x}) \quad \text{where} \quad \Phi(t, \mathbf{x}) \equiv (4\pi D t)^{-d/2} \exp\left(-\frac{x^2}{4D \cdot t}\right) \quad (3.12)$$

with initial condition $\Phi(0, \mathbf{x}) = \delta(\mathbf{x})$. Thus, the probability density function Φ is the *fundamental solution* or *heat kernel* for the diffusion equation with diffusion constant D .

A quick proof of the CLT (3.10), neglecting converging issues, is relatively easy and elucidating. Translational invariance in the spatial dimensions suggests to look at the Fourier transform a.k.a. the characteristic function:

$$\begin{aligned} \lim_{\epsilon \rightarrow 0} \text{PDF}(\mathbf{X}_t^\epsilon)(\mathbf{p}, t) &= \lim_{\epsilon \rightarrow 0} \langle \exp(-i \mathbf{X}_t^\epsilon \cdot \mathbf{p}) \rangle = \lim_{\epsilon \rightarrow 0} \prod_{i=0}^{t/\epsilon\tau} \langle e^{-i \sqrt{\epsilon} \mathbf{v}_i \cdot \mathbf{p}} \rangle \\ &= \lim_{\epsilon \rightarrow 0} \left(1 - \frac{\epsilon \sigma^2}{2} p^2\right)^{t/\epsilon\tau} = \exp(-D t p^2) \end{aligned}$$

³Note that \mathbb{R}^d replaces the lattice $\sqrt{\epsilon} L$ as the microscopic scale fades out of focus in the limit $\epsilon \rightarrow 0$.

(at the second equality sign, the definition of \mathbf{X}_i^ϵ and the independence of \mathbf{v}_i was used). This is the Fourier transform of (3.10). \square

The crux in this proof is that only the second moment $\langle \mathbf{v}_i^2 \rangle \equiv \sigma^2$ of the jump length distribution survives the limit $\epsilon \rightarrow 0$. This shows the insignificance of the precise form of the \mathbf{v}_i 's probability density. Hence, the central limit theorem demonstrates *par excellence*, how *universal* macroscopic properties can emerge from microscopics.

A different perspective on the CLT

A second, more physical (but less precise), way to view the central limit theorem, is to start with a master equation for the random walker [49]. The free action $S_0[\bar{\Phi}, \Phi]$ (3.5) is used to set up the idea. By using the notation of the discrete Laplacian ∇^2 (3.8) and the definition of the diffusion constant D (3.11), the action takes the simple form

$$S_0[\bar{\Phi}, \Phi] = \int_x \bar{\Phi}(x) \left(\partial_t + \frac{1}{\tau} \mathcal{F}^{-1} \epsilon \mathcal{F} \right) \Phi(x) = \int_x \bar{\Phi}(x) (\partial_t - D \nabla^2) \Phi(x).$$

The classical equation of motion is obtained by forcing the functional derivative with respect to $\bar{\Phi}(t, \mathbf{x})$ to vanish. We arrive at

$$\partial_t \Phi(t, \mathbf{x}) - D \nabla^2 \Phi(t, \mathbf{x}) = 0.$$

Although the notation reminds of the diffusion equation in the continuous space \mathbb{R}^d (3.12), the spatial coordinates \mathbf{x} are still confined to the discrete lattice $a \mathbb{Z}^d$.

The connection to the central limit theorem is established by looking at the *fundamental solution* (a.k.a. Green's function) of the operator $(\partial_t - D \nabla^2)$. In physical language one is interested in the *propagator* $\left(\frac{\delta^2 S_0}{\delta \Phi(x) \delta \Phi(y)} \right)^{-1} \equiv \left(S_0^{(2)} \right)^{-1}(x, y) = (\partial_t - D \nabla^2)^{-1} \delta(x - y)$. The calculation is most efficiently done in momentum space with (B.1):

$$\left(S_0^{(2)} \right)^{-1}(p, q) = \frac{1}{-i\omega + \frac{1}{\tau} \epsilon(\mathbf{p})} \widehat{\delta}(p - q).$$

Finally, to perform the inverse Fourier transform in the temporal direction, one uses the residue theorem. The positivity of $\epsilon(\mathbf{p}) > 0$ guarantees that the pole is always below the real axis. This yields

$$\int_{\omega} \frac{e^{-it_1\omega + it_2\omega}}{-i\omega + \frac{1}{\tau} \epsilon(\mathbf{p})} \widehat{\delta}(p - q) = \Theta(t_1 - t_2) \cdot \exp \left[-\frac{1}{\tau} \epsilon(\mathbf{p}) \cdot (t_1 - t_2) \right].$$

Up to now, no scale separation between the microscopic and the macroscopic scale took place, and the propagator still lives in the microscopic world. The scale separation is carried out by expanding the dispersion function $\epsilon(\mathbf{p})$ around $\mathbf{p} = 0$:

$$\epsilon(\mathbf{p}) \stackrel{(3.7)}{\approx} 1 - \frac{1}{d} \sum_{i=1}^d \cos(a p_i) \approx \frac{1}{2d} a^2 \mathbf{p}^2.$$

In this way the 'macroscopic propagator' reads

$$\left(S_0^{(2)} \right)^{-1}(t_1 - t_2, \mathbf{p}) = \Theta(t_1 - t_2) \exp \left[-D \mathbf{p}^2 \cdot (t_1 - t_2) \right], \quad \text{with } D = \frac{1}{2d} \frac{a^2}{\tau}.$$

On the macroscopic scale, the propagator takes the universal form predicted by the central limit theorem (3.10).

Some words of warning are necessary.

- The arguments used above are rather handwaving. Nevertheless, the main idea is correct: In the scaling limit, the rough knowledge of $\epsilon(\mathbf{p})$ in the vicinity of $\mathbf{p} = 0$ suffices to lead to the universal macroscopic description.
- The action S_0 describes the random walker on a microscopic scale. It is naive to obtain a macroscopic picture by using this action and merely restricting to small momenta p in $(S_0^{(2)})^{-1}$. In chapter 4 an improved formalism is introduced to define an effective, macroscopic action $\Gamma[\bar{\Phi}, \Phi]$ on the basis of some given microscopic action $S[\bar{\Phi}, \Phi]$.

3.3 Lévy flights

Contrary to the diffusion case (3.6), another choice for the jump length distribution is $(\mathbf{x}, \mathbf{y} \in a\mathbb{Z}^d)$

$$p(\mathbf{x} - \mathbf{y}) = \mathcal{N} \begin{cases} \left(\frac{|\mathbf{x} - \mathbf{y}|}{a}\right)^{-d-\mu} & , \text{ for } \mathbf{x} \neq \mathbf{y} \\ 0 & , \text{ for } \mathbf{x} = \mathbf{y} \end{cases} \quad \text{with } 0 < \mu < 2. \quad (3.13)$$

The parameter μ is called *Lévy flight exponent* (in short *Lévy exponent* or *Lévy parameter*). \mathcal{N} denotes the right normalization, such that (3.1) holds. For the simple one dimensional case $d = 1$, it is explicitly given in terms of the famous Riemann ζ function $\zeta(s) = \sum_{c=1}^{\infty} c^{-s}$, viz. $\mathcal{N} = [2\zeta(\mu + 1)]^{-1}$.

The main reason to expect new interesting behavior beyond diffusion, is the fact that the second moment

$$\sum_{\mathbf{x} \in L \setminus 0} \frac{|\mathbf{x}|^{2-\mu-d}}{a^{-d-\mu}},$$

diverges for $0 < \mu < 2$. The divergence is due to the slowly decaying power tail $\propto |\mathbf{x} - \mathbf{y}|^{-d-\mu}$ for long jumps. This long jump length characteristic has influence on the dispersion function $\epsilon(\mathbf{p})$ for small momenta: We split up the Fourier transform $\hat{p}(\mathbf{p})$ into a short and long jump length contribution:

$$\hat{p}(\mathbf{p}) = \underbrace{\sum_{\substack{\mathbf{x} \in L \\ x < c \cdot a}} p(\mathbf{x}) e^{-i\mathbf{x} \cdot \mathbf{p}}}_{\text{short jumps}} + \underbrace{\sum_{\substack{\mathbf{x} \in L \\ x \geq c \cdot a}} p(\mathbf{x}) e^{-i\mathbf{x} \cdot \mathbf{p}}}_{\text{long jumps}}. \quad (3.14)$$

The separation into short and long jumps is performed by an artificial constant c . Any reasonable result has to be insensitive to c . Let us concentrate on the long jumps. For large distances $|\mathbf{x}| > c \cdot a$, the distribution $p(\mathbf{x})$ is slowly varying. Therefore, the sum can be approximated by an integral:

$$\begin{aligned} \sum_{\substack{\mathbf{x} \in L \\ x \geq c \cdot a}} p(\mathbf{x}) e^{-i\mathbf{x} \cdot \mathbf{p}} &\approx \int_{|\mathbf{x}| > c \cdot a} \frac{d^d x}{a^d} p(\mathbf{x}) e^{-i\mathbf{x} \cdot \mathbf{p}} = \mathcal{N} \cdot a^\mu \int_{|\mathbf{x}| > c \cdot a} d^d x |\mathbf{x}|^{-d-\mu} e^{-i\mathbf{x} \cdot \mathbf{p}} \\ &\stackrel{\mathbf{z} = \frac{\mathbf{p}}{|\mathbf{p}|} \mathbf{x}}{=} \mathcal{N} \cdot (a|\mathbf{p}|)^\mu \int_{|\mathbf{z}| > c \cdot a|\mathbf{p}|} d^d z |\mathbf{z}|^{-d-\mu} e^{-i|\mathbf{z}| \cos(\langle \mathbf{p}, \mathbf{z} \rangle)}, \end{aligned}$$

$\sphericalangle(\mathbf{p}, \mathbf{z})$ being the angle enclosed by \mathbf{p} and $\mathbf{z} = |\mathbf{p}|\mathbf{x}$. In order to shed light onto the long range jumps, it suffices to know the integral for small $|\mathbf{p}|$. The form above already suggests $\epsilon(\mathbf{p}) \propto |\mathbf{p}|^\mu$. To be more precise, the integral is expanded around $|\mathbf{p}| = 0$ to obtain

$$\begin{aligned} \epsilon(\mathbf{p}) = 1 - \widehat{p}(\mathbf{p}) &\approx \widetilde{D}_A \cdot (a|\mathbf{p}|)^\mu + \mathcal{O}(p^2) \\ \text{where } \widetilde{D}_A &= -\mathcal{N} \frac{\pi^{d/2} \Gamma(-\mu/2)}{2^\mu \Gamma(\frac{\mu+d}{2})}. \end{aligned} \quad (3.15)$$

Comfortingly, this form is independent of the unphysical constant c as described above. Notice that the form of $|\mathbf{p}|^\mu$ is non analytic at $\mathbf{p} = 0$ for $\mu \neq 1$. Nevertheless, it is created in the Fourier series (3.14), which is analytic if one restricts the sum to be finite. Therefore, any non analytic term has to be a consequence of the infinitely extended space, perceived by the long distance jumps. In contrast, short range jumps can not grasp the infiniteness of the system and thus can only lead to analytic terms. This is the case for the diffusion described above where the dispersion (3.7) is analytic.

The finding in (3.15) motivates to generalize the discrete Laplace operator ∇^2 (3.8) to define the *discrete fractional derivative* operator ∇^μ

$$(\mathcal{F}^{-1} \epsilon \mathcal{F}) \Psi(\mathbf{x}) \equiv -\widetilde{D}_A \cdot a^\mu \nabla^\mu \Psi(\mathbf{x}) \quad (3.16)$$

(note that $[\nabla^\mu] = \text{length}^{-\mu}$). In contrast to ∇^2 , the operator ∇^μ acts on functions $\Psi: a\mathbb{Z}^d \rightarrow \mathbb{C}$ non locally due to the long jump length statistic.

Figure 3.3 shows the dispersion function $\epsilon(\mathbf{p})$ for $d = 1$.

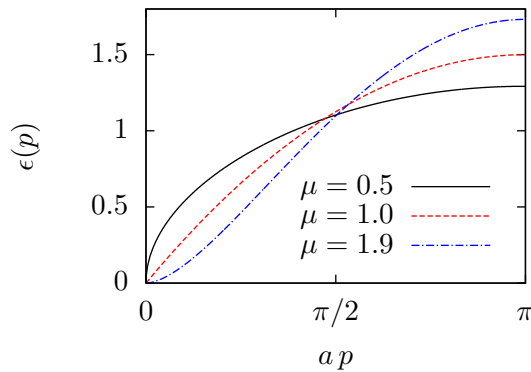


Figure 3.3: The dispersion relation $\epsilon(p) = 1 - \widehat{p}(p)$ for the d dimensional lattice $a\mathbb{Z}^d$ is defined on the first Brillouin zone $p \in [-\pi/a, \pi/a]^d$. The plot shows $d = 1$ for different μ . In the neighborhood around $\mathbf{p} = 0$ the dispersion function can be approximated by $\epsilon(p) \approx \widetilde{D}_A |ap|^\mu$ for $p \ll 1/a$ (compare eq. (3.15)). Consequently, the curvature of the dispersion function changes sign at $\mu = 1$.

Series expansion of the one dimensional dispersion function

We derive the series expansion (3.18) of $\epsilon(\mathbf{p})$ in powers of \mathbf{p} for $d = 1$. This expansion is an essential ingredient for the numerical considerations in chapters 6 and 8.

The analytic part of

$$\epsilon(\mathbf{p}) = 1 - \sum_{\mathbf{x} \in L} p(\mathbf{x}) e^{-i \mathbf{x} \cdot \mathbf{p}} \quad (3.17)$$

cannot be obtained by approximating the discrete sum by an integral as the integral ignores the crucial lattice structure. However, for the one dimensional lattice $L = a\mathbb{Z}^1$, the infinite sum over the lattice sites $\mathbf{x} \in L$ can be computed exactly by formally expanding $\epsilon(\mathbf{p})$ in powers of the momentum $\mathbf{p} \in [-\pi/a, \pi/a]$:

$$\begin{aligned} \epsilon(\mathbf{p}) &= 1 - \sum_{\mathbf{x} \in L} p(\mathbf{x}) e^{-i \mathbf{x} \cdot \mathbf{p}} = 1 - 2\mathcal{N} \sum_{c=1}^{\infty} c^{-1-\mu} \cos(c a \mathbf{p}) \\ &= 1 - 2\mathcal{N} \sum_{c=1}^{\infty} c^{-1-\mu} \sum_{n=0}^{\infty} \frac{(-1)^n}{(2n)!} (c a \mathbf{p})^{2n} \\ &\cong 1 - 2\mathcal{N} \sum_{n=0}^{\infty} \frac{(-1)^n}{(2n)!} \underbrace{\sum_{c=1}^{\infty} c^{-1-\mu+2n}}_{\cong \zeta(1+\mu-2n)} (a \mathbf{p})^{2n} \\ &\cong \tilde{D}_A (a \mathbf{p})^\mu - \sum_{n=1}^{\infty} \frac{(-1)^n}{(2n)!} \frac{\zeta(1+\mu-2n)}{\zeta(1+\mu)} (a \mathbf{p})^{2n}. \end{aligned}$$

The calculation involves three grains of salt, indicated by the modified ‘equality signs’ \cong . The naive interchanging (first grain of salt) of the two sums in the third line, leads to the formal expression $\sum_{c=1}^{\infty} c^{-1-\mu+2n}$. Although the sum $\sum_{c=1}^{\infty} c^{-1-\mu+2n}$ diverges for $n \geq 1$, it is formally substituted by the analytic continuation of the Riemann zeta function $\zeta(1+\mu-2n)$ (second grain of salt). This is where the magic happens and a formal power series in \mathbf{p} appears. At the same time, any non analytic part of $\epsilon(\mathbf{p})$ is lost. Therefore, the non analytic term $\tilde{D}_A (a|\mathbf{p}|)^\mu$ (3.15) is included by hand in the last line (third grain of salt).

The result

$$\epsilon(\mathbf{p}) = \tilde{D}_A (a \mathbf{p})^\mu - \sum_{n=1}^{\infty} \frac{(-1)^n}{(2n)!} \frac{\zeta(1+\mu-2n)}{\zeta(1+\mu)} (a \mathbf{p})^{2n} \quad \text{for } d = 1 \quad (3.18)$$

is *exact* for $\mathbf{p} \in [-\pi/a, \pi/a]$. Equation (3.18) can be derived mathematically rigorous by applying the expansion $\text{Li}_{\mu+1}(e^p) = \Gamma(-\mu) (-p)^\mu + \sum_{k=0}^{\infty} \zeta(\mu+1-k) p^k/k!$ [50] of the Polylogarithm $\text{Li}_{\mu+1} \equiv \sum_{k=1}^{\infty} z^k/k^{\mu+1}$. In contrast to (3.17), the expansion (3.18) converges fast (especially for small \mathbf{p}) which is important for accurate numerical considerations.

In the special case of $\mu = 1$, the sum in (3.18) becomes finite, as $\zeta(2-2n) = 0$ for $n \geq 2$. Using $\zeta(2) = \pi^2/6$, $\zeta(0) = -1/2$ and $\tilde{D}_A \xrightarrow{\mu \rightarrow 1} 3/\pi$ (3.15) in (3.18), yields

$$\epsilon(\mathbf{p}) = \frac{3}{\pi} a \mathbf{p} - \frac{3}{2\pi^2} (a \mathbf{p})^2 \quad \text{for } d = 1, \quad \mu = 1. \quad (3.19)$$

We do not know of an expansion of $\epsilon(\mathbf{p})$ in \mathbf{p} analog to (3.18) for $d \neq 1$.

Generalized Central Limit Theorem

Let us appreciate the result $\epsilon(\mathbf{p}) \propto |\mathbf{p}|^\mu$ for small $|\mathbf{p}|$. Similar to the discussion above, we look at a random flyer on $L = a\mathbb{Z}^d$, starting its flight at the origin. Every time step τ , the random flyer moves independently to a randomly chosen direction $\mathbf{v}_i \in a\mathbb{Z}^d$ (figure 3.1(b) shows a possible trajectory). However, the movements are not restricted to the nearest neighbors, but are distributed over the whole lattice according to the probability p in (3.13). Hence the variance $\langle \mathbf{v}_i^2 \rangle$ does not exist and prevents the central limit theorem to hold.

As in the case of diffusion, we are interested in the macroscopic behavior of the random flyer after an (almost) infinite amount of steps have been taken place. To get the coarse grained picture, one has to separate the microscopic model, given by the microscopic time τ and the lattice constant a , from the macroscopic world by scaling. In contrast to diffusion, the right scaling form is given by

$$\tau \mapsto \epsilon \cdot \tau, \quad a \mapsto \epsilon^{1/\mu} \cdot a \quad (3.20)$$

and the macroscopic position of the random flyer at some macroscopic time t is modeled by the random variable

$$\mathbf{X}_t^\epsilon \equiv \epsilon^{1/\mu} \sum_{i=0}^{t/\epsilon\tau} \mathbf{v}_i$$

as $\epsilon \rightarrow 0$. The special scaling of space and time (3.20) is the essence of the *generalized central limit theorem*. It states that the probability density of \mathbf{X}_t^ϵ universally converges to

$$\text{PDF}(\mathbf{X}_t^\epsilon)(\mathbf{p}, t) \xrightarrow{\epsilon \rightarrow 0} \exp(-D_A t |\mathbf{p}|^\mu), \quad (3.21)$$

where

$$D_A \equiv \tilde{D}_A \cdot \frac{a^\mu}{\tau} \quad \text{with} \quad [D_A] = \text{length}^\mu \cdot \text{time}^{-1} \quad (3.22)$$

is called the *anomalous diffusion constant*. Because the constant D_A is invariant under the scaling (3.20), it will maintain its value as $\epsilon \rightarrow 0$ and have an impact on the macroscopic regime.

The proof of (3.21) is as simple as the proof of (3.10):

$$\begin{aligned} \lim_{\epsilon \rightarrow 0} \text{PDF}(\mathbf{X}_t^\epsilon)(\mathbf{p}, t) &= \lim_{\epsilon \rightarrow 0} \langle \exp(-i \mathbf{X}_t^\epsilon \cdot \mathbf{p}) \rangle \\ &= \lim_{\epsilon \rightarrow 0} \prod_{i=0}^{t/\epsilon\tau} \langle e^{-i \epsilon^{1/\mu} \mathbf{v}_i \cdot \mathbf{p}} \rangle \\ &= \lim_{\epsilon \rightarrow 0} \hat{p} \left(\epsilon^{1/\mu} \mathbf{p} \right)^{t/\epsilon\tau} \\ &\stackrel{(3.15)}{=} \lim_{\epsilon \rightarrow 0} \left(1 - \tilde{D}_A (\epsilon^{1/\mu} a \mathbf{p})^\mu \right)^{t/\epsilon\tau} = \exp(-D_A t |\mathbf{p}|^\mu) \end{aligned}$$

(at the second equality the definition of \mathbf{X}_t^ϵ and the independence of \mathbf{v}_i was used). \square

The last line makes use of equation (3.15). It is this step in the derivation which motivates the scaling (3.20). The scaling guarantees that only the non analytic term $\propto |\mathbf{p}|^\mu$ survives the limit $\epsilon \rightarrow 0$.

A different perspective on the GCLT

We copy the discussion above and look at the free action, describing one random flyer

$$S_0[\bar{\Phi}, \Phi] = \int_x \bar{\Phi}(x) \left(\partial_t + \frac{1}{\tau} \mathcal{F}^{-1} \epsilon \mathcal{F} \right) \Phi(x) = \int_x \bar{\Phi}(x) (\partial_t - D_A \nabla^\mu) \Phi(x)$$

(the equality is obtained by the use of equations (3.16) and (3.22)). The classical equation of motion

$$\frac{\delta S_0}{\delta \bar{\Phi}} = 0 \quad \Longrightarrow \quad \partial_t \bar{\Phi} - D_A \nabla^\mu \bar{\Phi} = 0$$

is an anomalous diffusion equation with fractional spatial derivative in discrete space. As in the diffusive case, the propagator $(S_0^{(2)})^{-1}$ is calculated in momentum space

$$(S_0^{(2)})^{-1}(p, q) = \frac{1}{-i\omega + \frac{1}{\tau} \epsilon(\mathbf{p})} \hat{\delta}(p - q)$$

With the help of the residue theorem one transforms back in the temporal direction.

$$\int_\omega \frac{e^{-it_1\omega + it_2\omega}}{-i\omega + \frac{1}{\tau} \epsilon(\mathbf{p})} \hat{\delta}(p - q) = \Theta(t_1 - t_2) \exp \left[-\frac{1}{\tau} \epsilon(\mathbf{p}) \cdot (t_1 - t_2) \right].$$

Using the asymptotic behavior $\epsilon(\mathbf{p}) \approx a^\mu \tilde{D}_A \cdot |\mathbf{p}|^\mu$, to make the transition from the microscopic model to macroscopic world, yields

$$(S_0^{(2)})^{-1}(t_1 - t_2, \mathbf{p}) = \Theta(t_1 - t_2) \cdot \exp[-D_A \mathbf{p}^\mu \cdot (t_1 - t_2)], \quad \text{with } D_A = \tilde{D}_A \cdot \frac{a^\mu}{\tau}.$$

This coincides with the generalized central limit theorem (3.21).

3.4 Summary

This chapter concentrated on the random dynamics of (non interacting) particles inside the lattice $L = a\mathbb{Z}^d$. The randomness of the particle's movement is incorporated by defining the probability $p(\mathbf{x}, \mathbf{y})$ to jump from site $\mathbf{x} \in L$ to another site $\mathbf{y} \in L$ at a certain rate.

In section 3.1 some general properties of $p: L \times L \rightarrow \mathbb{R}_+$ were listed. In the hamiltonian way of speaking, the dynamics is captured by the kinetic term. The dispersion relation $\epsilon(\mathbf{p})$ expresses how much kinetic energy is contributed by the modes with momenta \mathbf{p} . The connection to the randomly jumping particles is established by $\epsilon(\mathbf{p}) = 1 - \hat{p}(\mathbf{p})$ and $\langle \Psi | \hat{H}_{kin} | \Phi \rangle = \frac{1}{\tau} (\hat{\Psi}, \epsilon \hat{\Phi})$.

The preceding sections 3.2 and 3.3 dealt with two concrete examples for the jump length distribution $p(\mathbf{x} - \mathbf{y})$: The random walk and the Lévy flight. Both of these microscopic models lead to a stable law describing the walker's (flyer's) position on a macroscopic scale. The transition from the microscopic to the macroscopic scale is the content of the (generalized) central limit theorem. Based on the randomly moving particles, the macroscopic impression of (super) diffusion is obtained. In the case of the Lévy flight, the crux is a slowly decaying power tail for large jumps leading to a super diffusive scaling between space and time and gives rise to the (discrete) fractional derivative operator ∇^μ . As described in section 3.3, the

mathematical reason for this is the divergence of the second moment, which circumvents the central limit theorem and enforces the generalized central limit theorem. The following table summarizes the main differences and similarities between normal diffusion and Lévy flights.

	Normal diffusion	Lévy flights
jump distribution	$p(\mathbf{x} - \mathbf{y}) \propto \begin{cases} 1, & \mathbf{x} - \mathbf{y} = a \\ 0, & \text{else} \end{cases}$	$p(\mathbf{x} - \mathbf{y}) \propto \begin{cases} \mathbf{x} - \mathbf{y} ^{-d-\mu}, & \text{else} \\ 0, & \mathbf{x} = \mathbf{y} \end{cases}$
diffusion constant	$D = \frac{1}{2d} \cdot \frac{a^2}{\tau}$ $[D] = \text{length}^2 \cdot \text{time}^{-1}$	$D_A = \tilde{D}_A \cdot \frac{a^\mu}{\tau}$ $[D_A] = \text{length}^\mu \cdot \text{time}^{-1}$
scaling	$\text{length}^2 \sim \text{time}$ diffusive	$\text{length}^\mu \sim \text{time}, \quad 0 < \mu < 2$ superdiffusive
dispersion	$\frac{1}{\tau} (\mathcal{F}^{-1} \epsilon \mathcal{F}) \Psi(\mathbf{x}) = -D \nabla^2 \Psi(\mathbf{x})$	$\frac{1}{\tau} (\mathcal{F}^{-1} \epsilon \mathcal{F}) \Psi(\mathbf{x}) = -D_A \nabla^\mu \Psi(\mathbf{x})$
asymptotics	$\frac{1}{\tau} \epsilon(\mathbf{p}) \approx D \cdot \mathbf{p} ^2$	$\frac{1}{\tau} \epsilon(\mathbf{p}) \approx D_A \cdot \mathbf{p} ^\mu$
propagator	$\exp(-\frac{1}{\tau} \epsilon(\mathbf{p}) \cdot t) \approx \exp(-D \mathbf{p}^2 \cdot t)$	$\exp(-\frac{1}{\tau} \epsilon(\mathbf{p}) \cdot t) \approx \exp(-D_A \mathbf{p} ^\mu \cdot t)$

Let us finish this chapter by briefly arguing why the problem of determining the macroscopic behavior of randomly moving particles becomes tremendously more difficult, when those particles react with each other. Without any reactions, the particles move independently⁴ from each other and the problem is reduced to a one particle problem. As described in sections 3.2 and 3.3, it is given by the (generalized) central limit theorem.

Imagine the pair annihilation reaction $A + A \rightarrow \emptyset$ is introduced among the random walkers (flyers). Due to the interaction, it is less likely to find a particle in the adjacency to another one. In this way, the dependence among the particles and the resulting (anti) correlations are serious difficulties in solving the pair annihilation process.

There are two prominent ways to account for (anti) correlation effects in the macroscopic description. The first method goes back to 1917 when Smoluchowski devised a phenomenological model [11]. As in every phenomenological theory, a lot of physical insight and intuition is necessary to account for the correlations ‘by hand’. The second possibility uses the ideas of statistical field theory and renormalization group theory to include fluctuation effects systematically. In this thesis the latter way is chosen and the following chapter prepares for this path.

⁴For a realistic physical system, this independence is a nontrivial assumption, based on the ansatz of molecular chaos.

4 Non perturbative renormalization group (NPRG)

Whenever a physical question is formulated with the help of a field theory, one can hope to get some insight into the problem via making use of the powerful technique of perturbative renormalization group (RG) theory. Two prominent areas in physics, that have profited by this strategy, are statistical physics and particle physics (see any textbook on QFT or many body physics such as [26, 51]). In both cases, one is interested in the partition function. Schematically this writes

$$Z[J] = \text{Tr}_{\Phi} \left(e^{-\frac{1}{k_B T} H[\Phi] + \Phi \cdot J} \right) \quad \text{and} \quad Z[J] = \text{Tr}_{\Phi} \left(e^{\frac{i}{\hbar} S[\Phi] + \Phi \cdot J} \right)$$

for statistical physics and particle physics, respectively. The trace is over all degrees of freedom represented by the field Φ coupled to an external source J . However, despite the success of perturbative RG, any perturbative study is doomed to fail if one of the following situations is encountered:

- There is no small parameter for which a perturbative expansion is meaningful [52]. In the special case of an $\epsilon = (d - d_c)$ expansion, the physically interesting dimension d might be far away from the critical dimension d_c .
- The quantities of interest are non universal [5].
- The properties of the investigation rely intrinsically on non perturbative features that are not captured within a perturbative approach [29, 53].

The framework of non perturbative renormalization group (NPRG) [8] has the potential to circumvent these difficulties. Using this technique, new progress in investigating critical phenomena in statistical physics has been made [54, 55].

In addition to equilibrium statistical physics and particle physics, the NPRG formalism was also established for out of equilibrium physics, first done by Canet et al. [29, 30, 31]. This thesis deals with non equilibrium physics. In particular, with the focus on the pair annihilation process. With this application in mind, the current chapter introduces the theory of NPRG. Extensive reviews are given by [52, 5].

4.1 Macroscopic behavior emerging from a microscopic model

As described in chapter 2, the physical space for the pair annihilation process is modeled by a lattice L . For the sake of concreteness, we restrict to the canonical, translational invariant, cubic lattice

$$L \equiv a \mathbb{Z}^d$$

with lattice constant a in d dimensions. Spacetime $\mathbb{R} \times L$ is defined by adding a continuous temporal direction to the spatial lattice. We denote spacetime points by $x = (t, \mathbf{x}) \in \mathbb{R} \times L$ and points in momentum space by $p = (\omega, \mathbf{p}) \in \mathbb{R} \times [-\pi/a, \pi/a]^d$ (see appendix A).

The field theory for the pair annihilation $A + A \rightarrow \emptyset$ is obtained by the Doi Peliti formalism and is given by the partition function (2.15)

$$Z[\bar{J}, J] = \int \mathcal{D}\Phi \mathcal{D}\bar{\Phi} \exp \left[-S[\bar{\Phi}, \Phi] + \int \Phi \cdot J + \int \bar{\Phi} \cdot \bar{J} \right]. \quad (4.1)$$

Characteristic for the Doi Peliti formalism are two fields: The Φ field with the physical interpretation of a particle density (compare eq. (2.17)), which couples to the auxiliary current J , and the so called response field $\bar{\Phi}$ with less physical content coupled to the particle input \bar{J} . Both, the fields, as well as the currents, are defined on spacetime, i.e. $\Phi: \mathbb{R} \times L \rightarrow \mathbb{R}$ and analog for $\bar{\Phi}$, J and \bar{J} . The microscopic action functional S directly carries the information of the reaction diffusion process given by the master equation. It is crucial to mention that no approximations were made in order to derive the field theory (4.1). Thus, the field theory is essentially non phenomenological and all the microscopic details (such as the reaction rate λ or the lattice structure L) are included.

The main task for solving *any* reaction diffusion process, is to leave the microscopic realm of its master equation and to investigate what happens on a macroscopic scale. As known from equilibrium statistical physics, this is a highly nontrivial task. Although the microscopic model happens to be simple (e.g. all reactions are short ranged), the emerging macroscopic behavior is likely to show a higher complexity:

- Correlations between distant space points can build up and lead to effectively long range interactions, although no long range interaction was present in the microscopic model.
- Critical phenomena with a diverging correlation length may occur (either in equilibrium [56] or in non-equilibrium [57] physics).
- Criticality is linked to a sudden change in the typical macroscopic behavior when certain microscopic parameters are changed only slightly. This intriguing curiosity, called phase transition, is difficult to predict quantitatively. It is a purely macroscopical effect without a counterpart in the microscopical world.

Mathematically, the macroscopical world is described by the partition function (4.1). Therefore, computing $Z[\bar{J}, J]$ is expected to be difficult as new macroscopical features will originate from simplicity. Once Z is computed, the model is considered to be solved and any macroscopical observable is cheaply obtained using (2.16).

Comparing the microscopic model given by S with the emerged macroscopical outcome given by Z , faces two problems.

1. The microscopic action S enters into the partition function Z as the argument of the exponential function.
2. The functional S depends on the fields Φ and $\bar{\Phi}$, whereas Z is a functional of the currents J and \bar{J} .

In this way, S and Z are poorly compatible. To resolve the first problem, define the *Helmholtz free energy* functional

$$W[\bar{J}, J] \equiv \ln Z[\bar{J}, J]$$

to be the logarithm of Z . Moreover, defining the *effective action*

$$\Gamma[\bar{\Psi}, \Psi] = -W[\bar{J}, J] + \int \Psi \cdot J + \int \bar{\Psi} \cdot \bar{J}, \quad (4.2)$$

where $\Psi(t, \mathbf{x}) = \frac{\delta W[\bar{J}, J]}{\delta J(t, \mathbf{x})}$ and $\bar{\Psi}(t, \mathbf{x}) = \frac{\delta W[\bar{J}, J]}{\delta \bar{J}(t, \mathbf{x})}$

to be the Legendre transform of W , solves the second difficulty. Since Ψ and $\bar{\Psi}$ are derived from the macroscopical object W , they are interpreted as *macroscopic fields* and Γ is the *macroscopic action*. In the terminology of statistical physics, Γ is also referred to as the *Gibbs free energy*. Notice the similarity between the macroscopic fields $\Psi(\mathbf{x})$, $\bar{\Psi}(\mathbf{x})$ and the one point functions

$$\langle \Phi(t, \mathbf{x}) \rangle \equiv \left. \frac{\delta W[\bar{J}, J]}{\delta J(t, \mathbf{x})} \right|_{\bar{J}=0, J=0} \quad \text{and} \quad \langle \bar{\Phi}(t, \mathbf{x}) \rangle \equiv \left. \frac{\delta W[\bar{J}, J]}{\delta \bar{J}(t, \mathbf{x})} \right|_{\bar{J}=0, J=0}.$$

The one point functions $\langle \Phi \rangle$ and $\langle \bar{\Phi} \rangle$ are obtained by evaluating the macroscopical fields Ψ and $\bar{\Psi}$ at vanishing currents $J = \bar{J} = 0$. This property will be used in the derivation of the Wetterich equation in section 4.3.

Going from Z to Γ , obviously preserves all the information and Z can be reobtained from Γ again. The reason why Γ is preferred over Z , is because S and Γ are on the same footing.

4.2 The idea of coarse graining

In nuce, the underlying idea of NPRG is to perform the transition from the microscopical to the macroscopical scale not at once, but peu à peu in an interpolating manner. For this purpose, a new parameter k with dimension $[k] = \text{length}^{-1}$ parametrizes the path from the microscopic world $k = \Lambda$ to the macroscopic world at $k = 0$ (Λ can be thought of as the inverse lattice spacing). Roughly speaking, at an intermediate mesoscopic scale $0 < k < \Lambda$, all short ranged degrees of freedom with $p > k$ are included in the formulation, while the long range modes $p < k$ are cut off. Therefore, k is also called the infrared (IR) cutoff. If $k = 0$, all physical degrees, especially the infrared ones, are integrated out and the macroscopic physics is obtained.

The idea is related to the block spin transformation according to Kadanoff [9]: At the mesoscopic scale k the ultraviolet lattice structure cannot be resolved any more. Instead, the lattice is blurred, showing a coarse grained image with the smallest resolvable blocks of size k^{-d} . Being incapable of seeing all the microscopic details has the advantage of sharpening the view for the fluctuations that coherently add up to form new mesoscopic physics. Macroscopic physics is obtained when all fluctuations are included as $k \rightarrow 0$. Metaphorically speaking, this coarse graining is similar to look at the details of brush strokes in a painting and, while going back, step by step, to finally recognize, how the single color patches blur and coherently create the big picture.

To quantify this coarse graining concept, the IR-cutoff operator R_k is used to define the cutoff term

$$\begin{aligned} \Delta S_k [\Phi, \bar{\Phi}] &= \frac{1}{2} \left(\begin{pmatrix} \bar{\Phi} \\ \Phi \end{pmatrix}, \begin{pmatrix} 0 & R_k \\ R_k & 0 \end{pmatrix} \begin{pmatrix} \bar{\Phi} \\ \Phi \end{pmatrix} \right) \\ &= \int_q \widehat{\Phi}(-q) \widehat{R}_k(q) \widehat{\Phi}(q) = \int_{x,y} \bar{\Phi}(x) R_k(x-y) \Phi(y). \end{aligned} \quad (4.3)$$

Equation (4.3) makes use of the fact that R_k is diagonal in momentum space (see appendix B), i.e.

$$K(\widehat{R}_k)(p_1, p_2) = \widehat{R}_k(p_1) \delta(p_1 - p_2).$$

When the cutoff (4.3) is added to the action, the partition function becomes scale dependent,

$$Z_k [\bar{J}, J] = \int \mathcal{D}\Phi \mathcal{D}\bar{\Phi} \exp \left[-S[\bar{\Phi}, \Phi] - \Delta S_k[\bar{\Phi}, \Phi] + \int \Phi \cdot J + \int \bar{\Phi} \cdot \bar{J} \right]. \quad (4.4)$$

The interpretation is as follows: Being proportional to the product $\bar{\Psi} \Psi$, the term ΔS_k gives an additional contribution to the dispersion function ϵ such that the total ‘energy’ of the p mode becomes $\tau^{-1} \epsilon(\mathbf{p}) + \widehat{R}_k(p)$. The propagation of the high energy modes is suppressed compared to the low energy modes. Hence, the artificial energy term \widehat{R}_k can be used to control how the fluctuations are integrated in. This is the key to implement the coarse graining described above. We require the following properties (recall $q = (\omega, \mathbf{q})$):

- $\lim_{k \rightarrow \Lambda} \widehat{R}_k(q) = \infty$ for all q , to guarantee that all fluctuations are frozen at the scale $k = \Lambda$. This is important in order to connect the macroscopic physics Γ to the microscopic model S (see section 4.4).
- $\lim_{k \rightarrow 0} \widehat{R}_k(q) = 0$ for all q , as the cutoff \widehat{R}_k is artificial and has to be absent in the physically meaningful, macroscopic limit $Z_{k=0} = Z$.
- $\widehat{R}_k(q) \simeq 0$ for $|\mathbf{q}| > k$: The modes with high momentum \mathbf{q} compared with the considered scale k are included and remain untouched.
- $\widehat{R}_k(q) \sim$ ‘large’ for $|\mathbf{q}| < k$: The modes with small momentum \mathbf{q} compared to the considered scale k are given a large artificial mass in order to damp their propagation. In other words, the cutoff \widehat{R}_k regularizes the IR behavior of the propagator.
- \widehat{R}_k is independent of ω : There is no coarse graining associated with the temporal direction.
- $\widehat{R}_k(q) \geq 0$ is non negative. The property is essential to guarantee causality (see section 5.2).

Analogously to section 4.1, we define the *scale dependent* Helmholtz free energy and effective action (Gibbs free energy) as

$$W_k [\bar{J}, J] \equiv \ln Z_k [\bar{J}, J]$$

and

$$\Gamma_k [\bar{\Psi}, \Psi] = -W_k [\bar{J}, J] + \int \Psi \cdot J + \int \bar{\Psi} \cdot \bar{J} - \Delta S_k [\bar{\Psi}, \Psi], \quad (4.5)$$

where $\Psi(x) = \frac{\delta W_k [\bar{J}, J]}{\delta J(x)}$ and $\bar{\Psi}(x) = \frac{\delta W_k [\bar{J}, J]}{\delta \bar{J}(x)}$,

respectively. Note that the additional ΔS_k term spoils (4.5) to be a true Legendre transform. Nevertheless, the right physical limit $\Gamma_{k=0} = \Gamma$ is recovered. As shown in section 4.4, the term is necessary to establish the connection between the microscopic action and the effective action in the sense $\Gamma_{k=\Lambda} = S$.

To further elaborate the investigation, a flow equation for the family of effective actions Γ_k is derived (section 4.3), and the initial condition $\Gamma_{k=\Lambda} = S$ is proven (section 4.4).

4.3 The derivation of the Wetterich flow equation

The flow equation in the context of NPRG characterizes how the effective action Γ_k behaves under the change of scale. Substituting the definition (4.5) of Γ_k , the flow equation is

$$\begin{aligned} \partial_k \Gamma_k [\bar{\Psi}, \Psi] &= -\partial_k W_k [\bar{J}, J] - \int_x \frac{\delta W_k [\bar{J}, J]}{\delta J(x)} \partial_k J(x) - \int_x \frac{\delta W_k [\bar{J}, J]}{\delta \bar{J}(x)} \partial_k \bar{J}(x) \\ &\quad + \int_x \Psi(x) \partial_k J(x) + \int_x \bar{\Psi}(x) \partial_k \bar{J}(x) - \partial_k \Delta S_k [\bar{\Psi}, \Psi] \\ &= -\partial_k W_k [\bar{J}, J] - \partial_k \Delta S_k [\bar{\Psi}, \Psi] \end{aligned} \quad (4.6)$$

(in the last line, the definition of the macroscopic fields Ψ and $\bar{\Psi}$ was used). The drawback of this equation is however, that the right hand side still depends on the functional W_k , and not on the appropriate functional Γ_k . The remaining task is to massage the expression

$$\partial_k W_k [\bar{J}, J] = -\langle \partial_k \Delta S_k [\bar{\Phi}, \Phi] \rangle$$

into a more suitable appearance, which depends on Γ_k only. Note that the definition¹ of the averaging bracket $\langle \cdot \rangle$ differs slightly from the one introduced in section 2.4.

In the first step, the following matrix notation

$$\tilde{R}_k \equiv \begin{pmatrix} 0 & R_k \\ R_k & 0 \end{pmatrix}, \quad \left(\Psi^{(n)}(x) \right)_{n \in \{1,2\}} \equiv (\bar{\Psi}(x), \Psi(x)) \quad \text{and} \quad \left(J^{(n)}(x) \right)_{n \in \{1,2\}} \equiv (\bar{J}(x), J(x))$$

is used to define two important operators:

¹The average of the functional $A[\bar{\Phi}, \Phi]$ is defined as

$$\langle A[\bar{\Phi}, \Phi] \rangle \equiv \frac{1}{Z_k[\bar{J}, J]} \int \mathcal{D}\Phi \mathcal{D}\bar{\Phi} A[\bar{\Phi}, \Phi] \exp \left[-S[\bar{\Phi}, \Phi] - \Delta S_k[\bar{\Phi}, \Phi] + \int \Phi J + \int \bar{\Phi} \bar{J} \right]$$

- The operator $G_k [\bar{J}, J] \equiv W_k^{(2)} [\bar{J}, J]$, defined through the integral kernel

$$K(G_k [\bar{J}, J])(x_1, x_2) \equiv G_k [\bar{J}, J] (x_1, x_2) = \left(\frac{\delta^2 W_k [\bar{J}, J]}{\delta J^{(n)}(x_1) \delta J^{(m)}(x_2)} \right)_{n,m \in \{1,2\}},$$

is called the *full field dependent propagator*. As $W = \ln Z$, the useful representation

$$\begin{aligned} G_k [\bar{J}, J] (x_1, x_2)_{n_1, n_2} &= \langle \Phi^{(n_1)}(x_1) \Phi^{(n_2)}(x_2) \rangle - \langle \Phi^{(n_1)}(x_1) \rangle \langle \Phi^{(n_2)}(x_2) \rangle \\ &= \langle \Phi^{(n_1)}(x_1) \Phi^{(n_2)}(x_2) \rangle - \Psi^{(n_1)}(x_1) \Psi^{(n_2)}(x_2). \end{aligned} \quad (4.7)$$

is obtained.

- Next, the operator $(\Gamma_k^{(2)} [\bar{\Psi}, \Psi] + \tilde{R}_k)$ with kernel

$$\left(\Gamma_k^{(2)} [\bar{\Psi}, \Psi] + \tilde{R}_k \right) (x_1, x_2) = \left(\frac{\delta^2 \Gamma_k [\bar{\Psi}, \Psi]}{\delta \Psi^{(n)}(x_1) \delta \Psi^{(m)}(x_2)} + K(\tilde{R}_k)_{n,m}(x_1, x_2) \right)_{n,m \in \{1,2\}}$$

is defined.

Both operators are inverses of each other:

$$G_k [\bar{J}, J] = \left(\Gamma_k^{(2)} [\bar{\Psi}, \Psi] + \tilde{R}_k \right)^{-1}. \quad (4.8)$$

A quick calculation reveals the claim

$$\begin{aligned} & \sum_m \int_y \frac{\delta^2 W_k [\bar{J}, J]}{\delta J^{(n_1)}(x_1) \delta J^{(m)}(y)} \left(\frac{\delta^2 \Gamma_k [\bar{\Psi}, \Psi]}{\delta \Psi^{(m)}(y) \delta \Psi^{(n_2)}(x_2)} + \tilde{R}_k(y - x_2)_{m, n_2} \right) \\ &= \sum_m \int_y \frac{\delta \Psi^{(m)}(y)}{\delta J^{(n_1)}(x_1)} \left(\frac{\delta J^{(n_2)}(x_2)}{\delta \Psi^{(m)}(y)} - \frac{\delta^2 \Delta S_k [\bar{\Psi}, \Psi]}{\delta \Psi^{(m)}(y) \delta \Psi^{(n_2)}(x_2)} + \tilde{R}_k(y - x_2)_{m, n_2} \right) \\ &= \sum_m \int_y \frac{\delta \Psi^{(m)}(y)}{\delta J^{(n_1)}(x_1)} \frac{\delta J^{(n_2)}(x_2)}{\delta \Psi^{(m)}(y)} = \delta_{n_1, n_2} \delta(x_1 - x_2) \end{aligned}$$

(in the second line $\frac{\delta \Gamma_k}{\delta \Psi^{(n)}} = J^{(n)} - \frac{\delta \Delta S_k}{\delta \Psi^{(n)}}$ is used).

Let us proceed with the plan to massage $\partial_k W_k$ into a form depending on Γ_k :

$$\begin{aligned} -\partial_k W_k [\bar{J}, J] &= \langle \partial_k \Delta S_k [\bar{\Phi}, \Phi] \rangle = \frac{1}{2} \int_{x_1, x_2} \sum_{n_1, n_2} \partial_k \tilde{R}_k(x_1 - x_2)_{n_1, n_2} \langle \Phi^{(n_1)}(x_1) \Phi^{(n_2)}(x_2) \rangle \\ &\stackrel{(4.7)}{=} \frac{1}{2} \int_{x_1, x_2} \sum_{n_1, n_2} \partial_k \tilde{R}_k(x_1 - x_2)_{n_1, n_2} \left(G_k [\bar{J}, J] (x_1, x_2)_{n_1, n_2} + \Psi^{(n_1)}(x_1) \Psi^{(n_2)}(x_2) \right) \\ &= \frac{1}{2} \text{Tr} \left(\partial_k \tilde{R}_k G_k [\bar{J}, J] \right) + \partial_k \Delta S_k [\bar{\Psi}, \Psi]. \end{aligned}$$

Plugging this into (4.6) and using (4.8), leads to the *Wetterich flow equation*

$$\boxed{\partial_k \Gamma_k [\bar{\Psi}, \Psi] = \frac{1}{2} \text{Tr} \left[\partial_k \tilde{R}_k \left(\Gamma_k^{(2)} [\bar{\Psi}, \Psi] + \tilde{R}_k \right)^{-1} \right]}. \quad (4.9)$$

It remains to show $\Gamma_{k=\Lambda} [\bar{\Psi}, \Psi] = S [\bar{\Psi}, \Psi]$. Pretending this equality holds, the strategy is set: Solving the Wetterich equation with this initial condition, forces $\Gamma_{k=0}$ to describe the coarse grained macroscopic physics connected *non phenomenologically* to the microscopic model S .

A selection of remarks concerning the structure of the Wetterich equation is listed:

- The Wetterich equation is an exact functional partial differential equation for the family of effective actions Γ_k .
- Going from a scale k to a scale $k - \Delta k$, involves only integrating over the degrees of freedom belonging to a narrow momentum range around $p = k$: For $p > k$ the property $\widehat{R}_k(p) \simeq 0$ turns $\partial_k \widetilde{R}_k$ into an ultraviolet (UV) cutoff. On the other hand, infrared (IR) modes with $p < k$ are damped by the propagator due to the large \widetilde{R}_k term in the denominator. In this way, the fluctuations on different scales are taken into account separately. This can be anticipated to be profitable for the description of critical phenomena, where fluctuations on all scales are important and have to be taken care of systematically [5].
- The syntactic structure of (4.9) motivates to represent the flow equation by a Feynman diagram:

$$\partial_k \Gamma = \frac{1}{2} \text{Tr} \left[\partial_k \widetilde{R}_k \left(\Gamma_k^{(2)} + \widetilde{R}_k \right)^{-1} \right] = \frac{1}{2} \text{loop} \text{ with cross} \quad (4.10)$$

Conveniently [5], the cross denotes the term $\partial_k \widetilde{R}_k$, and the line represents the full propagator $(\Gamma_k^{(2)} + \widetilde{R}_k)^{-1}$. The trace is depicted in a Feynman diagrammatic fashion by the fact that the propagator closes to form a loop. In contrast to perturbation theory, this one loop structure is exact due to the fact that the full field dependent propagator $(\Gamma_k^{(2)} [\bar{\Psi}, \Psi] + \widetilde{R}_k)^{-1}$ is used. The topological structure of the one loop diagram turns out to have important implications for the renormalization of the couplings in $A+A \rightarrow \emptyset$ (see section 5.3).

We conclude the chapter with the

4.4 Proof of $\Gamma_\Lambda = S$.

Rewriting the partition function Z_k (4.4) in terms of Γ_k , leads to (omitting the arguments for a condensed notation)

$$Z_k = e^{W_k} = \exp \left[-\Gamma_k - \Delta S_k + \int J \Psi + \int \bar{J} \bar{\Psi} \right] = \int \exp \left[-S - \Delta S_k + \int J \Phi + \int \bar{J} \bar{\Phi} \right].$$

Notice that the exponent on the left hand side is the macroscopical mirror image of the exponent appearing in the ‘Boltzmann factor’ on the right hand side. This symmetry is the essence of coarse graining. Making use of $J = \frac{\delta \Gamma}{\delta \Psi} + \frac{\delta \Delta S_k}{\delta \Psi}$ (and similarly for \bar{J}) and performing the field redefinition $\chi \equiv \Phi - \Psi$ and $\bar{\chi} \equiv \bar{\Phi} - \bar{\Psi}$, gives

$$\exp (-\Gamma_k [\bar{\Psi}, \Psi]) = \int \mathcal{D}\chi \mathcal{D}\bar{\chi} \exp \left[-S [\bar{\Psi} + \bar{\chi}, \Psi + \chi] + \int \frac{\delta \Gamma}{\delta \Psi} \chi + \int \frac{\delta \Gamma}{\delta \bar{\Psi}} \bar{\chi} - \Delta S_k [\bar{\chi}, \chi] \right].$$

The χ field measures the difference between the microscopical field Φ and the macroscopic field Ψ . In the limit $\widehat{R}_k \xrightarrow{k \rightarrow \Lambda} \infty$ the $-\Delta S_k[\bar{\chi}, \chi]$ term forces χ and $\bar{\chi}$ to be zero (this is a functional integration analogon to Laplace's method of the steepest descent)². Thus, the difference between the macroscopical and microscopical fields vanishes as $k \rightarrow \Lambda$. All fluctuations that lead to deviations from the microscopical picture are frozen by the cutoff \widehat{R}_Λ . Neglecting unimportant factors, completes the proof of:

$$\exp(-\Gamma_k[\bar{\Psi}, \Psi]) \xrightarrow{k \rightarrow \Lambda} \exp(-S[\bar{\Psi}, \Psi]) \implies \Gamma_\Lambda[\bar{\Phi}, \Phi] = S[\bar{\Phi}, \Phi].$$

□

²This rather handwaving argument can be made more waterproof by reintroducing the complex degree of freedom Φ , resulting in the fact that ΔS_k becomes quadratic in the real and imaginary part of the field. See the appendix in [27] for details.

5 The local potential approximation (LPA)

The previous chapters had a preliminary character and provided the tools for the investigation of the pair annihilation process. Chapter 2 introduced the Doi Peliti formalism and mapped the reaction diffusion process $A + A \rightarrow \emptyset$ to a field theory given by the action (compare eq. (2.15))

$$S[\bar{\Phi}, \Phi] = \int_x \bar{\Phi}(x) (\partial_t - D_A \nabla^\mu) \Phi(x) + U_\Lambda(\bar{\Phi}(x), \Phi(x)) \quad (5.1)$$

where

$$-D_A \nabla^\mu = \frac{1}{\tau} \mathcal{F}^{-1} \epsilon \mathcal{F} \quad \text{and} \quad U_\Lambda(\bar{\Phi}, \Phi) = \lambda \cdot (\bar{\Phi}^2 + 2\bar{\Phi}) \Phi^2. \quad (5.2)$$

Integration is performed over the whole spacetime $\mathbb{R} \times L$, i.e. $\int_x \equiv \int_{\mathbb{R}} dt \sum_{\mathbf{x} \in L}$ and $x = (t, \mathbf{x}) \in \mathbb{R} \times L$. For concreteness, we choose $L = a \mathbb{Z}^d$.

The action (5.1) consists of three different terms.

- The first term $\int \bar{\Phi} \partial_t \Phi$ includes a time derivative and results from the coherent state path integral prescription (compare section 2.3). It indicates the non equilibrium character of the process.
- The second term $-\int \bar{\Phi} D_A \nabla^\mu \Phi$ encodes the random movement of the particles. As explained in chapter 3, the dispersion function $\epsilon(\mathbf{p}) \equiv 1 - \hat{p}(\mathbf{p})$ is defined in terms of the jump length probability distribution $p(\mathbf{x} - \mathbf{y})$. In the case of Lévy flights one has $p(\mathbf{x} - \mathbf{y}) \propto |\mathbf{x} - \mathbf{y}|^{-d-\mu}$ (3.13) which leads to the fractional derivative (5.2). The anomalous diffusion constant D_A is defined by (3.22).
- The third term of (5.1) is the potential $\int U_\Lambda(\bar{\Psi}, \Psi)$, which incorporates the reaction $A + A \rightarrow \emptyset$.

Because the action (5.1) can be derived directly from the master equation (2.1), i.e. from the microscopic model, the action is understood to be part of the microscopic world. In contrast, the physical observables are macroscopical and are derived from the macroscopic partition function Z (4.1). The computation of the partition function Z can be viewed as the transition from the microscopical to the macroscopical world. A skillful way to perform this nontrivial transition is by the idea of coarse graining (see section 4.2): The IR cutoff ΔS_k is introduced and the family of scale dependent partition functions is defined to be

$$Z_k[\bar{J}, J] = \int \mathcal{D}\Phi \mathcal{D}\bar{\Phi} \exp \left[-S[\bar{\Phi}, \Phi] - \Delta S_k[\bar{\Phi}, \Phi] + \int \Phi J + \int \bar{\Phi} \bar{J} \right].$$

The scale $0 \leq k \leq \Lambda$ parametrizes the transition from microscopics ($k = \Lambda$) to macroscopics ($k = 0$). In the limit $k \rightarrow 0$, the IR cutoff vanishes and $Z_{k=0} = Z$ is recovered. The corresponding Gibbs free energy Γ_k is defined as the Legendre transform of the Helmholtz free

energy $W_k = \ln Z_k$. Γ_k is interpreted as an effective action, which describes the physics on an intermediate scale (see section 4.2). In particular, $\Gamma_{k=\Lambda} = S$ and $\Gamma_{k=0}$ are the microscopic and macroscopic extremes, respectively. In section 4.3, the *Wetterich equation*

$$\partial_k \Gamma_k [\bar{\Psi}, \Psi] = \frac{1}{2} \text{Tr} \left[\partial_k \tilde{R}_k \left(\Gamma_k^{(2)} [\bar{\Psi}, \Psi] + \tilde{R}_k \right)^{-1} \right] \quad (5.3)$$

was derived. If the initial condition $\Gamma_{k=\Lambda} = S$ is given, (5.3) relates the microscopic action S to the corresponding macroscopic action $\Gamma_{k=0}$. The flow equation (5.3) is exact and generally impossible to solve exactly. Nevertheless, the Wetterich equation is the right starting point for approximations [58].

Two famous methods to approximate the solution Γ_k of (5.3) are the *vertex expansion* and the *derivative expansion* [5]. The idea common to both approximations, is to truncate the space of possible functionals Γ_k on which the flow equation (5.3) is solved. In the following section, the *local potential approximation* (LPA) is introduced. The LPA is the simplest form of a derivative expansion. In the subsequent sections 5.2 and 5.3, we derive important consequences for the pair annihilation process.

5.1 The flow equation in LPA

Instead of solving the Wetterich equation (5.3) for $\Gamma_k [\bar{\Psi}, \Psi]$ exactly, the solution is approximated by restricting the space of functionals. In the simplest truncation, called the local potential approximation (LPA), the approximated solution is predicted to be of the form

$$\Gamma_k [\bar{\Psi}, \Psi] = \int_x [\bar{\Psi}(x) (\partial_t - D_A \nabla^\mu) \Psi(x) + U_k(\bar{\Psi}(x), \Psi(x))]. \quad (5.4)$$

This particular ansatz is intended to mimic the action (5.1) and has the same ‘dynamical part’ $\int \bar{\Psi}(x) (\partial_t - D_A \nabla^\mu) \Psi(x)$. In contrast to S however, (5.4) allows for a general *local potential* U_k that needs to be solved for. As we will see in section 5.3, the ‘dynamical part’ cannot be renormalized for the pair annihilation process, which justifies the ansatz (5.4). In the following, the constraints imposed on U_k by the Wetterich equation are examined.

We start with the computation of the propagator $(\Gamma_k^{(2)} + \tilde{R}_k)^{-1}$. The integral kernel of $\Gamma_k^{(2)}$ formally reads

$$\Gamma_k^{(2)}(x, y) = \begin{pmatrix} 0 & \partial_t - D_A \nabla^\mu \\ -\partial_t - D_A \nabla^\mu & 0 \end{pmatrix} \delta(x - y) + \begin{pmatrix} U_k^{(2,0)} & U_k^{(1,1)} \\ U_k^{(1,1)} & U_k^{(0,2)} \end{pmatrix} (\bar{\Psi}, \Psi) \delta(x - y)$$

in position space ($U^{(n,m)}(\bar{\Psi}, \Psi)$ being the derivative $\frac{\partial^{n+m} U(\bar{\Psi}, \Psi)}{\partial \bar{\Psi}^n \partial \Psi^m}$). To compute the inverse of $(\Gamma_k^{(2)} + \tilde{R}_k)$, it is tempting on one hand to do calculations in momentum space, because the cutoff \tilde{R}_k as well as the ‘dynamical part’ in $\Gamma_k^{(2)}$ become diagonal. On the other hand, the ‘potential’ part of $\Gamma_k^{(2)}$ is diagonal in position space and therefore, acts as a convolution in

momentum space (compare appendix B). To by-pass this difficulty, the fields $\Psi, \bar{\Psi}: \mathbb{R} \times L \rightarrow \mathbb{R}$ are chosen to be *constant* in space *and* time, such that $\Gamma_k^{(2)}$ is diagonal in momentum space:

$$\widehat{\Gamma}_k^{(2)}(p, q) = \begin{pmatrix} 0 & -i\omega + \frac{1}{\tau} \epsilon(\mathbf{p}) \\ i\omega + \frac{1}{\tau} \epsilon(\mathbf{p}) & 0 \end{pmatrix} \widehat{\delta}(p - q) + \begin{pmatrix} U_k^{(2,0)} & U_k^{(1,1)} \\ U_k^{(1,1)} & U_k^{(0,2)} \end{pmatrix} (\bar{\Psi}, \Psi) \widehat{\delta}(p - q).$$

We introduce the abbreviation

$$\Omega_k(p) \equiv -i\omega + \frac{1}{\tau} \epsilon(\mathbf{p}) + \widehat{R}_k(\mathbf{p}),$$

to ease the notation in the propagator at constant fields

$$\begin{aligned} (\widehat{\Gamma}_k^{(2)} + \widetilde{R}_k)^{-1}(p, q) &\stackrel{(B.6)}{=} \begin{pmatrix} U_k^{(2,0)} & \Omega_k(p) + U_k^{(1,1)} \\ \Omega_k(-p) + U_k^{(1,1)} & U_k^{(0,2)} \end{pmatrix}^{-1} \widehat{\delta}(p - q) \\ &= \left[\left(\Omega_k(p) + U_k^{(1,1)} \right) \left(\Omega_k(-p) + U_k^{(1,1)} \right) - U_k^{(2,0)} U_k^{(0,2)} \right]^{-1} \\ &\quad \cdot \begin{pmatrix} -U_k^{(0,2)} & \Omega_k(p) + U_k^{(1,1)} \\ \Omega_k(-p) + U_k^{(1,1)} & -U_k^{(2,0)} \end{pmatrix} \widehat{\delta}(p - q). \end{aligned} \quad (5.5)$$

Finally, the Wetterich equation for the ansatz (5.4) at constant fields, reads

$$\begin{aligned} \partial_k \Gamma_k = TV \partial_k U_k &= \frac{1}{2} \widehat{\delta}(0) \int_p \left[\omega^2 + \left(U_k^{(1,1)} + \widehat{R}_k(\mathbf{p}) + \frac{1}{\tau} \epsilon(\mathbf{p}) \right)^2 - U_k^{(2,0)} U_k^{(0,2)} \right]^{-1} \\ &\quad \text{tr} \partial_k \begin{pmatrix} 0 & \widehat{R}_k(\mathbf{p}) \\ \widehat{R}_k(\mathbf{p}) & 0 \end{pmatrix} \cdot \begin{pmatrix} -U_k^{(0,2)} & \Omega_k(p) + U_k^{(1,1)} \\ \Omega_k(-p) + U_k^{(1,1)} & -U_k^{(2,0)} \end{pmatrix} \end{aligned}$$

with $\widehat{\delta}(0) = \int_x \exp(i0 \cdot x) = \int_x 1 \equiv TV$ being the spacetime volume. Performing the ω integration (this is easy, because $\widehat{R}_k(p)$ is assumed to be independent of ω), yields

$$\partial_k U_k = \frac{1}{2} \int_{\mathbf{p}} \frac{\partial_k \widehat{R}_k(\mathbf{p}) \left(U_k^{(1,1)} + \widehat{R}_k(\mathbf{p}) + \frac{1}{\tau} \epsilon(\mathbf{p}) \right)}{\sqrt{\left(U_k^{(1,1)} + \widehat{R}_k(\mathbf{p}) + \frac{1}{\tau} \epsilon(\mathbf{p}) \right)^2 - U_k^{(2,0)} U_k^{(0,2)}}}. \quad (5.6)$$

Compared to the original Wetterich equation (5.3), being a functional partial differential equation for Γ_k , (5.6) is a significantly easier, partial differential equation for U_k . The price to pay for this simplification is the loss of exactness. Let us emphasize the approximation character of the flow equation (5.6). Assume the flow equation for the potential U_k (5.6) is solved exactly. Using this solution U_k in the ansatz (5.4) gives a functional Γ_k , which does

not need to solve the *full* Wetterich equation (5.3). The crucial point is that (5.6) was derived under the assumption of constant fields $\bar{\Psi}(x), \Psi(x) = \text{const}$. Therefore, even though (5.6) might be solved exactly, it is highly questionable whether this solution is still valid for non constant fields. The assumption of constant fields in the derivation of (5.6) is important to get a *consistent* flow equation for U_k , while the ansatz (5.4) does not need to solve the full Wetterich equation.

Remarkably, the derivation of (5.6) does not require to specify the microscopic model yet. Also, a particular choice for the cutoff function $\hat{R}_k(\mathbf{p})$ is not necessary (besides imposing independence on ω). Consequently, the flow equation (5.6) is capable to describe any one particle species, reaction diffusion process. The specific model enters the stage through a back door in fixing the initial condition $U_{k=\Lambda}$. In the case of $A + A \rightarrow \emptyset$, the initial condition is (5.2)

$$U_{k=\Lambda}(\bar{\Psi}, \Psi) = \lambda \cdot (\bar{\Psi}^2 + 2\bar{\Psi}) \Psi^2.$$

In the following sections 5.2 and 5.3, the crucial consequences of this particular initial condition are derived.

5.2 Causality

We evaluate the propagator (5.5) at *vanishing* fields $\bar{\Psi} = 0 = \Psi$:

$$\hat{G}_k [0, 0] (p_1, p_2) \equiv \left(\hat{\Gamma}_k^{(2)} [0, 0] + \tilde{R}_k \right)^{-1} (p_1, p_2) = \begin{pmatrix} 0 & \Omega_k(-p_1)^{-1} \\ \Omega_k(p_1)^{-1} & 0 \end{pmatrix} \hat{\delta}(p_1 - p_2)$$

(recall $\Omega_k(p) \equiv -i\omega + \frac{1}{\tau} \epsilon(\mathbf{p}) + \hat{R}_k(\mathbf{p})$). The temporal Fourier transform of this operator is performed by making use of the residue theorem. By abbreviating $c \equiv \frac{1}{\tau} \epsilon(\mathbf{p}_1) + \hat{R}_k(\mathbf{p}_1) \geq 0$,

$$\begin{aligned} \int_{\omega_1} \Omega(p_1)^{-1} e^{-i\omega_1(t_1-t_2)} \hat{\delta}(\mathbf{p}_1 - \mathbf{p}_2) &= - \int \frac{d\omega_1}{2\pi i} (\omega_1 + ic)^{-1} e^{-i\omega_1(t_1-t_2)} \hat{\delta}(\mathbf{p}_1 - \mathbf{p}_2) \\ &= \Theta(t_1 - t_2) \cdot \exp[-c \cdot (t_1 - t_2)] \hat{\delta}(\mathbf{p}_1 - \mathbf{p}_2) \end{aligned}$$

is obtained (since the Fourier transform is applied to an operator, equation (B.2) has to be used and results in the minus sign in the second argument t_2). Because $c \geq 0$ for every $\mathbf{p}_1 \in 1^{\text{st}}\text{B.Z.}$ and $0 \leq k \leq \Lambda$, the residue is always located in the lower half plane and entails the important Heaviside function $\Theta(t_1 - t_2)$. The result

$$\hat{G}_k [0, 0] ((t_1, \mathbf{p}_1), (t_2, \mathbf{p}_2)) \propto \begin{pmatrix} 0 & \Theta(t_2 - t_1) \\ \Theta(t_1 - t_2) & 0 \end{pmatrix} \hat{\delta}(\mathbf{p}_1 - \mathbf{p}_2) \quad (5.7)$$

sets up causality: It shows that the propagator connects only $\bar{\Psi}$ fields to later Ψ fields. Furthermore, the Ψ and $\bar{\Psi}$ fields cannot be connected among each other, as the propagator is off diagonal.

In a diagrammatic treatment, the propagator is represented by a straight line that connects a $\bar{\Psi}$ to a Ψ field

$$\Psi \longleftarrow \bar{\Psi}.$$

Causality is denoted by the arrow. As a convention, time always flows from the right to the left. Therefore, a $\bar{\Psi}$ field has to be attached at the right hand side of the propagator (earlier time) and the Ψ field, to which it connects, is on the left (later time).

5.3 The hierarchy of vertex functions

The scale dependent *vertex functions* $\Gamma_k^{(n,m)}$ are defined as the coefficients in the functional Taylor expansion of Γ_k around $\bar{\Psi} = 0 = \Psi$ [59],

$$\Gamma_k[\bar{\Psi}, \Psi] = \sum_{n,m=0} \frac{1}{n! m!} \int_{x_1, \dots, x_n} \int_{y_1, \dots, y_m} \Gamma_k^{(n,m)} \bar{\Psi}(x_1) \dots \bar{\Psi}(x_n) \Psi(y_1) \dots \Psi(y_m),$$

where
$$\Gamma_k^{(n,m)} = \frac{\delta^{n+m} \Gamma_k[\bar{\Psi}, \Psi]}{\delta \bar{\Psi}(x_1) \dots \delta \bar{\Psi}(x_n) \delta \Psi(y_1) \dots \delta \Psi(y_m)} \Big|_{\bar{\Psi}=0=\Psi}.$$

In this sense, the effective action Γ_k is the generating functional for all devisable vertex functions. The momentum space analogon is given by the functional $\hat{\Gamma}_k[\hat{\bar{\Psi}}, \hat{\Psi}] \equiv \Gamma_k[\bar{\Psi}, \Psi]$:

$$\hat{\Gamma}_k[\hat{\bar{\Psi}}, \hat{\Psi}] = \sum_{n,m=0} \frac{1}{n! m!} \int_{p_1, \dots, p_n} \int_{q_1, \dots, q_m} \hat{\Gamma}_k^{(n,m)} \hat{\bar{\Psi}}(p_1) \dots \hat{\bar{\Psi}}(p_n) \hat{\Psi}(q_1) \dots \hat{\Psi}(q_m),$$

where
$$\hat{\Gamma}_k^{(n,m)} = \frac{\delta^{n+m} \hat{\Gamma}_k[\hat{\bar{\Psi}}, \hat{\Psi}]}{\delta \hat{\bar{\Psi}}(p_1) \dots \delta \hat{\bar{\Psi}}(p_n) \delta \hat{\Psi}(q_1) \dots \delta \hat{\Psi}(q_m)} \Big|_{\hat{\bar{\Psi}}=0=\hat{\Psi}}.$$
 (5.8)

The vertex functions $\Gamma_k^{(n,m)}$ and $\hat{\Gamma}_k^{(n,m)}$ are interrelated by Fourier transform

$$\hat{\Gamma}_k^{(n,m)}(p_i, q_j) = \mathcal{F} \left(\Gamma_k^{(n,m)} \right) (-p_i, -q_j)$$

(notice the minus signs in the arguments).

Within the framework of the LPA, the vertex functions are directly related to the local potential U_k . Formally, by making use of (5.4), $m \geq 2$

$$\Gamma_k^{(n,m)}(x_i, y_j) = U_k^{(n,m)}(\bar{\Psi}, \Psi) \Big|_{\bar{\Psi}=0=\Psi} \prod_{i=2}^n \delta(x_1 - x_i) \prod_{i=1}^m \delta(x_1 - y_i)$$

$$\implies \hat{\Gamma}_k^{(n,m)}(p_i, q_i) = U_k^{(n,m)}(\bar{\Psi}, \Psi) \Big|_{\bar{\Psi}=0=\Psi} \hat{\delta}(\Sigma_i p_i + \Sigma_i q_i),$$

where $U_k^{(n,m)} = \partial^{n+m} U(\bar{\Psi}, \Psi) / \partial^n \bar{\Psi} \partial^m \Psi$ denotes the derivative. In the LPA, the momentum dependence of the vertex functions is only due to the momentum conservation. This feature is induced by the fact that the effective action Γ_k is expanded around homogeneous (especially zero) fields.

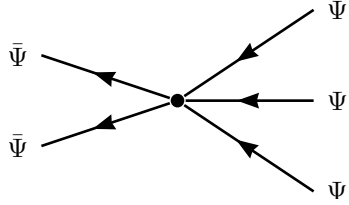
Assuming that U_k is analytic¹

$$U_k(\bar{\Psi}, \Psi) = \sum_{n,m} G_k(n, m) \bar{\Psi}^n \Psi^m,$$

and calling the Taylor coefficients $G_k(n, m)$ the *coupling constants*, the vertex function is proportional to the coupling

$$\widehat{\Gamma}_k^{(n,m)}(p_i, q_j) = n! m! G_k(n, m) \widehat{\delta}(\Sigma_i p_i + \Sigma_j q_j). \quad (5.9)$$

To relax the way of speaking (and writing), we call $G_k(n, m)$ the (n, m) coupling and $\Gamma_k^{(n,m)}$ the (n, m) vertex. The vertex functions are illustrated in a Feynman diagrammatic form: (choosing $(2, 3)$ as an example)



Their naming results from their vertex like, geometric structure. As a convention, we always draw the associated Ψ fields on the right hand side and call these the *ingoing* legs, whereas the *outgoing* legs, associated to the $\bar{\Psi}$ fields, are drawn on the left hand side (recall that time flows from right to left). The terminology of *ingoing* and *outgoing* comes from the fact that the Ψ fields of one vertex are infinitesimally earlier in time than the $\bar{\Psi}$ fields due to the Doi Peliti formalism (see also the explanation in footnote 2 on page 41). Note that the factors $n!$ and $m!$ in (5.9) appear naturally in the diagram as the combinatorial number of ways how the legs can be attached to the knot.

The Wetterich equation induces flow equations for each vertex function. The common feature which all of these flow equations share, is their one loop structure inherited from the original Wetterich equation (4.10). In what follows, we will make productive use of this instance.

At the microscopic level, the only non vanishing couplings for pair annihilation are $G_\Lambda^{(2,2)}$ and $G_\Lambda^{(1,2)}$. We deduce two important properties:

P1. For any non vanishing vertex function $\Gamma_\Lambda^{(n,m)}$, the number of ingoing Ψ fields is greater than or equal to the number of outgoing $\bar{\Psi}$ fields: $m \geq n$.

P2. From $U_\Lambda = \lambda(2\bar{\Psi} + \bar{\Psi}^2) \Psi^2$ it follows $G_\Lambda(1, 2) = 2 \cdot G_\Lambda(2, 2) = 2\lambda$ and therefore, $\Gamma_\Lambda^{(1,2)} = 2 \cdot \Gamma_\Lambda^{(2,2)}$.

Remarkably, both symmetries, initially only present at $k = \Lambda$, are preserved along the flow and subsequently hold on all scales $0 \leq k \leq \Lambda$.

¹It is still possible to derive non analytic results from this ansatz.

To prove the symmetry (P1) on all scales, it suffices to show that no vertex with more outgoing than ingoing legs can exist. The proof goes by induction. Assuming the absence of vertices with more outgoing than ingoing legs on some scale k , we have to show their absence on the scale $k - \Delta k$. New, contradicting vertices at scale $k - \Delta k$ are created through the Wetterich equation (4.10) out of the present vertices at scale k . The claim follows from the topological constraint imposed by the one loop character: Starting with any selection of N (n_i, m_i) vertices ($i = 1 \dots N$) with $n_i \leq m_i$ by induction hypothesis, the total number of outgoing legs trivially cannot be larger than the total number of ingoing legs: $\sum_i n_i \leq \sum_i m_i$. Forging a one loop diagram out of these building blocks by linking vertices with propagators, reduces the number of free outgoing and ingoing legs. As described in the previous section 5.2, a propagator can only connect a $\bar{\Psi}$ (i.e. outgoing leg) to a Ψ (i.e. ingoing leg). To complete a connected, irreducible one loop structure, N propagators are needed. Hence, the total number of ingoing and outgoing legs is reduced by the same amount N . We have $\sum_i n_i - N \leq \sum_i m_i - N$. \square

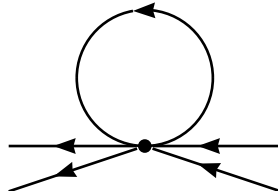
To prove the second symmetry (P2) on all scales, we look at the precise diagrammatic structure of the $(1, 2)$ and $(2, 2)$ vertex flow. As explained above, one has to obey the rule to use only (n, m) vertices with $n \leq m$ in building up the one loop flow. This topological limitation restricts the valid one loop structures to a simple form. Figure 5.1 shows the only allowed Feynman diagram for the $(1, 2)$ and $(2, 2)$ vertex flow². Both diagrams differ only by one vertex: The flow of the $(2, 2)$ vertex is obtained from the $(1, 2)$ vertex flow by replacing the $(1, 2)$ vertex by another $(2, 2)$ vertex. At $k = \Lambda$ one has $\Gamma_\Lambda^{(1,2)} = 2 \cdot \Gamma_\Lambda^{(2,2)}$ and thus $\partial_k \Gamma_k^{(1,2)}|_{k=\Lambda} = 2 \cdot \partial_k \Gamma_k^{(2,2)}|_{k=\Lambda}$. Therefore, the symmetry becomes inherited to the lower scale $\Lambda - \Delta k$. By induction, $\Gamma_k^{(1,2)} = 2 \cdot \Gamma_k^{(2,2)}$ holds for every $0 \leq k \leq \Lambda$. \square

The two preceding symmetries (P1) and (P2) already reveal some features of the vertex structure. We proceed by investigating the vertex scheme further and prove the following additional properties:

P3. It is not allowed to connect two legs of the same vertex with a propagator.

P4. The propagator does not become renormalized: $\partial_k \Gamma_k^{(1,1)} = 0$. This is the justification for the LPA ansatz (5.4).

²The reason why the flow for the $(2, 2)$ vertex does not contain the following *skull diagram*



lies in the Doi Peliti prescription. As described in chapter 2, the hamiltonian $H(\bar{\Phi}_t, \Phi_t)$, appearing in the action and giving birth to the couplings, was obtained by blurring the time difference in $H(\Phi_t, \Phi_{t-\Delta t})$ as $\Delta t \rightarrow 0$. This means, the ingoing Φ fields of a vertex are slightly earlier in time than the outgoing $\bar{\Phi}$ fields. The causality characteristic that the propagator only connects earlier $\bar{\Phi}$ fields to later Φ fields, prohibits the connection of legs of the same vertex. Hence, the skull diagram is excluded.

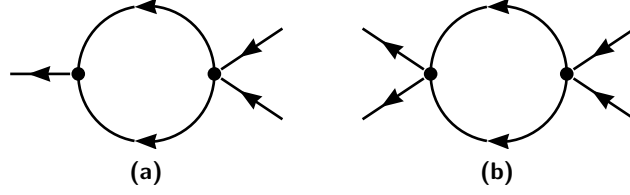


Figure 5.1: The proof of (P2), $\Gamma_k^{(1,2)} = 2 \cdot \Gamma_k^{(2,2)}$: (a) shows the flow $\partial_k \Gamma_k^{(1,2)}$ of the vertex $\Gamma_k^{(1,2)}$ in a diagrammatic way. Similarly, (b) depicts the flow $\partial_k \Gamma_k^{(2,2)}$.

Both diagrams differ only by the vertex on the left. Replacing the (1, 2) vertex in (a) by a (2, 2) vertex, gives the second diagram (b). Consequently, the initial condition $\Gamma_\Lambda^{(1,2)} = 2 \cdot \Gamma_\Lambda^{(2,2)}$ is inherited to all scales $0 \leq k < \Lambda$ by the flow equations.

- P5.** The flow of any vertex cannot depend on vertices, of which the difference between ingoing and outgoing legs is more severe. In other words, the flow of the (n, m) vertex with $m - n = l \geq 0$ cannot depend on a (\tilde{n}, \tilde{m}) vertex, whenever $\tilde{m} - \tilde{n} = \tilde{l} > l$.
- P6.** The flow equation of any (n, m) vertex cannot depend on a (\tilde{n}, \tilde{m}) vertex, with more than m ingoing legs.
- P7.** With the exception of the (2, 2) vertex, the flow of all other vertices (n, m) is linear in $\Gamma_k^{(n,m)}$. Moreover, the only diagram in the flow $\partial_k G_k(n, m)$ which contains the (n, m) vertex, contains exactly one additional (2, 2) vertex.
- P8.** The flow of the (n, m) vertex always contains a diagram which is build out of (1, 2) and (2, 2) vertices only. The total number N of vertices and internal lines in this particular diagram is $N = m$.

The rule (P3) was already used in the proof of $\Gamma_k^{(1,2)} = 2 \cdot \Gamma_k^{(2,2)}$ (P2). As explained in the footnote 2 on page 41, (P3) is a consequence of causality (section 5.2) and the Doi Peliti prescription (see chapter 2). \square

The fourth property (P4) was first realized by Peliti [60] in the context of perturbative RG theory. As shown in figure 5.2 the propagator cannot be dressed by loops without contradicting (P1) or (P3). \square

To prove property (P5), assume that the flow of the (n, m) vertex contains a loop with N vertices of the form (n_i, m_i) , $i = 1 \dots N$. As argued in the proof of property (P1), $(n, m) = (\sum_i n_i - N, \sum_i m_i - N)$. Therefore, $l = m - n = \sum_i (m_i - n_i) = \sum_i l_i$. Since all $l_i \geq 0$, this necessary condition fails if one of the $l_i > l$. \square

(P6) follows by similar means: If the flow of a (n, m) vertex is created by a loop with $N > 1$ vertices of the form (n_i, m_i) , the condition $m = \sum_i m_i - N$ has to hold. Every $m_i \geq 2$, because (P4) excludes the (1, 1) vertex. Finally, pretending there is a $m_j = \tilde{m} > m$, we obtain $m = \tilde{m} + \sum_{i \neq j} m_i - N \geq \tilde{m} + 2(N - 1) - N \geq \tilde{m}$. A contradiction. \square

Looking at the flow of the (1, 2) coupling in figure 5.1(a) explicitly, confirms the claim (P7) for this instance. Moreover, figure 5.1(b) shows that the flow of the (2, 2) vertex is quadratic

in $\Gamma_k^{(2,2)}$, which manifests the exceptional character of the $(2,2)$ coupling. To prove the rest of (P7), it remains to concentrate on (n,m) vertices with $m \geq 3$. Assume the flow of (n,m) contains at least two (n,m) vertices (this spoils linearity). Using $m_i \geq 2$ and $N \geq 2$, one has $m = \sum_i m_i - N \geq 2m + 2(N - 2) - N \Leftrightarrow m \leq 4 - N \leq 2$. This contradicts $m \geq 3$ and proves the absence of diagrams containing more than one (n,m) vertex. Further assume, the diagram contributing to the flow of the (n,m) vertex is build out of (n_i, m_i) , $i = 1, \dots, N$ vertices with $(n_1, m_1) = (n, m)$. As $m = \sum_{i=1} m_i - N = m + \sum_{i=2} m_i - N$ and $m_i \geq 2$, we conclude $N = 2$ and $m_2 = 2$. Similarly, $n_2 = 2$. The corresponding diagram is shown in figure 5.3. \square

Property (P8) is easily confirmed by drawing a circle and attaching sufficiently $(1,2)$ and $(2,2)$ vertices without contradicting the properties (P1) to (P7). As we have $m = \sum_i m_i - N$ with all $m_i = 2$, we get $N = m$. The condition $n = \sum_i n_i - N = \sum_i n_i - m \leq m$ on the number of outgoing legs can always be fulfilled by choosing the right number of $n_i = 1$. \square

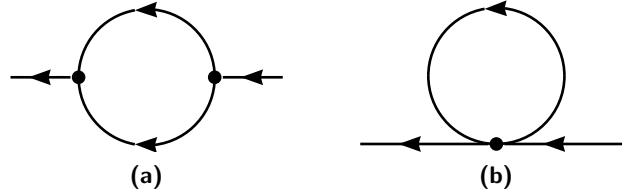


Figure 5.2: The proof of the absence of propagator renormalization (P4): Hypothetical one loop diagrams, that dress the propagator, are shown in (a) and (b). Both diagrams have to be ruled out, since they contradict property (P1) and (P3), respectively.

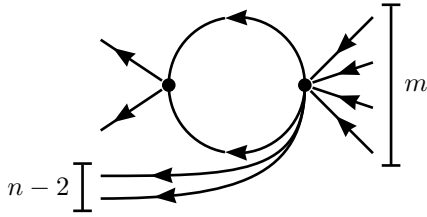


Figure 5.3: Property (P7) ensures that the flow $\partial_k G_k(n,m)$ of any $(n,m) \neq (2,2)$ vertex is linear in the coupling constant $G_k(n,m)$. The typical diagram which gives the term proportional to $G_k(n,m)$ is shown in this figure.

The backbone underlying all proof leading arguments used for (P1) to (P8), is the topology of the one loop structure in the Feynman diagrams imposed by the Wetterich equation (4.10) and the causality of the propagator (5.7). Equipped with the initial condition $G_\Lambda(n,m)$ for the couplings, the properties (P1) to (P8) follow. In principle, all the results could be derived without ever using any diagrammatic technique and just expanding the Wetterich equation (5.6) in the fields by setting $U_k(\bar{\Psi}, \Psi) = \sum_{n,m} G_k(n,m) \bar{\Psi}^n \Psi^m$. Equating coefficients, leads to a hierarchy of ordinary differential equations (ODEs) for the couplings $G_k(n,m)$ with initial condition $G_\Lambda(2,2) = 1/2 \cdot G_\Lambda(1,2) = \lambda$ and $G_\Lambda(n,m) = 0$. All the properties (P1) to (P8) are then read off in an algebraic manner.

Seen this way, Feynman diagrams provide a powerful topological tool to exploit the algebraic structure of the Wetterich equation (5.3).

The upshot of this section can be summarized with the help of the diagram in figure 5.4. The arrows denote the dependence in the flow of the couplings. The flow of any coupling (n, m) can only depend on the couplings prior (with respect to the arrows) to (n, m) . The arrangement of the arrows expresses properties (P5) and (P6). The resulting hierarchy implies a crucial property: Starting at the $(2, 2)$ coupling and including all couplings along the path in the direction of the arrows, up to an arbitrary coupling (\tilde{n}, \tilde{m}) , gives a closed system of flow equations for the couplings (i.e. coupled ODEs). In general, this system is too difficult to be solved analytically.

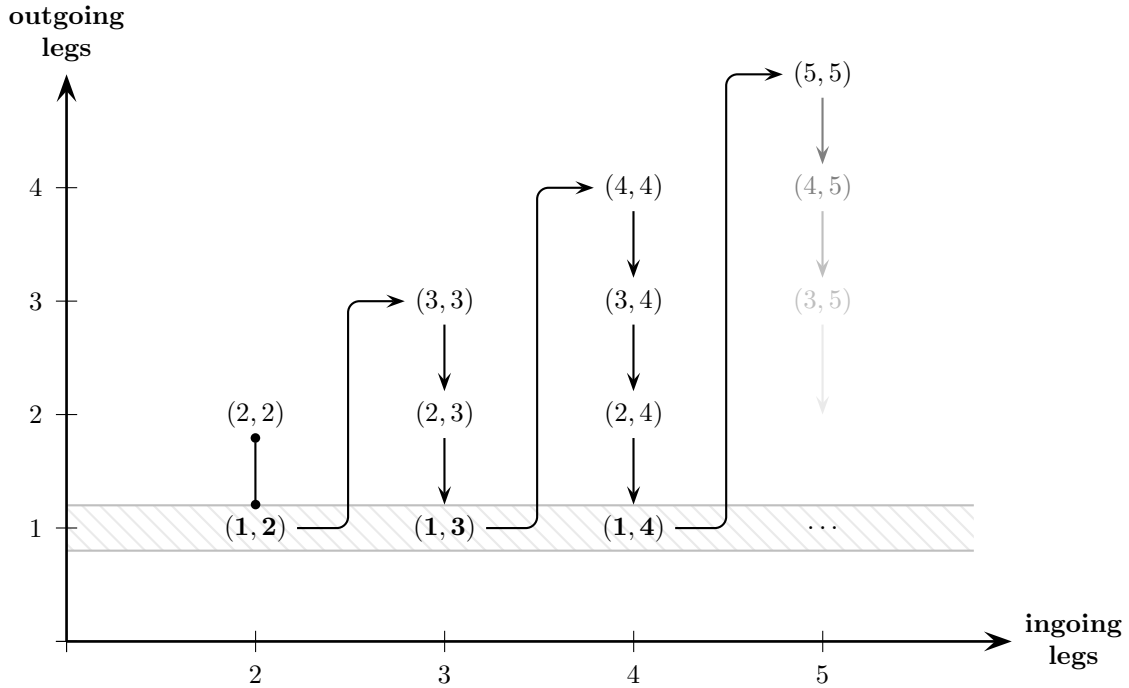


Figure 5.4: The structure of the vertex hierarchy for pair annihilation in the LPA approximation: All non vanishing vertex functions are placed according to their number of ingoing and outgoing legs (notice the absence of $(1, 1)$ and all vertices with more outgoing than ingoing legs). The arrows show the dependence among them, imposed by the Wetterich flow equation: The flow of the vertex (n, m) can only depend on vertices prior to it. A special link between the vertices $(2, 2)$ and $(1, 2)$ indicates the symmetry $\Gamma_k^{(1,2)} = 2 \cdot \Gamma_k^{(2,2)}$. The shaded region marks the vertices with direct physical relevance. They determine the particle density (see chapter 6).

6 Corrections to the law of mass action in $d > d_c$

We concentrate on the description of the process $A + A \rightarrow \emptyset$ where the A particles perform Lévy flights (see section 3.3) inside the lattice $L = a\mathbb{Z}^d$. As in chapters 4 and 5, spacetime points are denoted by $x = (t, \mathbf{x}) \in \mathbb{R} \times L$. The main goal is to predict the particle density $\rho(t)$ as a function of time.

In a simple mean field approach, where correlations between particles are neglected, the probability for two particles to collide is assumed to be given by the product of the particle density $\rho(t) \cdot \rho(t)$. If the reaction $A + A \rightarrow \emptyset$ occurs at the rate λ , the rate equation

$$\partial_t \rho(t) = -2\lambda \rho(t)^2 \quad (6.1)$$

describes the particle decrease for pair annihilation in the *mean field approximation*. The solution of (6.1) predicts the power law decay $\rho(t) \approx (\lambda t)^{-1}$ for late times t . We refer to (6.1) as the *microscopic law of mass action*, which states that the reaction rate is proportional to the concentration of the reacting particles [61, 57]. This mean field law is justified for systems, in which the particles are well stirred and consequently, the correlations between particles are absent or at least sufficiently low. The stirring is the result of the particle's random movement [62]. The antagonist of the random stirring is the reaction, which leads to (anti) correlations [63] between the reacting particles. Therefore, the validity of the mean field approximation depends on the balance between the dynamics of the particles and the particle's reactions.

For Lévy flights with Lévy exponent μ , we will show in section 6.3 that the law of mass action (6.1) is qualitatively correct up to the leading order if $d > d_c = \mu$. The spatial dimension d_c , where the law of mass action breaks down, is called the *critical dimension*. The fact that the critical dimension is lower for small Lévy exponents is conform with the intuition: For small Lévy exponents, large jumps happen more frequently and the particles stir more efficiently. Consequently, the law of mass action remains valid on a larger domain.

In this chapter we go beyond the mean field calculation (6.1) by means of field theoretical NPRG in $d > d_c$. After discussing the fluctuation improved law of mass action in section 6.3, we focus on the correction terms to this law in sections 6.4 and 6.5. The theoretical findings are compared to computer simulations in section 6.6. The following two sections are intended to make contact to the NPRG formalism in the local potential approximation.

6.1 Macroscopic rate equation

As described in section 2.5, the mean particle density $\rho(t)$ is given by (2.17)

$$\rho(x) = \langle \Phi(x) \rangle = \left. \frac{\delta W[\bar{J}, J]}{\delta J(x)} \right|_{\bar{J}=0, J=0} \quad (6.2)$$

and the one point function $\langle \bar{\Phi} \rangle$ fulfills the constraint (2.18)

$$\langle \bar{\Phi}(t) \rangle = \left. \frac{\delta W[\bar{J}, J]}{\delta \bar{J}(t, \mathbf{x}_0)} \right|_{\bar{J}=0, J=0} = 0.$$

Rewriting both equations in terms of the effective action $\Gamma[\bar{\Psi}, \Psi]$ (see section 4.1), yields

$$\left. \frac{\delta \Gamma[\bar{\Psi}, \Psi]}{\delta \Psi(x)} \right|_{\Psi=\langle \Phi \rangle, \bar{\Psi}=0} = J(x) = 0 \quad \text{and} \quad \left. \frac{\delta \Gamma[\bar{\Psi}, \Psi]}{\delta \bar{\Psi}(x)} \right|_{\Psi=\langle \Phi \rangle, \bar{\Psi}=0} = \bar{J}(x) = 0. \quad (6.3)$$

Solving the equations (6.3) for $\langle \Phi(x) \rangle$ is equivalent to calculating the one point function $\langle \Phi(x) \rangle$ by means of (6.2). The advantage of the equations (6.3) is the fact that they phrase the problem of determining the mean particle density $\langle \Phi \rangle$ in terms of the effective action Γ . Consequently, the framework of NPRG theory described in chapters 4 and 5 becomes applicable.

We give two related interpretations for (6.3).

- As $\Gamma_{k=0} = \Gamma$, the equations (6.3) can be viewed as the macroscopic extreme of

$$\frac{\delta \Gamma_k[\bar{\Psi}, \Psi]}{\delta \Psi(x)} = 0 \quad \text{and} \quad \frac{\delta \Gamma_k[\bar{\Psi}, \Psi]}{\delta \bar{\Psi}(x)} = 0.$$

The microscopic extreme is the *microscopic (classical) equations of motion*

$$\frac{\delta S[\bar{\Psi}, \Psi]}{\delta \Psi(x)} = 0 \quad \text{and} \quad \frac{\delta S[\bar{\Psi}, \Psi]}{\delta \bar{\Psi}(x)} = 0.$$

Against this background, equations (6.3) are called the *macroscopic equations of motion*.

- As known from statistical physics, the *equations of state* describing the system in thermodynamic equilibrium are obtained by minimizing the Gibbs free energy Γ . In this way, (6.3) could be called the *equations of state* despite its non equilibrium character.

Replacing the effective action Γ in (6.3) by the LPA ansatz (compare section 5.1)

$$\Gamma_k[\bar{\Psi}, \Psi] = \int_x [\bar{\Psi}(x) (\partial_t - D_A \nabla^\mu) \Psi(x) + U_k(\bar{\Psi}(x), \Psi(x))],$$

yields the *macroscopic* rate equation for the density ρ :

$$\partial_t \rho(t) = -U_0^{(1,0)}(0, \rho(t)) \quad (6.4)$$

($U_0^{(1,0)}$ being the first derivative of U_0 with respect to the first argument). Note, that the *microscopic* rate equation

$$\partial_t \rho(t) = -U_\Lambda^{(1,0)}(0, \rho(t)) = -2\lambda \rho(t)^2$$

is equivalent to the mean field equation (6.1).

With the results derived in section 5.3, the Taylor expansion of U_0 is known to be of the form

$$U_0(\bar{\Psi}, \Psi) = \sum_{\substack{n, m \geq 2 \\ n \leq m}} G_0(n, m) \bar{\Psi}^n \Psi^m$$

with $G_0(1, 2) = 2 G_0(2, 2)$ (see properties (P1), (P2) and (P4) on pages 40 and (P41). Consequently, expanding (6.4) yields

$$\partial_t \rho(t) = - \sum_{n \geq 2} G_0(1, n) \rho(t)^n = \underbrace{-2 G_0(2, 2) \rho(t)^2}_{\text{law of mass action}} - \underbrace{\sum_{n \geq 3} G_0(1, n) \rho(t)^n}_{\text{corrections}} \quad (6.5)$$

The first term is the *macroscopic* analogon of the *microscopic law of mass action* (6.1). The only quantitative difference is the fact that the macroscopic reaction rate $G_0(2, 2)$ replaces the microscopic reaction rate λ . The subsequent terms $-\sum_{n \geq 3} G_0(1, n) \rho(t)^n$ are corrections to the macroscopic law of mass action. This shows that the couplings $G_0(1, m \geq 2)$ effect the particle density directly. The vertex hierarchy, visualized in figure 5.4, indicates that it is nontrivial to compute the couplings $G_0(1, m)$ for large m since they depend on many previous couplings in the hierarchy.

As long as $G_0(2, 2) \neq 0$ the first term of (6.5) dominates the behavior for sufficiently small densities $\rho(t)$ and the scaling $\rho(t) \approx (2 G_0(2, 2) t)^{-1}$ is valid for large t . The exponent of this power law is exact and was investigated for diffusion [20, 12] and Lévy flights [15]. However, less effort was made to determine the amplitude $G_0(1, 2)$ or the corrections beyond the law of mass action.

In what follows, we will make use of the LPA flow equation (see section 5.1)

$$\partial_k U_k = \frac{1}{2} \int_{\mathbf{p}} \frac{\partial_k \widehat{R}_k(\mathbf{p}) \left(U_k^{(1,1)} + \widehat{R}_k(\mathbf{p}) + \frac{1}{\tau} \epsilon(\mathbf{p}) \right)}{\sqrt{\left(U_k^{(1,1)} + \widehat{R}_k(\mathbf{p}) + \frac{1}{\tau} \epsilon(\mathbf{p}) \right)^2 - U_k^{(2,0)} U_k^{(0,2)}}, \quad (6.6)$$

to determine the macroscopic coupling $G_0(2, 2)$ (section 6.3) and the effect of the corrections in (6.5) (sections 6.4 and 6.5). Prior to this, the following section defines the yet undetermined IR cutoff function \widehat{R}_k in (6.6).

6.2 The cutoff function

In section 4.2 a list of properties of the cutoff function \widehat{R}_k is given. The properties are motivated by the idea of coarse graining. However, most of the properties are not mandatory. There are only two indispensable requirements:

- $\lim_{k \rightarrow 0} \widehat{R}_k(\mathbf{p}) = 0$ for all \mathbf{p} , in order to guarantee that the true, physical limit $\boxed{\Gamma_{k=0} = \Gamma}$ is obtained macroscopically.
- $\lim_{k \rightarrow \Lambda} \widehat{R}_k(\mathbf{p}) = \infty$ for all \mathbf{p} to connect the initial microscopic action S to the effective action: $\boxed{\Gamma_{k=\Lambda} = S}$ (see section 4.4).

Since the Wetterich equation is an *exact* flow equation for Γ_k , these two inevitable conditions guarantee that the flow connects the initial condition $\Gamma_{k=\Lambda} = S$ to the final outcome $\Gamma_{k=0} = \Gamma$, independent of the concrete choice for \widehat{R}_k . The remaining freedom in \widehat{R}_k can be used to simplify the flow equation without changing the macroscopic outcome. Only the intermediate, mesoscopic functionals Γ_k are sensitive to the cutoff. In the limit $k \rightarrow 0$, where all degrees are integrated out, the unique physical limit Γ is obtained without ambiguities [64].

Things are different as soon as approximations such as the LPA (see chapter 5) are used. The loss of exactness leads to spurious, unphysical dependences of Γ_0 on the IR-cutoff [64, 54, 65] and $\Gamma_0 \neq \Gamma$ is not unique. A ‘good’ choice for \widehat{R}_k can improve the results, whenever approximations are used.

We do not follow the line of finding an optimal cutoff function \widehat{R}_k , but choose a form, which keeps analytic calculations simple. A convenient form, proposed by Litim [64], is

$$\widehat{R}_k(q) = \widehat{R}_k(\mathbf{q}) = \frac{1}{\tau} (\epsilon_k - \epsilon(\mathbf{q})) \cdot \Theta(\epsilon_k - \epsilon(\mathbf{q})). \quad (6.7)$$

At a given scale k , the Heaviside step function separates the physical modes into two regimes. The low energy (long ranged) modes with $\epsilon(\mathbf{q}) < \epsilon_k$ and the high energy (short ranged) modes with $\epsilon(\mathbf{q}) > \epsilon_k$. Hence, the ϵ_k functions as a energy reference. The precise dependence of the reference ϵ_k on the scale parameter k is given in equation (6.8).

Using the cutoff (6.7) in the effective propagator (5.5) at scale k and vanishing fields, yields

$$\left(\widehat{\Gamma}_k^{(1,1)}[0,0] + \widehat{R}_k \right)^{-1} (p_1, p_2) = \widehat{\delta}(p_1 - p_2) \begin{cases} (i\omega_1 + \frac{1}{\tau}\epsilon_k)^{-1} & \text{for } \epsilon(\mathbf{p}_1) < \epsilon_k \\ (i\omega_1 + \frac{1}{\tau}\epsilon(\mathbf{p}_1))^{-1} & \text{for } \epsilon(\mathbf{p}_1) > \epsilon_k. \end{cases}$$

In the case of $\epsilon(\mathbf{p}) < \epsilon_k$, the propagator is independent of the momenta (apart from the momentum conserving delta function) and all the low energy modes propagate the same way. The property that the propagator can not distinguish among the low energy modes is intended by the construction of (6.7) and simplifies the analytic considerations. The propagation of the high energy modes with $\epsilon(\mathbf{p}) > \epsilon_k$ is unaltered, because $\widehat{R}_k(\mathbf{p}) = 0$ in this case. Consequently, as soon as $\epsilon(\mathbf{p}) > \epsilon_k$, the \mathbf{p} modes are included completely into Γ_k and do no longer contribute to the Wetterich flow. Algebraically, this fact manifests in the factor $\partial_k \widehat{R}_k(\mathbf{q})$ of the Wetterich equation (4.9), which becomes zero for the high energy modes $\epsilon(\mathbf{p}) > \epsilon_k$.

The energy reference ϵ_k is chosen to fulfill the following properties.

- In the limit $k \rightarrow 0$ all modes are integrated out. Hence $\boxed{\epsilon_{k=0} = 0}$, which is equivalent to $R_{k=0} = 0$.
- $\boxed{\epsilon_{k=\Lambda} = \infty}$ to guarantee $R_{k=\Lambda} = \infty$.
- The positivity of $\epsilon(\mathbf{q})$ (3.4) implies $\boxed{\epsilon_k \geq 0}$ for all $0 \leq k \leq \Lambda$.
- ϵ_k is monotonically increasing in k .

The remaining freedom is fixed by the choice

$$\epsilon_k \equiv \widetilde{D}_A (ak)^\mu, \quad \Lambda = \infty \quad (6.8)$$

where \widetilde{D}_A is given by (3.15). The form (6.8) is proposed to mimic the dispersion relation $\epsilon(\mathbf{p})$ for small $|\mathbf{p}|$, i.e. $\epsilon(\mathbf{p}) \approx \widetilde{D}_A (a|\mathbf{p}|)^\mu$ for $|\mathbf{p}| \ll \pi/a$ [46].

The above properties of ϵ_k lead to a momentum scale k^* which separates the onsite fluctuations from long range fluctuations. We define the cross over scale k^* by

$$\max_{\mathbf{p}} \epsilon(\mathbf{p}) = \epsilon_{k^*}, \quad (6.9)$$

where the maximum is taken over all momenta $\mathbf{p} \in 1^{\text{st}}\text{B.Z.}$ (see figure 6.1). In the case of one dimensional Lévy flights, the maximum of $\epsilon(\mathbf{p})$ is obtained at the boundary of the Brillouin zone and k^* can be determined exactly:

$$k^* = \frac{1}{a} \left(\frac{2 - 2^{-\mu}}{\tilde{D}_A} \right)^{1/\mu} \quad \text{for Lévy flights in } d = 1. \quad (6.10)$$

For $k > k^*$, all momenta $\mathbf{p} \in 1^{\text{st}}\text{B.Z.}$ are treated as low energy modes ($\epsilon(\mathbf{p}) < \epsilon_k$) and contribute to the Wetterich flow. The fluctuations being integrated out for $k \gg k^*$ are extremely short ranged (smaller than the lattice spacing) and therefore, called onsite [46]. On the other hand, if $k < k^*$, the first Brillouin zone splits up into two parts. The first part corresponds to the low energy modes with $\epsilon(\mathbf{p}) < \epsilon_k$ and the second contains the high energy modes with $\epsilon(\mathbf{p}) > \epsilon_k$. Since the high energy modes are already included into Γ_k completely, they no longer contribute to the flow. In the limiting case $k \ll k^*$, only a small neighborhood around $\mathbf{0} \in 1^{\text{st}}\text{B.Z.}$ contains the remaining low energy modes. For \mathbf{p} in this small neighborhood the dispersion function is approximated by $\epsilon(\mathbf{p}) \approx \tilde{D}_A (a|\mathbf{p}|)^\mu$ and the flow cannot be distinguished from the continuum case [46]. The fluctuations integrated out for $k \ll k^*$ are long ranged and propagate through the whole lattice.

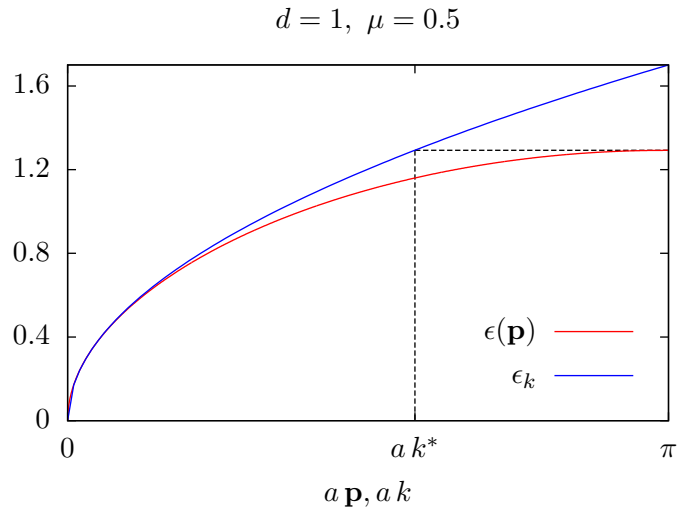


Figure 6.1: Schematic plot of the dispersion relation $\epsilon(\mathbf{p})$ and the energy reference ϵ_k for Lévy flights in $a\mathbb{Z}^1$ and $\mu = 0.5$. The energy reference ϵ_k is chosen to approximate the dispersion function $\epsilon(\mathbf{p})$ for small momenta $|\mathbf{p}| \approx 0$. The characteristic momentum scale k^* is defined as the smallest k such that $\epsilon_k > \epsilon(\mathbf{p})$ for all $\mathbf{p} \in 1^{\text{st}}\text{B.Z.}$. An explicit expression for k^* in the one dimensional case is given in (6.10). k^* separates onsite fluctuations from long range fluctuations (see eq. (6.9) and the discussion thereafter).

6.3 The leading term

For the Litim regulator (6.7), the flow equation of the local potential (6.6) becomes

$$\partial_k U_k = \frac{1}{2} \mathcal{V}(k) \frac{\frac{1}{\tau} \partial_k \epsilon_k \left(U_k^{(1,1)} + \frac{1}{\tau} \epsilon_k \right)}{\sqrt{\left(U_k^{(1,1)} + \frac{1}{\tau} \epsilon_k \right)^2 - U_k^{(2,0)} U_k^{(0,2)}}, \quad (6.11)$$

where

$$\mathcal{V}(k) \equiv \int_{\mathbf{p}} \Theta(\epsilon_k - \epsilon(\mathbf{p})), \quad \text{with dimension } [\mathcal{V}(k)] = 1$$

denotes the percental fraction of the Brillouin zone belonging to the low energy modes with $\epsilon(\mathbf{p}) < \epsilon_k$. For $k > k^*$ we have $\mathcal{V}(k) = 1$ as discussed in the previous section. Moreover, the fact that ϵ_k was chosen to approximate the dispersion function $\epsilon(\mathbf{p})$ for small momenta (compare eq. (6.8)), gives the useful scaling

$$\mathcal{V}(k) \xrightarrow{k \rightarrow 0} \frac{V(B^d(1))}{(2\pi)^d} (ak)^d, \quad (6.12)$$

where $V(B^d(1)) = \pi^{d/2} \cdot \Gamma(d/2 + 1)^{-1}$ denotes the volume of the d dimensional ball with unit radius.

Equation (6.11) imposes the flow equation

$$\partial_k G_k(2, 2) = \tau^{-1} \mathcal{V}(k) \partial_k \left(-\frac{1}{\epsilon_k} \right) (\tau G_k(2, 2))^2 = \text{Feynman diagram} \quad (6.13)$$

for the coupling $G_k(2, 2)$. The right hand side is quadratic in $G_k(2, 2)$ and does not depend on any other coupling as shown in the Feynman diagram (see section 5.3 and figure 5.1(b) therein). The solution of (6.13) with initial condition $G_\Lambda(2, 2) = \lambda$ is

$$G_k(2, 2) = \left[\frac{1}{\lambda} + \tau \int_k^\Lambda dk' \mathcal{V}(k') \partial_{k'} \left(-\frac{1}{\epsilon_{k'}} \right) \right]^{-1}. \quad (6.14)$$

Figure 6.2 plots the dependence of $G_k(2, 2)$ on k for $d = 2$ and $\mu = 1.5$. To calculate the macroscopic coupling $G_0(2, 2)$, the flow is divided into two regimes (compare the discussion in section 6.2 and the definition of k^* in eq. (6.9)).

- ① $k > k^*$, $\mathcal{V}(k) = 1$: The fluctuations are short ranged and the whole lattice contributes to $G_k(2, 2)$.
- ② $k < k^*$: The fluctuations are long ranged and can propagate through the lattice. Some small scale details of the lattice no longer contribute to $G_k(2, 2)$. In the limit $k \ll k^*$ the lattice structure has no influence on the flow.

Consequently, the integral splits up into

$$\int_0^\Lambda dk' \mathcal{V}(k') \partial_{k'} \left(-\frac{1}{\epsilon_{k'}} \right) = \underbrace{\int_{k^*}^\Lambda dk' \mathcal{V}(k') \partial_{k'} \left(-\frac{1}{\epsilon_{k'}} \right)}_{\text{①}} + \underbrace{\int_0^{k^*} dk' \mathcal{V}(k') \partial_{k'} \left(-\frac{1}{\epsilon_{k'}} \right)}_{\text{②}}.$$

and each part is investigated separately.

$$\begin{aligned} \textcircled{1} &= \int_{k^*}^{\Lambda} dk' \partial_{k'} \left(-\frac{1}{\epsilon_{k'}} \right) = \frac{1}{\epsilon_{k^*}} - \frac{1}{\epsilon_{\Lambda}} = \frac{1}{\epsilon_{k^*}}, \\ \textcircled{2} &= \int_0^{k^*} dk' \int_{\mathbf{p}} \Theta(\epsilon_{k'} - \epsilon(\mathbf{p})) \partial_{k'} \left(-\frac{1}{\epsilon_{k'}} \right) = \int_{\mathbf{p}} \int_{\epsilon_{\epsilon(\mathbf{p})}^{-1}}^{k^*} dk' \partial_{k'} \left(-\frac{1}{\epsilon_{k'}} \right) = \int_{\mathbf{p}} \left(\frac{1}{\epsilon(\mathbf{p})} - \frac{1}{\epsilon_{k^*}} \right). \end{aligned}$$

The monotonicity of ϵ_k was used to give $\Theta(\epsilon_{k'} - \epsilon(\mathbf{p})) = 1 \Leftrightarrow k' > \epsilon_{\epsilon(\mathbf{p})}^{-1}$ in the last line.

Combining $\textcircled{1}$ and $\textcircled{2}$ in equation (6.14), yields

$$G_0(2, 2) = \left[\frac{1}{\lambda} + \tau \int_{\mathbf{p}} \frac{1}{\epsilon(\mathbf{p})} \right]^{-1} \stackrel{\lambda \neq \infty}{=} \lambda \cdot \left[1 + \lambda \tau \int_{\mathbf{p}} \frac{1}{\epsilon(\mathbf{p})} \right]^{-1}. \quad (6.15)$$

As long as $G_0(2, 2) > 0$, the macroscopic rate equation reads

$$\partial_t \rho(t) = -2G_0(2, 2) \rho(t)^2 \quad (6.16)$$

up to the leading order as $\rho \rightarrow 0$ (6.5). We call (6.16) the *macroscopic law of mass action*. Equation (6.16) has the same mean field characteristic as the *microscopic law of mass action* (6.1). For $G_0(2, 2) = 0$ the *macroscopic law of mass action* breaks down and the corrections take over the leading position (see chapter 7). In order for $G_0(2, 2)$ to vanish, the integral $\int_{\mathbf{p}} \epsilon(\mathbf{p})^{-1}$ in equation (6.15) has to diverge. As the domain of integration is finite and $\epsilon(\mathbf{p}) > 0$ for $\mathbf{p} \neq 0$, any possible divergence has to originate from the IR behavior of $\epsilon(\mathbf{p})^{-1}$ in the vicinity of $\mathbf{p} = 0$. Using $\epsilon(\mathbf{p}) \approx \tilde{D}_A (a|\mathbf{p}|)^\mu$ for small $a|\mathbf{p}| < \eta$ in the integrand, leads to

$$\int_{\mathbf{p}} \epsilon(\mathbf{p})^{-1} \approx (2\pi)^{-d} \int_{a|\mathbf{p}| < \eta} d^d(ap) \frac{(a|\mathbf{p}|)^{-\mu}}{\tilde{D}_A} + \text{finite} = \begin{cases} \text{finite} & d > \mu \\ \text{logarithmically divergent} & d = \mu \\ \text{divergent} & d < \mu. \end{cases}$$

Hence, the criterion for the *macroscopic law of mass action* (6.16) to be valid is

$$G_0(2, 2) > 0 \iff d > d_c = \mu. \quad (6.17)$$

The dimension $d_c = \mu$ separates the regime $G_0(2, 2) > 0$ from the regime $G_0(2, 2) = 0$ and is called the *critical dimension*. The interpretation was already mentioned at the beginning of this chapter. The crux is the competition between the stirring of the particles and the tendency to build up correlations. On the one hand, the mixing property of the particles originates from the Lévy flights. On the other hand, reactions tend to build up correlations and thereby, work against the stirring. In the case of $A + A \rightarrow \emptyset$ anti correlations between the particles makes it less likely to find particles close to each other [63]. Mean field assumes perfect stirring and neglects the correlations completely. For $d > d_c = \mu$ the stirring dominates upon the correlations. Hence, the mean field result (6.1) is only altered quantitatively in (6.16). This is justified for $d < d_c = \mu$ where the stirring is less efficient, as the Lévy jumps are small and the correlations become strong enough to break down the law of mass action. More precisely, the fluctuations which are responsible for this breakdown are infinitely extended in space. This is rooted in the fact that $G_0(2, 2)$ vanishes due to the IR divergence of $\int \epsilon(\mathbf{p})^{-1}$ at $\mathbf{p} = 0$. The discussion of the fluctuation dominated regime $d \leq d_c$ is postponed to chapter 7.

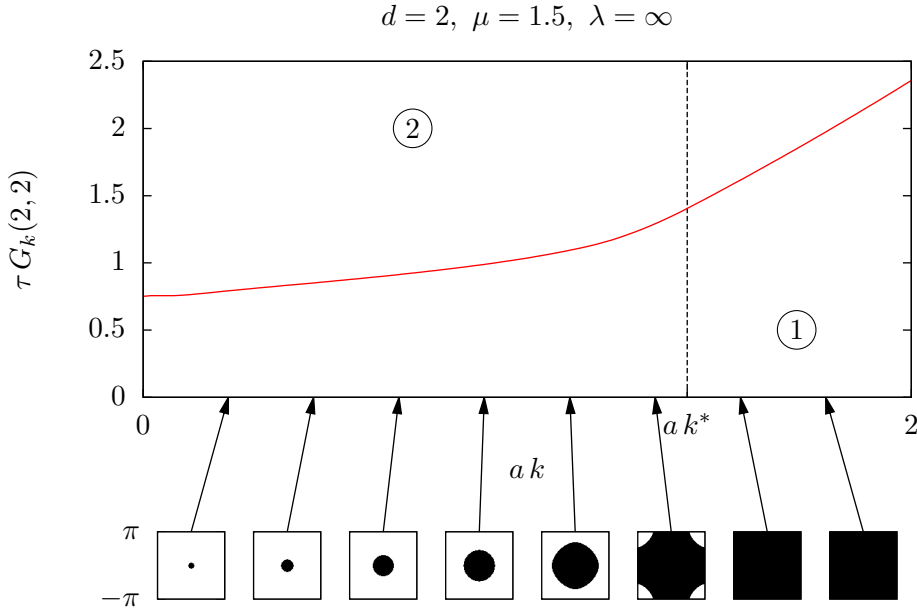


Figure 6.2: The running of the reaction rate $G_k(2, 2)$ (6.14) is demonstrated for the process $A + A \xrightarrow{\lambda} \emptyset$ on the lattice $a\mathbb{Z}^2$ with Lévy exponent $\mu = 1.5$ and $G_\Lambda(2, 2) = \lambda = \infty$. The plot shows the last piece of flow for $0 \leq ak \leq 2$ before the macroscopic limit at $k = 0$ is reached. The square images below indicate the fraction of the Brillouin zone $[-\pi/a, \pi/a]^2$ which contributes to the flow at the certain scale k indicated by the corresponding arrow.

The \mathbf{p} modes (colored in black), which contribute to the flow at the scale k , are low energetic with respect to the reference energy, i.e. $\epsilon(\mathbf{p}) < \epsilon_k$ (see section 6.2). Each of these low energy modes contributes the same amount to the flow at scale k in the sense that they propagate the same way. The scale $ak^* \approx 1.417$ (see eq. (6.9)) separates the regime of short range fluctuations $k > k^*$ from the regime of long range fluctuations $k < k^*$. At the scales $k > k^*$, all modes are treated as low energy fluctuations and consequently, the whole Brillouin zone influences the flow. However, at a coarse grained scale k below k^* , the Brillouin zone splits up into a high energy part with $\epsilon(\mathbf{p}) > \epsilon_k$ (white) and the remaining low energy contribution (black). The high energy (small distance) modes are completely included into $G_k(2, 2)$ and no longer influence the flow. The short scale details of the lattice corresponding to this part of the Brillouin zone cannot be resolved at this coarse grained scale k . Just below k^* , the low energy part is anisotropic, which reflects the anisotropy of the lattice $a\mathbb{Z}^2$ at small distances compared to the lattice spacing a . For $k \rightarrow 0$ the flow behaves as if the space was continuous, because the lattice structure approximates the continuum \mathbb{R}^2 at large distances $\gg a$.

Macroscopic vs. microscopic reaction rate

This paragraph discusses the dependence of the macroscopical reaction rate $G_0(2, 2)$ (6.15) on the microscopic rate λ and on the Lévy flight exponent μ for $d > d_c$. The microscopic time scale between two jumps τ is used to render the reaction rates $G_0(2, 2)$ and λ dimensionless. Equation (6.15) can be written in terms of the dimensionless rates as

$$\tau G_0(2, 2) = \left(\frac{1}{\tau \lambda} + \int_{\mathbf{p}} \frac{1}{\epsilon(\mathbf{p})} \right)^{-1} \quad \text{for } \tau \neq 0. \quad (6.18)$$

This rescaled equation demonstrates the feature of data collapse in the sense, that the dimensionless macroscopic coupling $\tau G_0(2, 2)$ depends only on the product $\lambda \tau$ and not on the microscopic parameters τ and λ individually. The following list of properties can be extracted from (6.18) and is visualized by the plot in figure 6.3.

- P1.** $G_0(2, 2) < \infty$ for all $0 < \mu < d$ and all $0 \leq \lambda \leq \infty$.
- P2.** $G_0(2, 2) \geq 0$ for all $0 < \mu < d$ and λ and $G_0(2, 2) = 0 \Leftrightarrow \lambda = 0$.
- P3.** $G_0(2, 2) < \lambda$, as $\epsilon(\mathbf{p}) > 0$ (see eq. (3.4)).
- P4.** $G_0(2, 2)$ is monotonically increasing in λ .
- P5.** $G_0(2, 2)$ is monotonically decreasing in μ .
- P6.** $G_0(2, 2) \xrightarrow{\lambda \rightarrow 0} \lambda$ and the rate $G_0(2, 2)$ becomes insensitive to μ .
- P7.** $G_0(2, 2) \propto D_A$ as $\lambda \rightarrow \infty$.
- P8.** $G_0(2, 2) \xrightarrow{\mu \rightarrow 0} (1/\lambda + \tau)^{-1}$.
- P9.** $G_0(2, 2) < 1/\tau$ for all $0 < \mu < d$ and all $0 \leq \lambda \leq \infty$.
- P10.** The macroscopic reaction rate obeys the power law

$$\tau G_0(2, 2) = \mathcal{A} \cdot (d - \mu)^1 \quad (6.19)$$

as the critical dimension approaches $\mu \rightarrow d$. In the $d = 1$ dimensional case, the amplitude is given by $\mathcal{A} = 3$.

The three properties (P1), (P3) and (P4) can be interpreted in terms of coarse graining: For the sake of concreteness, the microscopic reaction rate is considered to be infinite, $\lambda = \infty$. This means that two particles react immediately when they collide, i.e. if they meet at the same lattice site. Two nearby particles separated by a finite, microscopic distance (at least of the size of the lattice spacing) do not react. In the process of coarse graining, there is a scale k at which the small distance between the close particles is not resolvable (at the order of $k \sim a^{-1}$). At this mesoscopic scale, it looks as if the particles are colliding, but no reaction occurs. Thus, $G_k(2, 2)$ cannot be infinite. This interpretation also suggests that $G_k(2, 2)$ is monotonically decreasing with k , such that $G_0(2, 2) < G_k(2, 2) < \infty$. The monotonicity can be verified algebraically in (6.14) and is illustrated in figure 6.2.

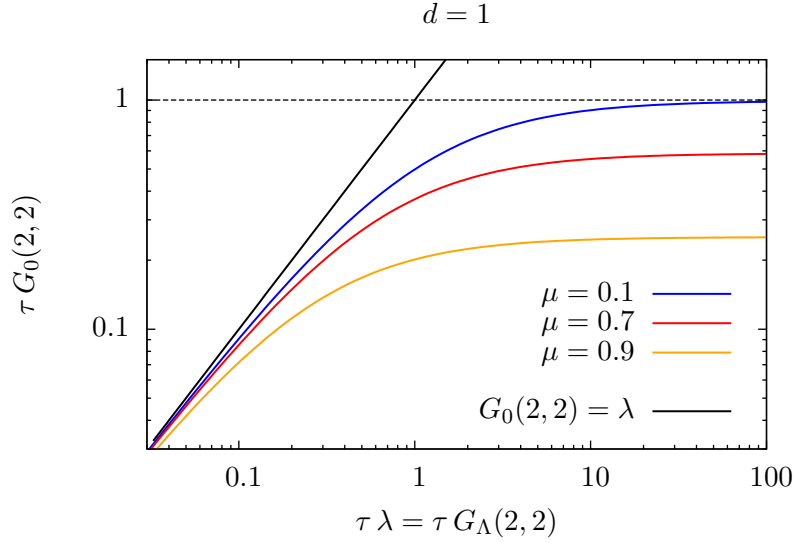


Figure 6.3: The macroscopic reaction rate $\tau G_0(2,2) = \tau\lambda (1 + \tau\lambda \int_{\mathbf{p}} 1/\epsilon)^{-1}$ is plotted against the corresponding microscopic rate $\tau\lambda$ for different μ in one spatial dimension $d = 1$. The solid black line represents the mean field result $G_0(2,2) = \lambda$. The dotted black line marks the upper limit $\tau G_0(2,2) = 1$, which is only reached for $\mu = 0$ and $\lambda = \infty$ (see property P9).

The property (P2) was already discussed during the derivation of the criterion (6.17).

Property (P5) is equivalent to the fact that the integral $\int_{\mathbf{p}} \epsilon(\mathbf{p})^{-1}$ is monotonically increasing in μ . As already mentioned above, the integral $\int_{\mathbf{p}} \epsilon(\mathbf{p})^{-1}$ gets its main contribution from the neighborhood $|\mathbf{p}| < \eta/a$ around $\mathbf{p} = 0$ where $\epsilon(\mathbf{p})$ is small. Using the asymptotic behavior $\epsilon(\mathbf{p}) \approx \tilde{D}_A (a|\mathbf{p}|)^\mu$ (see eq. (3.15)) leads to

$$\int_{\mathbf{p}} \epsilon(\mathbf{p})^{-1} \approx (2\pi)^{-d} \int_{a|\mathbf{p}| < \eta} d^d(ap) \left(\tilde{D}_A (a|\mathbf{p}|)^\mu \right)^{-1} + \text{const} = \frac{V(S^{d-1})}{(2\pi)^d \tilde{D}_A} \frac{1}{d-\mu} \eta^{d-\mu} + \text{const}, \quad (6.20)$$

where $V(S^{d-1}) = 2\pi^{n/2}/\Gamma(n/2)$ is the surface of the $(d-1)$ dimensional unit sphere. Assuming that the dependence of \tilde{D}_A and the remaining constant on μ is weak, this supports the claim of (P5). From a physical point of view, (P5) is obvious: For small μ , particles perform large jumps more frequently and the particles stir more efficiently. As a consequence, the effective reaction rate is large in this case (see figure 6.4).

(P6) states that the mean field result $G_0(2,2) = \lambda$ is recovered in the limit $\lambda \rightarrow 0$. Recall that the mean field approximation relies on the thought that the particles are perfectly mixed due to their random movement and that correlations caused by the reaction $A + A \rightarrow \emptyset$ can be ignored completely. In the weak coupling limit $\lambda \rightarrow 0$, the correlations are insignificant, as they are washed out by the dominant random movement. The limit $\lambda = 0$ is rather dull, as the particles do not react and the particle density is conserved: $\partial_t \rho(t) = -2\lambda \rho(t)^2 = 0$.

The statement (P7) focuses on $\lambda \rightarrow \infty$. Although (P7) follows directly from (6.18), let us emphasize how it can be obtained by simple dimensional analysis. If $\lambda < \infty$, there are two microscopic time scales, viz. the characteristic time scale $1/\lambda$ for a reaction to happen and the time τ between the two jumps of a particle. Writing the macroscopic coupling $G_0(2, 2)$ as a function of all possible dimensional microscopic parameters, yields $G_0(2, 2) = f(1/\lambda, \tau, a)$. As $G_0(2, 2)$ has the dimension of inverse time, and the lattice spacing a is the only parameter with dimension of length, $G_0(2, 2)$ cannot depend on a . Moreover, using τ to gauge the units of time, we obtain

$$G_0(2, 2) = \frac{1}{\tau} \tilde{f}(\tau\lambda).$$

The dimensionless product $\tau\lambda$ reflects the competition between stirring (enforced by the random jumps at every time step τ) and correlations (due to the particle interaction given by λ). The remaining dimensionless function \tilde{f} cannot be determined by dimensional considerations. However, things simplify in the limit $\lambda \rightarrow \infty$:

$$G_0(2, 2) \xrightarrow{\lambda \rightarrow \infty} \frac{1}{\tau} \tilde{f}(0) \propto \frac{1}{\tau}.$$

By performing the limit, we assume that \tilde{f} is continuous [66]. The time scale τ is expressed as $1/\tau \propto D_A/a^\mu$ (3.22). Therefore,

$$G_0(2, 2) \propto \frac{D_A}{a^\mu} \quad \text{for } \lambda \rightarrow \infty.$$

This is the content of (P7). Using (6.18), the dimensionless proportionality factor takes the form

$$\left[\tilde{D}_A \int_{\mathbf{p}} \epsilon(\mathbf{p})^{-1} \right]^{-1} \quad \text{with } \tilde{D}_A \text{ given in (3.15)} \quad (6.21)$$

and encodes the microscopic details, such as the lattice structure and the dynamics of the particles. In his seminal paper [11], Smoluchowski devised a phenomenological model to determine the proportionality factor for the case of spherical particles diffusing in the continuum \mathbb{R}^3 and reacting immediately on contact ($\lambda = \infty$). His result takes the form $G_0(2, 2) = D 4\pi r^2$, where r denotes the particles' radius. We do not know of any phenomenological way to obtain the factor (6.21) for Lévy flights in a 'Smoluchowski fashion'. This emphasizes the power of NPRG.

The crux of property (P8) is that the limit $\mu \rightarrow 0$ enhances the particle's tendency to stir and subsequently, to wash out correlations. For $\mu = 0$, the probability for a jump of length $|\mathbf{x}|$ to happen decays as $p(\mathbf{x}) \propto |\mathbf{x}|^{-d}$ (compare eq. (3.13)). At the same time, the number of possible target sites at the distance $|\mathbf{x}|$ grows $\propto |\mathbf{x}|^d$. Consequently, the probability to jump to any lattice site becomes homogenous in the limit $\mu = 0$. In this sense, every lattice site is equally well connected to any other site and the lattice structure is lost. As a consequence, the dispersion function is flat $\epsilon(\mathbf{p}) = 1$ (this can also be seen algebraically, at least for $d = 1$). The macroscopic coupling (6.18) becomes

$$G_0(2, 2) = \left(\frac{1}{\lambda} + \tau \right)^{-1} \quad \text{for } \mu = 0. \quad (6.22)$$

The interpretation of (6.22) is straightforward: The microscopic reaction rate λ gives a typical time scale $1/\lambda$ for a reaction to take place. A second time scale is given by the mean time τ between two jumps of a particle. As the particles have to meet before a reaction can happen, both time scales have to be added. The reciprocal of this sum gives the new effective reaction rate $G_0(2, 2) = (1/\lambda + \tau)^{-1}$. The fact that particles are spatially separated and have to meet in order to react is neglected in the mean field approach. Only if the time between two jumps vanishes, $\tau = 0$, mean field is recovered.

(P9) is a refined version of property (P1). As a consequence of the monotonic dependence of $G_0(2, 2)$ on the microscopic rate λ and the Lévy exponent μ (see properties (P4) and (P5)), the maximum of $G_0(2, 2)$ is attained for $\mu = 0$ and $\lambda = \infty$. The claim follows by setting $\mu = 0$ and $\lambda = \infty$ in (6.22).

To prove the last property (P10), we use the fact that the main contribution to the integral $\int_{\mathbf{p}} \epsilon(\mathbf{p})^{-1}$ is given by the small momenta $a|\mathbf{p}| \leq \eta \ll 1$. Using (6.20) in (6.18) for $\lambda = \infty$, gives

$$\tau G_0(2, 2) = \left[\int_{\mathbf{p}} \epsilon(\mathbf{p})^{-1} \right]^{-1} \approx \left[\frac{V(S^{d-1})}{(2\pi)^d \tilde{D}_A} \frac{1}{d - \mu} \eta^{d-\mu} + \text{const} \right]^{-1}.$$

In the limit $\mu \rightarrow d$, we can approximate $\eta^{d-\mu} \rightarrow 1$ for fixed $\eta < 1$ and neglect the second term in the square bracket. This proves the power law $\tau G_0(2, 2) = \mathcal{A} \cdot (d - \mu)^1$ (6.19). In particular for $d = 1$ we have $\tilde{D}_A \xrightarrow{\mu \rightarrow 1} 3/\pi$ by (3.19) and get $\mathcal{A} = 3$. Figure 6.4 confirms this result by plotting the exact numerical data of $\tau G_0(2, 2)$ in $d = 1$.

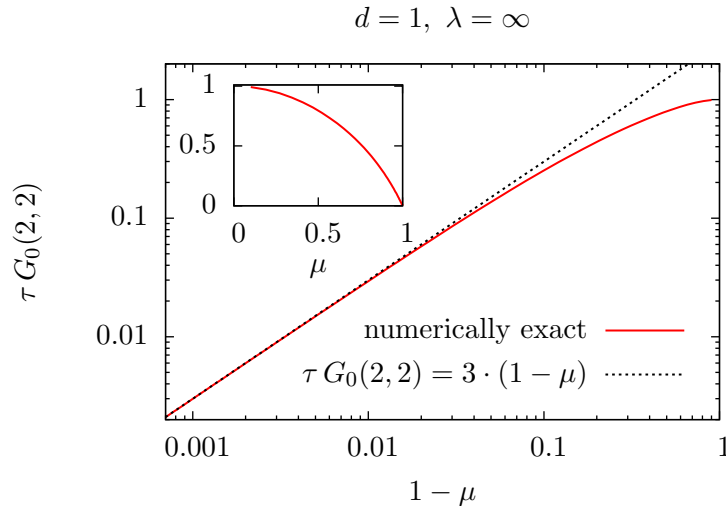


Figure 6.4: The macroscopic reaction rate $G_0(2, 2)$ is plotted against $(1 - \mu)$ for the microscopic rate $\lambda = \infty$ in one spatial dimension. The dotted black line represents the power law $G_0(2, 2) = 3 \cdot (1 - \mu)$ which is approached in the limit $\mu \rightarrow 1$ (see property (P10) and equation (6.19)). The red graph is obtained by using the expansion (3.18) of $\epsilon(p)$ in (6.18) and computing the integral numerically. The lack of an analogous expansion in two dimensions makes the integration numerically unfaithful for $d = 2$.

6.4 Analytic and non analytic corrections

In the previous section, the leading coupling $G_0(2, 2)$ of the macroscopic rate equation

$$\partial_t \rho(t) = -2 G_0(2, 2) \rho(t)^2 - \sum_{n \geq 3} G_0(1, n) \rho(t)^n \quad (6.23)$$

was computed by solving the flow equation (6.13) for the running coupling $G_k(2, 2)$ imposed by the Wetterich equation (6.11). The renormalization of the macroscopic reaction rate $G_0(2, 2)$ was discussed in the properties (P1) to (P10) (see also figure 6.3). As $\rho(t) \rightarrow 0$, the macroscopic rate equation can be replaced by the macroscopic law of mass action $\partial_t \rho(t) = -2 G_0(2, 2) \rho(t)^2$, as long as $d > d_c \equiv \mu$. In the present section, we go beyond this leading order and try to include the correction $\sum_{n \geq 3} G_0(1, n) \rho^n$.

The cascade of subordinate critical dimensions

Proceeding in the same way as for the $G_k(2, 2)$ coupling in section 6.3, the LPA Wetterich equation (6.11) induces coupled ODEs for higher coupling constants $G_k(n, m)$. The dependence among the couplings was derived by general topological arguments in section 5.3 (see figure 5.4). In the concrete case of the (1, 3) coupling, this means that the flow of $G_k(1, 3)$ depends on the (2, 2), (3, 3) and (2, 3) couplings. The coupled ODEs in the hierarchy up to the $G_k(1, 3)$ read explicitly

$$\begin{aligned} G_k(1, 2) &= 2 G_k(2, 2) \\ \partial_k G_k(2, 2) &= \tau^{-1} \mathcal{V}(k) \partial_k \epsilon_k \epsilon_k^{-2} \tau G_k(2, 2)^2 \\ \partial_k G_k(3, 3) &= \tau^{-1} \mathcal{V}(k) \partial_k \epsilon_k \left[-8 \epsilon_k^{-3} \tau G_k(2, 2)^3 + 6 \epsilon_k^{-2} \tau G_k(2, 2) \tau G_k(3, 3) \right] \end{aligned} \quad (6.24a)$$

$$\begin{aligned} \partial_k G_k(2, 3) &= \tau^{-1} \mathcal{V}(k) \partial_k \epsilon_k \left[-12 \epsilon_k^{-3} \tau G_k(1, 2) \tau G_k(2, 2)^2 \right. \\ &\quad \left. + 3 \epsilon_k^{-2} \tau G_k(1, 2) \tau G_k(3, 3) + 4 \epsilon_k^{-2} \tau G_k(2, 2) \tau G_k(2, 3) \right] \end{aligned} \quad (6.24b)$$

$$\begin{aligned} \partial_k G_k(1, 3) &= \tau^{-1} \mathcal{V}(k) \partial_k \epsilon_k \left[-4 \epsilon_k^{-3} \tau G_k(1, 2)^2 \tau G_k(2, 2) \right. \\ &\quad \left. + \epsilon_k^{-2} \tau G_k(1, 2) \tau G_k(2, 3) + 3 \epsilon_k^{-2} \tau G_k(1, 3) \tau G_k(2, 2) \right]. \end{aligned} \quad (6.24c)$$

This is too complicated to be exactly solved, but the structure is easy. An accessible way to extract the structure out of (6.24) is by Feynman diagrams (see chapter 5). To this end, the algebraic flow equations are translated into its pictorial representation by applying the following *Feynman rules*.

- The factor $\tau^{-1} \mathcal{V}(k) \partial_k \epsilon_k$, common to each flow equation, is represented by the one loop structure of each diagram. As in ordinary field theory, the loop originates from an integration in momentum space. The integration over the momentum \mathbf{p} hides in $\mathcal{V}(k)$, whereas the integration over ω is only indirectly given by ϵ_k/τ (the reason for this indirect appearance is the fact that the ω integration was already performed in eq. (5.6)). In addition, the derivative ∂_k is characteristic for the Wetterich approach. As in

(4.10), this derivative is usually indicated by a cross appearing in the diagrams. In the following, we do not draw the cross but understand the derivative ∂_k to be part of the loop.

- The coupling $G_k(n, m)$ appears as a vertex with m ingoing (right hand side) and n outgoing (left hand side) legs.
- Each factor ϵ_k^{-1} contributes one propagator, i.e. a line connecting two *different* vertices. The propagator can only connect an outgoing leg of one vertex to the ingoing leg of another vertex.
- The resulting diagram has to be irreducible. Consequently, all vertices lie on the loop.
- The numerical factors appear as the combinatorial number of ways to draw the diagram and to attach the term $\partial_k \epsilon_k$ to one of the propagators. We draw only one diagram representative for all possibilities.

The pictorial version of (6.24) is

$$\partial_k G_k(2, 2) = \text{Diagram 1} \quad (6.25a)$$

$$\partial_k G_k(3, 3) = \text{Diagram 2} + \text{Diagram 3} \quad (6.25a)$$

$$\partial_k G_k(2, 3) = \text{Diagram 4} + \text{Diagram 5} + \text{Diagram 6} \quad (6.25b)$$

$$\partial_k G_k(1, 3) = \text{Diagram 7} + \text{Diagram 8} + \text{Diagram 9} \quad (6.25c)$$

Compared to (6.24), the notation is crucially simplified. One essential property which is apparent in this graphical representation is the fact that the flow of $G_k(n, 3)$ depends solely linearly on the $(n, 3)$ vertex. In section 5.3, this feature was proven to hold for any coupling $G_k(n, m)$ except $G_k(2, 2)$ (see property (P7) on page 42). Hence, if all couplings prior to $G_k(n, m)$ in the vertex hierarchy are known, the flow equation of $G_k(n, m)$ is a linear, first order ODE.

A second advantage of the Feynman diagram notation is to organize the power counting of k in the flow $\partial_k G_k(n, m)$ as $k \rightarrow 0$. As described in the previous section, the reaction rate $G_0(2, 2)$ is finite for $d > d_c$. Hence, any $(2, 2)$ vertex scales as $\sim k^0$ in the limit $k \rightarrow 0$. An internal line of some Feynman diagram represents ϵ_k^{-1} and therefore, scales as $\sim k^{-\mu}$ (see eq (6.8)). Lastly, the one loop structure, encoding the term $\tau^{-1} \mathcal{V}(k) \partial_k \epsilon_k$, gives three contributions: **First** $\sim k^d$ from the momentum integration in $\mathcal{V}(k)$ (see equation (6.12)), **second** $\sim k^\mu$ from the ω integration and **third** $\sim k^{-1}$ from the derivative ∂_k . *Summa summarum*, a loop contributes $k^{d+\mu-1}$ as $k \rightarrow 0$. Using this scaling behavior, the flow equation (6.25a) is written as

$$\partial_k G_k(3, 3) \sim k^{d+\mu-1} k^{-3\mu} + k^{d+\mu-1} k^{-2\mu} \cdot G_k(3, 3) \quad (6.26)$$

in the macroscopic limit $k \rightarrow 0$ (constant factors are omitted). We are going to use a simple lemma about linear, first order, ordinary differential equations.

Lemma. *Let $f : (0, \epsilon] \rightarrow \mathbb{R}$ be the solution to the differential equation*

$$\partial_x f(x) = C_1 x^{\alpha_1 - 1} + C_2 x^{\alpha_2 - 1} + \dots + C_n x^{\alpha_n - 1} + C x^{\alpha - 1} \cdot f(x) \quad (6.27)$$

with the initial condition $f(\epsilon) = f_\epsilon \in \mathbb{R}$,

where $\alpha_i, \alpha, C_i, C \in \mathbb{R} \setminus \{0\}$, such that

$$\alpha_1 < \alpha_2 < \dots < \alpha_n < \alpha \quad \text{and} \quad \alpha > 0.$$

- If $\alpha_1 > 0$, $f(x)$ approaches the finite value $f(0)$ and behaves asymptotically as

$$f(x) \xrightarrow{x \rightarrow 0} x^0.$$

- If $\alpha_i < 0$ for some i , then $\alpha_1 < 0$ and $f(x)$ diverges in the limit $x \rightarrow 0$ as

$$f(x) \xrightarrow{x \rightarrow 0} x^{\alpha_1}.$$

This means, that the term $C_1 x^{\alpha_1 - 1}$ in (6.27) dominates the behavior of $f(x)$ as $x \rightarrow 0$.

- In the marginal case of $\alpha_1 = 0$, the divergence is logarithmic

$$f(x) \xrightarrow{x \rightarrow 0} \log(x).$$

Proof. The solution of (6.27) is given by the sum of the homogenous solution

$$f_h(x) = \tilde{C} \cdot \exp \left[\frac{C}{\alpha} x^\alpha \right]$$

and a particular solution of the non homogenous equation, given by

$$f_{nh} = - \exp \left[\frac{C}{\alpha} x^\alpha \right] \cdot \int_x^1 d\xi (C_1 \xi^{\alpha_1 - 1} + \dots + C_n \xi^{\alpha_n - 1}) \exp \left[-\frac{C}{\alpha} \xi^\alpha \right]. \quad (6.28)$$

The remaining free coefficient \tilde{C} is determined by matching the initial condition $f(x = \epsilon) = f_h(\epsilon) + f_{nh}(\epsilon) = f_\epsilon$. As $\alpha > 0$, the homogeneous part obeys $f_h(x) \xrightarrow{x \rightarrow 0} x^0$. Any deviation from x^0 has to come from the non homogenous contribution $f_{nh}(x)$. For $\alpha_1 > 0$, the integral in (6.28) remains finite, as the lower boundary x goes to $x \rightarrow 0$. For $\alpha_i < 0$, the term $C_1 \xi^{\alpha_1}$ dominates the asymptotic behavior of the integral and leads to $f_{nh}(x) \xrightarrow{x \rightarrow 0} x^{\alpha_1}$. Likewise, $f_{nh}(x) \xrightarrow{x \rightarrow 0} \log(x)$ is obtained for $\alpha_1 = 0$. \square

Applying the lemma to (6.26) gives

$$G_k(3, 3) \xrightarrow{k \rightarrow 0} \begin{cases} k^{d-2\mu}, & \text{for } \mu > d/2 \\ k^0, & \text{for } \mu < d/2. \end{cases}$$

Using this finding in the power counting of (6.25b), yields

$$\partial_k G_k(2, 3) \sim k^{d+\mu-1} k^{-3\mu} + k^{d+\mu-1} k^{-2\mu} \begin{cases} k^{d-2\mu}, & \mu > d/2 \\ k^0, & \mu < d/2 \end{cases} + k^{d+\mu-1} k^{-2\mu} \cdot G_k(2, 3)$$

Again, this is a linear, first order ODE and the lemma is applicable. It gives

$$G_k(2, 3) \xrightarrow{k \rightarrow 0} \begin{cases} k^{d-2\mu}, & \text{for } \mu > d/2 \\ k^0, & \text{for } \mu < d/2. \end{cases}$$

Analogous results hold for $G_k(1, 3)$. In summary, we extract the asymptotic behavior of the $G_k(*, 3)$ couplings in the macroscopic limit $k \rightarrow 0$ above the critical dimension $d > \mu$:

$$G_k(*, 3) \xrightarrow{k \rightarrow 0} \begin{cases} k^{d-2\mu} \rightarrow \infty, & \text{for } \mu > d/2 \\ k^0 \rightarrow \text{finite}, & \text{for } \mu < d/2 \end{cases} \quad (6.29)$$

(the asterisk stands for 1, 2 or 3). The drastic change in the behavior of $G_k(*, 3)$ from diverging to converging at $\mu = d/2$, is analogous to the change of $G_k(2, 2)$ at $\mu \equiv d_c = d$ (see eq. (6.17)). In this sense, $\mu = d/2$ is a critical Lévy flight exponent for the $G_k(*, 3)$ couplings. In other words, $d = 2\mu$ is a second, *subordinate critical dimension*. At the transition of this second critical dimension, the macroscopic rate equation keeps the form of the macroscopic law of mass action $\partial_t \rho(t) = -2 G_0(2, 2) \rho(t)^2$, as the leading coupling $G_0(2, 2)$ is not affected by the critical change of $G_k(*, 3)$. Hence, the effect of the second critical dimension can only be observed in the corrections to the law of mass action.

The following theorem generalizes (6.29) and gives rise to an infinite cascade of subordinate critical dimensions.

Theorem (see figure 6.5). *Above the critical dimension, i.e. for $d > \mu$, the coupling constant $G_k(n, m)$ scales as*

$$G_k(*, m) \xrightarrow{k \rightarrow 0} \begin{cases} k^{d-(m-1)\mu} \rightarrow \infty, & \text{for } \mu > d/(m-1) \\ \log(k) \rightarrow \infty, & \text{for } \mu = d/(m-1) \\ k^0 \rightarrow \text{finite}, & \text{for } \mu < d/(m-1) \end{cases} \quad \text{where } m \geq 3 \quad (6.30)$$

in the macroscopic limit $k \rightarrow 0$. The critical value $\mu = d/(m-1)$ separates the regime $G_0(n, m) = \text{finite}$ from $G_0(n, m) = \text{infinite}$.

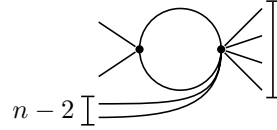
Proof. The proof is given by induction with respect to m . The base case $m = 3$ was proven in (6.29) above. Let us proceed with the inductive step.

The crucial observation is the fact, that the flow $\partial_k G_k(n, m)$ of any coupling constant $G_k(n, m)$ with $m \geq 3$ contains the following two important diagrams.

- Property (P8) on page 42 guarantees the existence of the diagram which contains only (1, 2) and (2, 2) vertices has m internal lines. In the limit $k \rightarrow 0$, this diagram gives a contribution $\sim k^{d+\mu-1} k^{-m\mu} = k^{d-(m-1)\mu-1}$ to the flow of $G_k(n, m)$:

$$\begin{array}{c} \text{Diagram: A circle with } n \text{ external lines on the left and } m-2 \text{ external lines on the right.} \\ \sim k^{d-(m-1)\mu-1}. \end{array} \quad (6.31)$$

- Property (P7) on page 42 guarantees the existence of the diagram which is proportional to $G_k(n, m)$. Besides the (n, m) coupling, the diagram can only contain one additional $(2, 2)$ vertex and has two internal lines. As $k \rightarrow 0$, this diagram contributes $\sim k^{d+\mu-1} k^{-2\mu} \cdot G_k(n, m) = k^{d-\mu-1} \cdot G_k(n, m)$ to the flow of $G_k(n, m)$:



$$\sim k^{d-\mu-1} \cdot G_k(n, m). \quad (6.32)$$

Usually, the flow of $G_k(n, m)$ consists of more than those two diagrams. The additional diagrams do not contain the (n, m) vertex and have strictly less than m internal lines. We write (omitting constant factors)

$$\partial_k G_k(n, m) \sim k^{d-(m-1)\mu-1} + \sum_i k^{\alpha_i-1} + k^{d-\mu-1} \cdot G_k(n, m) \quad (6.33)$$

where the first and the last term represent the diagrams (6.31) and (6.32). The intermediate sum $\sum_i k^{\alpha_i-1}$ accounts for the remaining diagrams. Although we do not know the exponents α_i exactly, we can estimate $\alpha_i > d - (m-1)\mu$. To prove this lower bound on α_i , we start with the diagram consisting of $(*, 2)$ vertices as a raw model for the i^{th} diagram. This prototype scales as $\sim k^{d+\mu-m\mu-1}$ (see eq. (6.31)). The i^{th} diagram is obtained from the prototype by contracting some of the $(*, 2)$ vertices to a $(*, l)$ vertex with $l \geq 3$. This contraction reduces the number of internal lines by $(l-2)$. As the vertex $(*, l)$ is prior to $(*, m)$ in the vertex hierarchy, we can use the induction hypothesis $G_k(*, l) \sim k^{d-(l-1)\mu}$ in the case $\mu < d/(l-1)$ (which is the worst case). Hence, any contraction adds at most a factor $k^{(l-2)\mu+d-(l-1)\mu} = k^{d-\mu}$ to the prototype. For $d > \mu$ this gives $\alpha_i \geq d - (m-1)\mu + d - \mu > d - (m-1)\mu$. This lower bound on the α_i allows to apply the lemma on page 59 to (6.33). The claim (6.30) follows. \square

The exponent of the first non analytic correction

Let us use the knowledge about the couplings $G_k(*, m)$ condensed in the theorem of the previous paragraph to calculate the first correction to the law of mass action. The deviation from the law of mass action is given by the sum

$$\sum_{n \geq 3} G_0(1, n) \rho(t)^n \quad (6.34)$$

(see eq. (6.23)). The theorem (6.30) states, that most of the couplings $G_0(1, n)$, $n \geq 3$ are infinite. Nevertheless, the sum (6.34) still converges to a finite, meaningful result¹. A simple way to extract meaningful and *finite* results out of (6.34) is by using a scaling argument. We split the sum (6.34) into $n \leq \lfloor 1 + d/\mu \rfloor$ for which $G_0(1, n) = \text{finite}$ and use $G_k(1, n) \sim$

¹Consider $\exp(-1/k) = \sum_{n=0}^{\infty} (-k)^{-n}/n!$ as a simple toy example. Even though each individual summand diverges in the limit $k \rightarrow 0$, the divergences cancel in the sum.

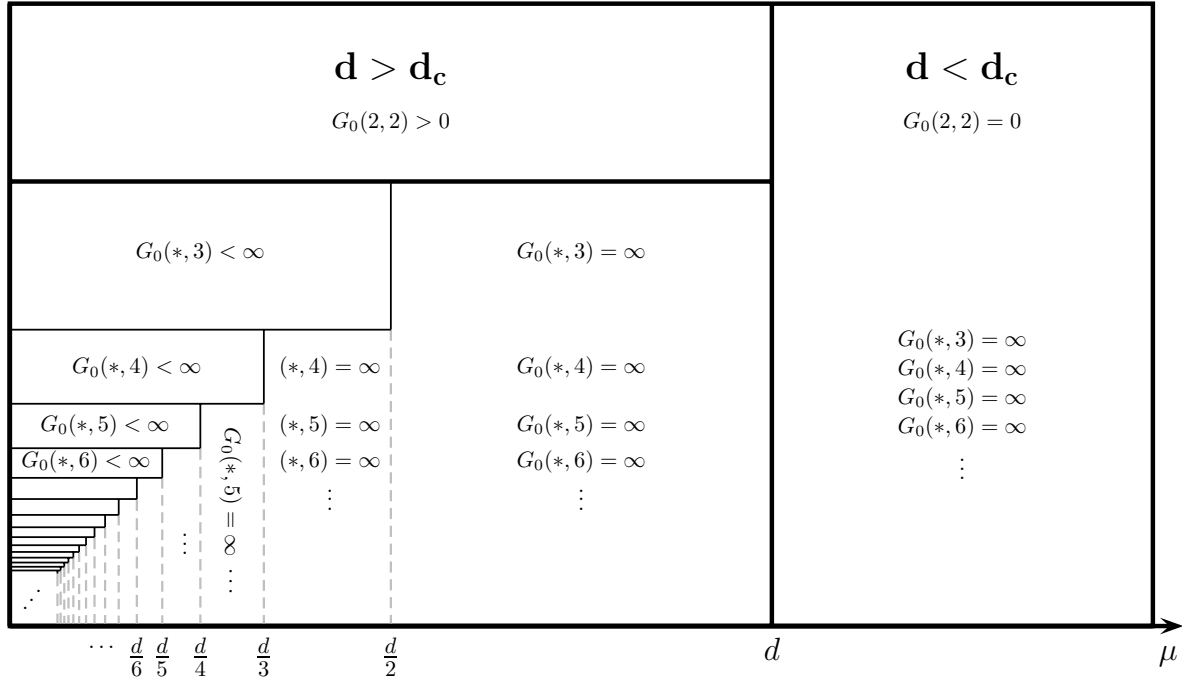


Figure 6.5: Schematic diagram of the critical dimension $d_c = \mu$ (6.17) and the cascade of subordinate critical dimensions at $\mu = d/2, d/3, \dots$ (6.30). The critical dimension $d_c = \mu$ separates regime of $G_0(2,2) > 0$ ($\mu < d$) from the regime where $G_0(2,2) = 0$ ($\mu > d$). The significant consequence of $G_0(2,2) = 0$ is the breakdown of the law of mass action (see chapter 7). The critical value $\mu = d/n$ ($n = 2, 3, \dots$) separates the regime of $G_0(*, n+1) < \infty$ from $G_0(*, n+1) = \infty$ (see equation 6.30). The change in $G_0(n+1)$ at $\mu = d/n$ is not relevant enough to change the leading term in the macroscopic rate equation. However, the critical character of $\mu = d/n$ is visible in the corrections to the law of mass action.

In general, nontrivial values for the macroscopic couplings $G_0(n, m)$ encode some coarse grained, non universal information about the microscopic model at $k = \Lambda$. For $\mu > d$ all couplings $G_0(n, m)$ are trivial. Consequently, the microscopic details of the model (such as reaction rate λ or lattice structure) are lost (see chapter 7). Contrary, for $\mu < d$, the macroscopic reaction rate $G_0(2,2)$ survives the limit $k \rightarrow 0$ and carries information about the microscopic reaction rate λ or the lattice structure to the coarse grained macroscopic scale. The lower the Lévy exponent μ , the more couplings $G_0(n, m)$ will take finite values and encode (different) coarse grained aspects of the microscopic theory.

$k^{d-(n-1)\mu}$ for $n > [1 + d/\mu]$ (here $[x]$ denotes the largest integer smaller than x):

$$\begin{aligned} \sum_{n \geq 3} G_k(1, n) \rho(t)^n &\xrightarrow{k \rightarrow 0} \sum_{\substack{n \geq 3 \\ n \leq [1+d/\mu]}} G_k(1, n) \rho(t)^n + \sum_{\substack{n \geq 3 \\ n > [1+d/\mu]}} G_k(1, n) \rho(t)^n \\ &\sim \sum_{\substack{n \geq 3 \\ n \leq [1+d/\mu]}} \rho(t)^n + k^{d+\mu} \cdot \underbrace{\sum_{\substack{n \geq 3 \\ n > [1+d/\mu]}} \left(\frac{\rho(t)}{k^\mu}\right)^n}_{\equiv f(k^{-\mu}\rho(t))}. \end{aligned}$$

We interpret the last sum as a unknown function f of $k^{-\mu}\rho$. Demanding a nontrivial, macroscopic limit $k \rightarrow 0$ of $k^{d+\mu} \cdot f(k^{-\mu}\rho)$, enforces $f(k^{-\mu}\rho) \sim \rho^{1+d/\mu}$. Using this finding in (6.23), yields

$$\partial_t \rho(t) = \underbrace{-2 G_0(2, 2) \rho(t)^2}_{\text{law of mass action}} - \underbrace{\sum_{\substack{n \geq 3 \\ n \leq [1+d/\mu]}} \underbrace{G_0(1, n) \rho(t)^n}_{\text{analytic}} - \underbrace{\mathcal{A} \rho(t)^{1+d/\mu}}_{\text{non analytic}} - \dots}_{\text{corrections}}. \quad (6.35)$$

Let us discuss this result.

- The correction to the law of mass action term consists of an analytic part and a non analytic part. The number of analytic correction terms depends on the Lévy exponent μ . Whenever μ drops below the critical value d/n , a new analytic correction $G_0(1, n + 1) \rho^{n+1}$ is frozen out.
- The exponent $1 + d/\mu$ of the non analytic correction is always greater than the largest exponent $[1 + d/\mu]$ of the analytic corrections.
- Non analytic terms can only be created in the renormalization group flow as $k \rightarrow 0$, i.e. in the macroscopic limit. We will see how this is linked to universality.
- For $\mu > d/2$, the analytic corrections in (6.35) are absent and the non analytic term is the leading correction

$$\partial_t \rho(t) = \underbrace{-2 G_0(2, 2) \rho(t)^2}_{\text{law of mass action}} - \underbrace{\mathcal{A} \rho(t)^{1+d/\mu}}_{\text{corrections}} - \dots, \quad (6.36)$$

where $2 < 1 + d/\mu < 3$.

The amplitude of the first correction

We compute the amplitude \mathcal{A} of the correction term

$$\mathcal{A} \rho(t)^{1+d/\mu} \quad (6.37)$$

in (6.35). For the sake of simplicity, let us assume that $d/2 < \mu < d$, so that the rate equation takes the form of (6.36). As described in the previous paragraph, the correction (6.37) is obtained by approximating the flow

$$\partial_k G_k(1, n) \xrightarrow{k \rightarrow 0} \approx \text{diagram}$$

by the diagram which contains only $(*, 2)$ vertices. The approximation is justified, as it gives the dominating contribution for $k \rightarrow 0$ (see the lemma on page 59). The fact that the $(*, 2)$ vertices give the essential contribution to the correction $\sim \rho^{1+d/\mu}$, motivates to approximate the local potential by

$$U_k(\bar{\Psi}, \Psi) = G_k(2, 2) \bar{\Psi}^2 \Psi^2 + 2 G_k(2, 2) \bar{\Psi} \Psi^2. \quad (6.38)$$

This is a crude approximation in the sense, that all Feynman diagrams are now forced to be build out of $(*, 2)$ vertices *only*. Nevertheless, those Feynman diagrams are sufficient to generate the correction term $\mathcal{A} \rho^{1+d/\mu}$ *exactly*.

Using the ansatz (6.38) in the Wetterich equation (6.11) leads to

$$\begin{aligned} \partial_k U_k^{(1,0)}(\bar{\Psi} = 0, \Psi) &= \frac{2}{\tau} \mathcal{V}(k) \partial_k \epsilon_k \frac{(\tau G_k(2, 2))^2 \Psi^2}{[\epsilon_k + 4 \tau G_k(2, 2) \Psi]^2} \\ &\xrightarrow{k \rightarrow 0} \frac{2a}{\tau} \frac{V(B^d(1))}{(2\pi)^d} \mu \tilde{D}_A (ak)^{d+\mu-1} \frac{(\tau G_0(2, 2))^2 \Psi^2}{[\tilde{D}_A (ak)^\mu + 4 \tau G_0(2, 2) \Psi]^2} \end{aligned} \quad (6.39)$$

(the definition of ϵ_k (6.8) and the asymptotic behavior of $\mathcal{V}(k)$ (6.12) was used in the last line). Since the correction (6.37) is created at $k \rightarrow 0$, it is sufficient to start the integration of (6.39) at some arbitrary small \tilde{k}

$$U_0^{(1,0)}(0, \Psi) = U_{\tilde{k}}^{(1,0)} - \frac{2}{\tau} \frac{V(B^d(1))}{(2\pi)^d} \mu \tilde{D}_A \int_0^{\tilde{k}} d(ak) (ak)^{d+\mu-1} \frac{(\tau G_0(2, 2))^2 \Psi^2}{[\tilde{D}_A (ak)^\mu + 4 \tau G_0(2, 2) \Psi]^2}.$$

The correction term (6.37) is created in the integral of the right hand side. We extract the correction $\mathcal{A} \rho^{1+d/\mu}$ with the help of a computer algebra system and determined the amplitude to be

$$\mathcal{A} = -\frac{2^{-3}}{\tau} \frac{V(B^d(1))}{(2\pi)^d} \frac{d}{d+\mu} \Gamma(2+d/\mu) \Gamma(-d/\mu) \tilde{D}_A c^{1+d/\mu} \quad (6.40)$$

(where c is given by $c = 4 \tau G_0(2, 2) / \tilde{D}_A$). Two important properties of (6.40) are:

- The only dependence of \mathcal{A} on the microscopic model at $k = \Lambda$ is indirect through the macroscopic coupling $\tau G_0(2, 2)$. In other words, \mathcal{A} is a *universal function* of $G_0(2, 2)$. This crucial feature is a direct consequence of two things: **Firstly**, the non analytic correction (6.37) are created at $k = 0$. This leads to universality in the sense that non analytic terms can only depend on the microscopic model indirectly through the renormalization flow as $k \rightarrow 0$. **Secondly**, the Feynman diagrams, which substantially contribute to the correction $\mathcal{A} \rho^{1+d/\mu}$, consist of $(*, 2)$ vertices only. Since $G_k(*, 2)$ takes the finite value $G_0(*, 2)$ for $k \rightarrow 0$, \mathcal{A} depends universally on $G_0(2, 2)$. In this way, non analytic terms are related to universality. Schematically,

$$\mathcal{A} \xleftarrow{(6.40)} \left\{ \begin{array}{l} \text{macroscopic data} \\ d, \mu \\ \tau G_0(2, 2) \end{array} \right. \xleftarrow{(6.18)} \left\{ \begin{array}{l} \text{microscopic details} \\ d, \mu \\ \lambda \\ \tau \\ \epsilon(\mathbf{p}) \end{array} \right.$$

shows, how the amplitude \mathcal{A} depends on the microscopic details only through the real numbers $\tau G_0(2, 2)$ and μ .

- The gamma function $\Gamma(-d/\mu)$ in (6.40) leads to divergences of \mathcal{A} at $\mu = d/n$ for every $n \in \mathbb{N}$, $n \geq 2$ (see figure 6.6). The divergences are explained by the following observation: At $\mu = d/n$ the exponent of $\mathcal{A} \rho^{1+d/\mu}$ becomes the integer $(n+1) \geq 3$ and the non analyticity is lost. Consequently, the amplitude \mathcal{A} has to incorporate also non universal contributions for $\mu = d/n$. The divergence of \mathcal{A} at $\mu = d/n$ is an artifact of the fact that these non universal contributions are neglected in the derivation of (6.40).

Metaphorically speaking, the divergences of the amplitude \mathcal{A} at $\mu = d/n$ is the formalism's way to warn about the loss of universality which is linked to the loss of non analyticity.

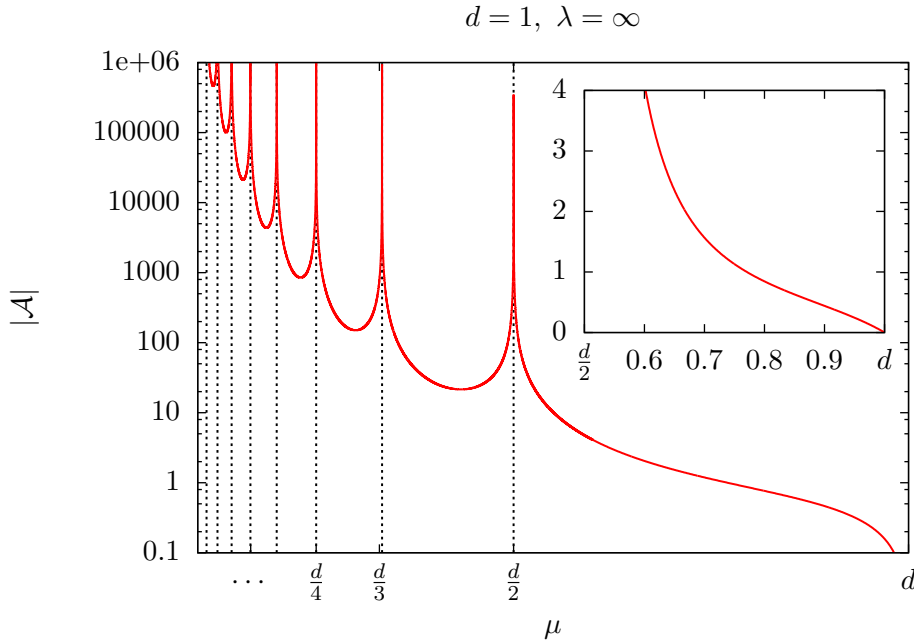


Figure 6.6: The corrections to the law of mass action are given in (6.35). This plot focuses on the non analytic correction term $\mathcal{A} \rho^{1+d/\mu}$. The modulus of the amplitude $|\mathcal{A}|$ (6.40) is plotted against the Lévy flight exponent μ for the microscopic reaction rate $\lambda = \infty$ in $d = 1$ dimensions. The divergences at $\mu = d/n$ with $n \in \mathbb{N}$, $n \geq 2$, mathematically originate from the poles of the gamma function $\Gamma(-d/\mu)$ in (6.40). The physical interpretation is the loss of universality of \mathcal{A} at $\mu = d/n$ (see the discussion after eq. (6.40)). Note that the divergences occur at the critical values $\mu = d/n$ where the non universal couplings $G_0(1, n+1)$ attain finite values (compare figure 6.5).

6.5 Further non analytic corrections

The non analytic correction $\mathcal{A}\rho^{1+d/\mu}$ was discussed in the previous section. $\mathcal{A}\rho^{1+d/\mu}$ originates from the flow given by Feynman diagrams consisting only of $(*, 2)$ vertices, where each vertex is treated as $G_0(*, 2)$. Mathematically, this corresponds to using

$$U_k(\bar{\Psi}, \Psi) = G_0(2, 2) \bar{\Psi}^2 \Psi^2 + 2 G_0(2, 2) \bar{\Psi}^2 \Psi^2 \quad (6.41)$$

as an ansatz in the Wetterich equation (6.11). The flow of the macroscopic reaction rate $G_0(2, 2)$ is ignored completely in this approach. In the following, we will refine the ansatz (6.41) in the sense that we include the k -dependence of $G_k(*, 2)$ for small k . This will lead to further non analytic corrections which give important contributions close to the critical dimension.

The flow of the (2,2) vertex revisited

The solution to the flow equation (6.13) of $G_k(2, 2)$ is given by (6.14)

$$G_k(2, 2) = \left[\frac{1}{\lambda} + \tau \int_k^\Lambda dk' \mathcal{V}(k') \partial_{k'} \left(-\frac{1}{\epsilon_{k'}} \right) \right]^{-1} \quad (6.42)$$

The flow of $G_k(2, 2)$ is separated into three regimes (in section 6.3, the distinction between ② and ③ was omitted).

- ① $k > k^*$: The flow of $G_k(2, 2)$ is driven by fluctuations with momenta in the whole Brillouin zone. The boundary k^* is defined by (6.9) such that $\mathcal{V}(k) = 1$ for $k > k^*$. Using $\mathcal{V}(k) = 1$ in (6.42), gives

$$G_k(2, 2) = \left[\frac{1}{\lambda} + \frac{\tau}{\epsilon_k} \right]^{-1} = \left[\frac{1}{\lambda} + \tau \tilde{D}_A^{-1} (ak)^{-\mu} \right]^{-1} \quad \text{for } k > k^* \quad (6.43)$$

- ② $\tilde{k} < k < k^*$: The onsite fluctuations are completely included into $G_k(2, 2)$ and consequently, some short scale details of the lattice no longer contribute to $G_k(2, 2)$. However, the lattice structure has still significant influence on $G_k(2, 2)$ and cannot be replaced by a continuum. Characteristic for this intermediate scale is the fact that the low energy modes ($\epsilon(\mathbf{p}) < \epsilon_k$) are treated different to the high energy modes ($\epsilon(\mathbf{p}) > \epsilon_k$):

$$G_k(2, 2) = \left[\frac{1}{\lambda} + \tau \int_{\mathbf{p}} \left(\frac{\Theta(\epsilon_k - \epsilon(\mathbf{p}))}{\epsilon_k} + \frac{\Theta(\epsilon(\mathbf{p}) - \epsilon_k)}{\epsilon(\mathbf{p})} \right) \right]^{-1}.$$

This equation is actually valid for all $0 \leq k \leq \Lambda$. For $k > k^*$, (6.43) is recovered and $k = 0$ yields (6.15).

- ③ $k < \tilde{k}$: The short range fluctuations are integrated out. The remaining long range fluctuations are not affected by the lattice and the flow behaves as in a continuum

model. In contrast to k^* , the boundary \tilde{k} is not sharp. The boundary \tilde{k} is chosen such that the estimate $\mathcal{V}(k) \approx V(B^d(1))/(2\pi)^d (ak)^d$ (6.12) is valid for $k < \tilde{k}$. Thus,

$$\begin{aligned} G_k(2,2) &= \left[\frac{1}{G_{\tilde{k}}(2,2)} + \tau \int_k^{\tilde{k}} dk' \frac{V(B^d(1))}{(2\pi)^d} (ak')^d \partial_{k'} \left(-\frac{1}{\epsilon_{k'}} \right) \right]^{-1} \\ &= G_{\tilde{k}}(2,2) \cdot \left[1 + \tau G_{\tilde{k}} \frac{V(B^d(1))}{(2\pi)^d} \frac{1}{\tilde{D}_A} \frac{\mu}{d-\mu} \cdot \left((a\tilde{k})^{d-\mu} - (ak)^{d-\mu} \right) \right]^{-1}. \end{aligned}$$

Expanding in $(ak)^{d-\mu}$ and matching the term $\propto (ak)^0$ with $G_0(2,2)$, gives a condition which can be solved for the intermediate coupling $G_{\tilde{k}}(2,2)$. We arrive at

$$\boxed{G_k(2,2) = \left[\frac{1}{G_0(2,2)} - \tau \frac{\mu}{d-\mu} \frac{\mathcal{V}(k)}{\epsilon_k} \right]^{-1} \quad \text{for } k < \tilde{k}}. \quad (6.44)$$

The similarity to (6.43) is charming. Expanding (6.44) in powers of $(ak)^{d-\mu}$, yields

$$\begin{aligned} G_k(2,2) &= G_0(2,2) \sum_{n=0}^{\infty} \left[\mathcal{C} (ak)^{d-\mu} \right]^n \quad \text{for } k < \tilde{k}, \\ \text{where } \mathcal{C} &\equiv \frac{\mu}{d-\mu} \frac{V(B^d(1))}{(2\pi)^d} \frac{\tau G_0(2,2)}{\tilde{D}_A}. \end{aligned} \quad (6.45)$$

Figure 6.7 demonstrates the validity of formula (6.44).

Non analytic corrections induced by the flow of $G_k(2,2)$

Using the ansatz $U_k = G_k(2,2) \bar{\Psi}^2 \Psi^2 + 2 G_k(2,2) \bar{\Psi}^2 \Psi^2$ in the Wetterich flow equation (6.11), leads to

$$\partial_k U_k^{(1,0)}(\bar{\Psi} = 0, \Psi) = \frac{2}{\tau} \mathcal{V}(k) \partial_k \epsilon_k \frac{(\tau G_k(2,2))^2 \Psi^2}{[\epsilon_k + 4 \tau G_k(2,2) \Psi]^2}.$$

The idea is to use the macroscopic approximation (6.44) of the flow of $G_k(2,2)$ to generate non analytic corrections in the course of integrating

$$U_0^{(1,0)}(0, \Psi) = U_{\tilde{k}}^{(1,0)}(0, \Psi) - \frac{2}{\tau} \int_0^{\tilde{k}} dk \mathcal{V}(k) \partial_k \epsilon_k \frac{(\tau G_k(2,2))^2 \Psi^2}{[\epsilon_k + 4 \tau G_k(2,2) \Psi]^2}.$$

The first non analytic correction reads $\mathcal{A} \rho^{1+d/\mu}$ and is obtained by setting $G_k(2,2) = G_0(2,2)$ in the last equation (see section 6.4). Using (6.13), the above integral is rewritten as

$$-2 \int_0^{\tilde{k}} dk \partial_k G_k(2,2) \frac{\Psi^2}{[1 + 4 \tau G_k(2,2)/\epsilon_k \Psi]^2}. \quad (6.46)$$

It is tempting to use the expansion (6.45) of $G_k(2,2)$ in (6.46) to get more non analytic corrections. However, there is a crucial caveat to this strategy: If the denominator of the

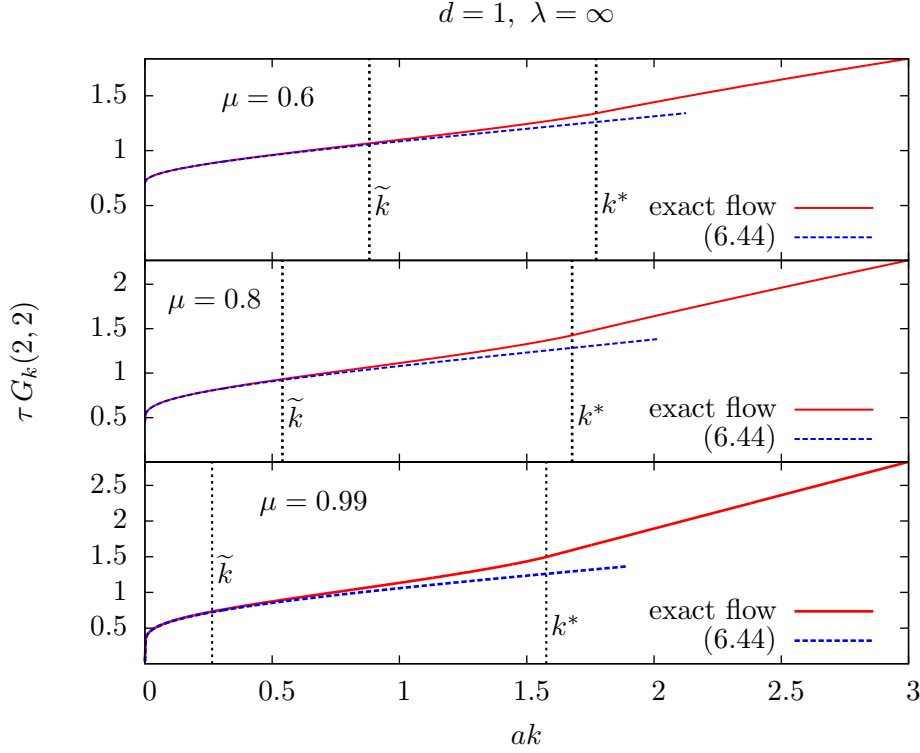


Figure 6.7: The flow of $G_k(2, 2)$ is plotted against $0 \leq k < 3$ in $d = 1$ with the initial rate $G_\Lambda(2, 2) = \lambda = \infty$ for different μ . The two vertical dotted lines at k^* and \tilde{k} separate three regions: **First**, $k > k^*$: the whole Brillouin zone contributes to the flow, **second**, $\tilde{k} < k < k^*$: short range fluctuations are integrated out, but the lattice still affects the flow, and **third**, $k < \tilde{k}$: the lattice is blurred and the continuum becomes a good approximation. While k^* is exactly defined by (6.9), the definition of \tilde{k} is fuzzy. In the plot, we choose \tilde{k} to be the scale, at which the relative error of (6.44) compared to exact value of $G_k(2, 2)$ becomes larger than 1%. It is shown that \tilde{k} decreases as μ increases. Nevertheless, even for values of μ very close to $d = 1$ the approximation (6.44) applies on a notable domain $0 \leq k < \tilde{k}$ (see the plot on the bottom). The fact that the approximation (6.44) does not hold for all $0 < k < \Lambda$, marks the breakdown of scale invariance due to the lattice.

integrand (6.46) contains terms with different powers of k , the scaling argument which leads to non analytic power law corrections, is not applicable. Let us demonstrate this by using $G_k(2, 2) \approx G_0(2, 2) + G_0(2, 2) C (ak)^{d-\mu}$ in the denominator of (6.46). Schematically (i.e. by omitting constant factors), the integral in (6.46) becomes ($c = 4 \tau G_0(2, 2) / \tilde{D}_A$)

$$\begin{aligned}
& \int_0^{\tilde{k}} d(ak) (ak)^{d-\mu-1} \frac{\Psi^2}{[1 + c \Psi (ak)^{-\mu} + c \Psi (ak)^{d-2\mu}]^2} \\
&= \int_0^1 dz (a\tilde{k})^{d-\mu} z^{d-\mu-1} \frac{\Psi^2}{[1 + c \Psi (a\tilde{k})^{-\mu} z^{-\mu} + c \Psi (a\tilde{k})^{d-2\mu} z^{d-2\mu}]^2} \\
&= \Psi^2 (a\tilde{k})^{d-\mu} F(c \Psi (a\tilde{k})^{-\mu}, c \Psi (a\tilde{k})^{d-2\mu}),
\end{aligned}$$

where $F(x, y) = \int_0^1 dz z^{d-\mu-1} [1 + x z^{-\mu} + y z^{d-2\mu}]^{-2}$. Non analytic corrections are independent of \tilde{k} . There is no unique way to obtain this independence by conjecturing the scaling form $F(x, y) \sim x^{\alpha_x} y^{\alpha_y}$. This makes it impossible to extract universal power law terms.

The conclusion is: In order to guarantee that the non analytic corrections created in the integral of (6.46) are of the form of a power law $\mathcal{A}_\alpha \rho^\alpha$ with some non integer exponent α , we have to replace $G_k(2, 2)$ in the denominator of the integrand (6.46) by $G_0(2, 2)$. Hence, we compute

$$\begin{aligned} & -2 \int_0^{\tilde{k}} dk \partial_k G_k(2, 2) \frac{\Psi^2}{[1 + 4\tau G_0(2, 2)/\epsilon_k \Psi]^2} \\ & \stackrel{(6.45)}{=} -2 G_0(2, 2) \sum_{n=1} n(d-\mu) C^n \int_0^{\tilde{k}} d(ak) (ak)^{n(d-\mu)-1} \frac{\Psi^2}{[1 + c(ak)^{-\mu} \Psi]^2}. \end{aligned}$$

The non analytic power law terms, being independent of \tilde{k} , are extracted with the help of a computer algebra system:

$$\sum_{n=1} \mathcal{A}_n \Psi^{n\left(\frac{d}{\mu}-1\right)+2}, \quad (6.47)$$

where the amplitudes \mathcal{A}_n are given by:

$$\mathcal{A}_n \equiv -2 G_0(2, 2) \frac{n\left(\frac{d}{\mu}-1\right)}{n\left(\frac{d}{\mu}-1\right)+2} C^n c^{n(d/\mu-1)} \cdot \Gamma\left[3+n\left(\frac{d}{\mu}-1\right)\right] \Gamma\left[-n\left(\frac{d}{\mu}-1\right)\right], \quad (6.48)$$

$$\text{with } C \equiv \frac{\mu}{d-\mu} \frac{V(B^d(1))}{(2\pi)^d} \frac{\tau G_0(2,2)}{\bar{D}_A} \quad \text{and} \quad c \equiv \frac{4\tau G_0(2,2)}{\bar{D}_A}.$$

The non analytic corrections (6.47) are added to the macroscopic reaction rate (6.35):

$$\partial_t \rho(t) = \underbrace{-2 G_0(2, 2) \rho(t)^2}_{\text{law of mass action}} - \underbrace{\sum_{\substack{n \geq 3 \\ n \leq [1+d/\mu]}} \underbrace{G_0(1, n) \rho(t)^n}_{\text{analytic}} - \sum_{n=1} \underbrace{\mathcal{A}_n \rho(t)^{n\left(\frac{d}{\mu}-1\right)+2}}_{\text{non analytic}}}_{\text{corrections}} - \dots \quad (6.49)$$

Some properties of \mathcal{A}_n are listed.

- *Formally*, performing the limit $n \rightarrow 0$ in (6.48), yields $\mathcal{A}_0 = 2 G_0(2, 2)$ and gives the law of mass action term $\mathcal{A}_0 \rho^2$.
- For $n = 1$, the power law $\mathcal{A} \rho^{1+d/\mu}$ is recovered (see eq. (6.40) and its discussion).
- The amplitudes \mathcal{A}_n are *universal* functions of $G_0(2, 2)$. This is a consequence of the fact that the non analytic corrections are created by Feynman diagrams build out of $(*, 2)$ vertices as $k \rightarrow 0$.
- The amplitude \mathcal{A}_n diverges at $\mu = dn/(m+n)$, $m \in \mathbb{N}$ due to the gamma function $\Gamma(-n(d/\mu-1))$ (see figure 6.8). The reason for the divergence of \mathcal{A}_n at $\mu = dn/(m+n)$ is that the exponent of the correction term becomes the integer $(m+2)$. The loss of non analyticity is linked to the loss of universality and hence, the derivation of (6.48) becomes incorrect. The divergences are an artifact of this instance (see also the discussion after eq. (6.40)).

- As $\mu \rightarrow d$, the exponent of the n^{th} correction, $n(d/\mu - 1) + 2 \approx 2$ (for n not too large), becomes comparable to the exponent of the law of mass action. Hence, close to the critical dimension ($\mu \rightarrow d$), we expect the non analytic terms (6.47) to give significant corrections to the law of mass action. This is an indication for the breakdown of the law of mass action below the critical dimension $d < \mu$ (see chapter 7).
- For $\mu \rightarrow d$ all amplitudes $\mathcal{A}_n \rightarrow 0$ (see figure 6.8). This decrease is compensated by the fact, that many correction terms with similar exponents add up coherently.

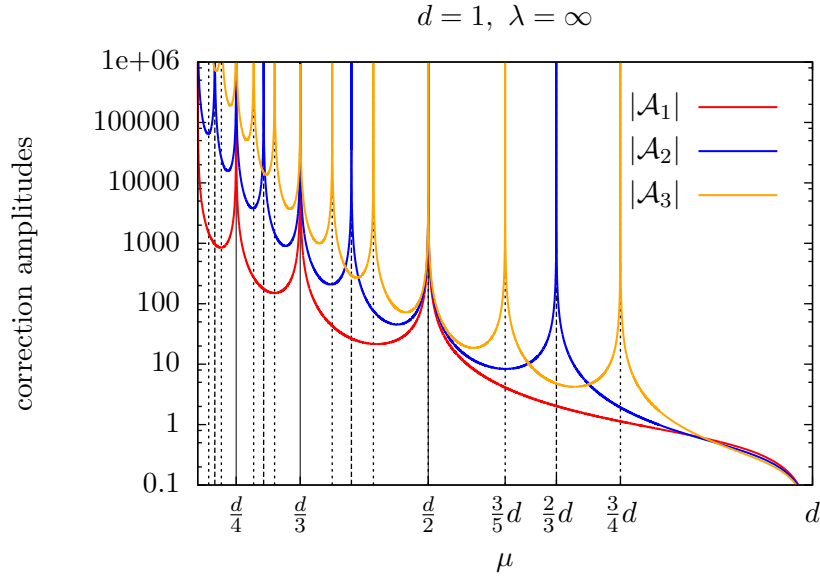


Figure 6.8: The first three amplitudes \mathcal{A}_1 to \mathcal{A}_3 of (6.47) are plotted against μ (compare the plot of figure 6.6). The divergences of \mathcal{A}_n occur at the values μ , where the corresponding exponent $n(d/\mu - 1) + 2$ becomes an integer and the non analyticity is lost.

On the validity of the amplitudes \mathcal{A}_n

As the corrections (6.47) are expected to be important for $\mu \rightarrow d$, we assume $\mu > d/2$. By the theorem on page 60, the macroscopic behavior of $G_k(1, n)$ is given by

$$\partial_k G_k(1, n) \stackrel{k \rightarrow 0}{\approx} \text{diagram} \implies G_k(1, n) \stackrel{k \rightarrow 0}{\approx} \left(\frac{G_0(*, 2)}{D_A} \right)^n k^{d - (n-1)\mu}. \quad (6.50)$$

The diagram is a circle with a vertex on the left and $n-2$ vertices on the right. A vertical bracket on the right side of the circle is labeled $n-2$.

There are two ways to go beyond this approximation.

A The flow of the $(*, 2)$ vertices is included into the analysis, i.e. $G_0(*, 2)$ is replaced by $G_k(*, 2)$.

B More diagrams with other vertices than the $(*, 2)$ vertices are considered.

In the last paragraph, we followed the first prescription **A** by using the expression

$$G_k(2, 2) \approx G_0 \left[1 + \mathcal{C} (ak)^{d-\mu} + \dots \right] \quad (6.51)$$

(compare eq. (6.44)). Let us have a look at the second possibility **B** and argue why it gives only a minor contribution for $\mu \rightarrow d$. Adding a diagram with one $(*, 3)$ vertex to the flow of $G_k(1, n)$, yields

$$\partial_k G_k(1, n) \stackrel{k \rightarrow 0}{\approx} \underbrace{\text{Diagram (1)}}_{\textcircled{1}} + \underbrace{\text{Diagram (2)}}_{\textcircled{2}} + \dots$$

The second diagram is obtained from the first diagram by contracting two $(1, 2)$ vertices to one $(1, 3)$ vertex and thereby reducing the number of internal lines by one. Approximating $G_k(1, 3) \sim G_0(2, 2)^3 k^{d-2\mu}$ (6.50) in the diagram $\textcircled{2}$ shows that the difference between the diagrams $\textcircled{1}$ and $\textcircled{2}$ scales as

$$\frac{\textcircled{2}}{\textcircled{1}} \sim \frac{G_0(2, 2)^3 k^{d-2\mu}}{G_0(2, 2)^2 \epsilon_k^{-1}} = \frac{G_0(2, 2)}{\tilde{D}_A} k^{d-\mu}.$$

Hence,

$$G_k(1, n) \sim \left(\frac{G_0(2, 2)}{\tilde{D}_A} \right)^n k^{d-(n-1)\mu} \left[1 + \frac{G_0(2, 2)}{\tilde{D}_A} k^{d-\mu} + \dots \right]. \quad (6.52)$$

This is the analog of (6.51) of the approach **B**. The fact that the corrections in (6.51) and (6.52) both scale as $\sim k^{d-\mu}$ shows that approach **A** and **B** lead to the same non analytic corrections². This challenges the calculation of \mathcal{A}_n in (6.48), which relies solely on the prescription **A** and ignores the corrections of the type **B**. Nevertheless, the result (6.48) remains valid in the limit $\mu \rightarrow d$, where $G_0(2, 2) \xrightarrow{\mu \rightarrow d} \infty$ ($d - \mu$) (see property (P10) on page 53). Accordingly, the prefactor $G_0(2, 2)/\tilde{D}_A$ of the correction in (6.52) becomes arbitrarily small, whereas the prefactor \mathcal{C} in (6.51) remains of order $\mathcal{O}(1)$ in the limit $\mu \rightarrow d$.

6.6 Comparison with simulations

In 1976, Daniel Gillespie proposed an exact method to simulate stochastic processes defined by a master equation on a computational device [67]. We apply the Gillespie algorithm to

²This can be verified explicitly by a scaling argument

$$\sum_n G_k(1, n) \Psi^n \stackrel{(6.52)}{\sim} \underbrace{k^{d+\mu} \sum_n \frac{\Psi^n}{k^\mu}}_{\sim \Psi^{1+d/\mu}} + \underbrace{k^{2d} \sum_n \frac{\Psi^n}{k^\mu}}_{\sim \Psi^{2d/\mu}}.$$

Therefore, the correction term in (6.52) also contributes to the amplitude \mathcal{A}_2 (6.47).

the process



The role of the particle input \bar{J} (6.53c) is twofold.

- For vanishing particle input $\bar{J} = 0$, any initial particle configuration reaches the absorbing state of zero particle density $\rho = 0$. To guarantee that correlations build up *before* the absorbing state is obtained, the simulations have to start with a huge initial particle number on a large lattice. Hence, a lot of computational effort and memory is required for the simulations. A positive particle input $\bar{J} > 0$ has the consequence that the particle density $\rho(t)$ fluctuates around its equilibrium steady state value $\bar{\rho}$ after some relaxation time. This reduces the computational effort and improves the numerical data without neglecting correlation effects.
- A positive side effect of $\bar{J} > 0$ is that the simulations become directly comparable to theoretical considerations. Using the LPA ansatz (5.4) in the equations of motion (6.3) for $\bar{J} > 0$, gives the relation

$$U_0^{(1,0)}(0, \bar{\rho}) = \bar{J} \quad (6.54)$$

between the particle input \bar{J} and the stationary density $\bar{\rho}$. As the corresponding pairs of \bar{J} and $\bar{\rho}$ can be measured in simulations, the relation (6.54) is used to test the theoretical prediction (6.49):

$$U_0^{(1,0)}(0, \bar{\rho}) = 2G_0(2, 2)\bar{\rho}^2 + \sum_{\substack{n \geq 3 \\ n \leq \lfloor 1+d/\mu \rfloor}} G_0(1, n)\bar{\rho}^n + \sum_{n=1} \mathcal{A}_n \bar{\rho}^{n \left(\frac{d}{\mu}-1\right)+2} + \dots \quad (6.55)$$

$G_0(2, 2)$ and \mathcal{A}_n are explicitly calculated in (6.15) and (6.48), respectively.

The Lévy step (6.53a) accounts for the possibility that a particle at site $\mathbf{x} \in a\mathbb{Z}^d$ jumps to a site $\mathbf{y} \in a\mathbb{Z}^d$ with probability $p(|\mathbf{x} - \mathbf{y}|)$. In the simulations, the infinitely large lattice $a\mathbb{Z}^d$ is replaced by an finite lattice with periodic boundary conditions. We varied the size of the lattice from a minimal size of 10^6 to a maximal size of 10^9 lattice sites. We found that the simulations are insensitive to the lattice size and therefore finite size effects can be excluded. The target site \mathbf{y} of a Lévy jump starting at \mathbf{x} is determined by giving the 10^6 nearest sites of \mathbf{x} a weight $\propto |\mathbf{x} - \mathbf{y}|^{-d-\mu}$ (3.13) and making a random choice according to this distribution. This is an approximation in the sense, that the maximal jump length is bounded, whereas ‘true’ Lévy flights are characterized by unbounded jump lengths (see section 3.3). We found that this approximation is valid, as long as $\mu \gtrsim 0.3$, such that long jumps occur sufficiently seldom. We improved the runtime of the simulations by storing the particle positions in a skip list [68].

Simulations in 1D

Figures 6.9 and 6.10 compare the theoretical prediction (6.55) to the simulations for the initial reaction rate $\lambda = \infty$ and $\tau\lambda = 1$, respectively. In addition to the law of mass action

$\bar{J} \approx 2 G_0(2, 2) \bar{\rho}^2$ (dotted line), the first $N = \lfloor (d/\mu - 1)^{-1} \rfloor$ non analytic correction terms $\sum_{n=1}^N \mathcal{A}_n \bar{\rho}^{n(d/\mu-1)+2}$ are included in the blue graph. N is chosen in such a way that the non analytic exponents $n(d/\mu - 1) + 2$ are below 3 for $n \leq N$.

The simulations of $\lambda = \infty$ (figure 6.9) differ from $\tau \lambda = 1 < \infty$ (figure 6.10) for large densities $\bar{\rho}$: Due to the fact that each lattice site cannot contain more than one particle in the case of $\lambda = \infty$, the largest density is obtained when statistically every second site is occupied by one particle. Consequently, the particle input \bar{J} diverges at $\rho = 0.5$. This divergence does not occur in the case $\lambda < \infty$ since the sites may contain more than one particle.

For small densities $\bar{\rho}$ the two cases of $\lambda = \infty$ and $\lambda < \infty$ are qualitatively alike. Hence, the following description of the low density regime applies to both figures 6.9 and 6.10. As long as the critical dimension μ is not too close to the spatial dimension $d = 1$ (i.e. $\mu \lesssim 0.9$), the non analytic corrections are small and give only marginal contributions to the law of mass action. In this case, the simulations are fitted well by the simple law of mass action $\bar{J} \approx 2 G_0(2, 2) \bar{\rho}^2$. For $\mu \gtrsim 0.9$, the correction terms give a crucial contribution to the law of mass action. The closer the critical dimension $d_c = \mu$ is to the spatial dimension $d = 1$, the larger is the discrepancy between the law of mass action and the correction improved law of mass action. For $\mu = 0.999$, a remarkably large number of $\lfloor (d/\mu - 1)^{-1} \rfloor = 999$ non analytic terms $\mathcal{A}_n \bar{\rho}^{n(d/\mu-1)+2}$ correct the law of mass action. The amplitude \mathcal{A}_n of each individual term becomes arbitrarily small for $\mu \rightarrow d$ (see figure 6.8). At the same time, the number N of terms increases and thereby compensates the smallness of \mathcal{A}_n . If the non analytic corrections are included, (6.55) fits the simulations well for $\mu \gtrsim 0.9$. The largest possible value is $\mu = 0.999$ until the calculation of $G_0(2, 2)$ (6.15) becomes numerically unstable. Even for this μ the plot is satisfying.

In nuce: For sufficiently low stationary densities $\bar{\rho} \lesssim 0.1$, the theoretical calculation (6.55) agrees well with the simulations. For small $\mu \lesssim 0.9$, the non analytic corrections are small and the law of mass action $U_0^{1,0}(0, \bar{\rho}) \approx 2 G_0(2, 2) \bar{\rho}^2$ describes the system well. Contrary, for $\mu \gtrsim 0.9$, the corrections have a significant impact on the law of mass action and cannot be neglected. This confirms the interpretation that the corrections indicate the breakdown of the law of mass action for $\mu > d$.

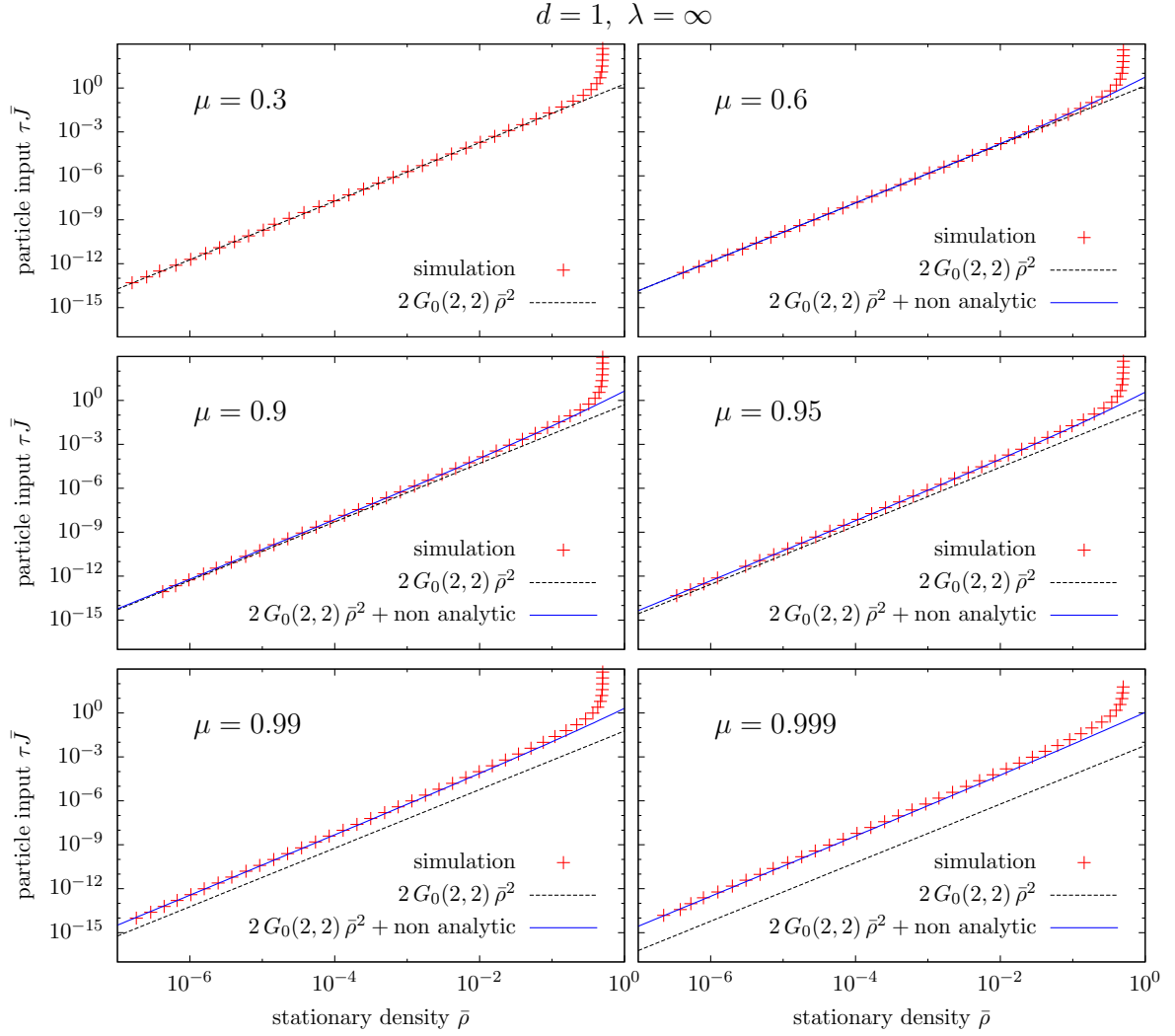


Figure 6.9: The validity of the law of mass action $\bar{J} \approx 2G_0(2,2)\bar{\rho}^2$ (dotted line) is tested for different Lévy flight exponents μ and initial reaction rate $\lambda = \infty$. In addition, for $\mu > d/2$, the non analytic corrections $\sum_{n=1}^N \mathcal{A}_n \bar{\rho}^{n(d/\mu-1)+2}$ are included in the blue graph. The number of non analytic correction terms N is chosen such that the exponents $n(d/\mu-1)+2$ are less than 3 for $n < N$. The deviation from the law of mass action for $\mu \gtrsim 0.9$ indicates the importance of corrections when the critical dimension μ is close to the spatial dimension $d = 1$. Figure 6.10 shows an analogous plot for finite initial reaction rate.

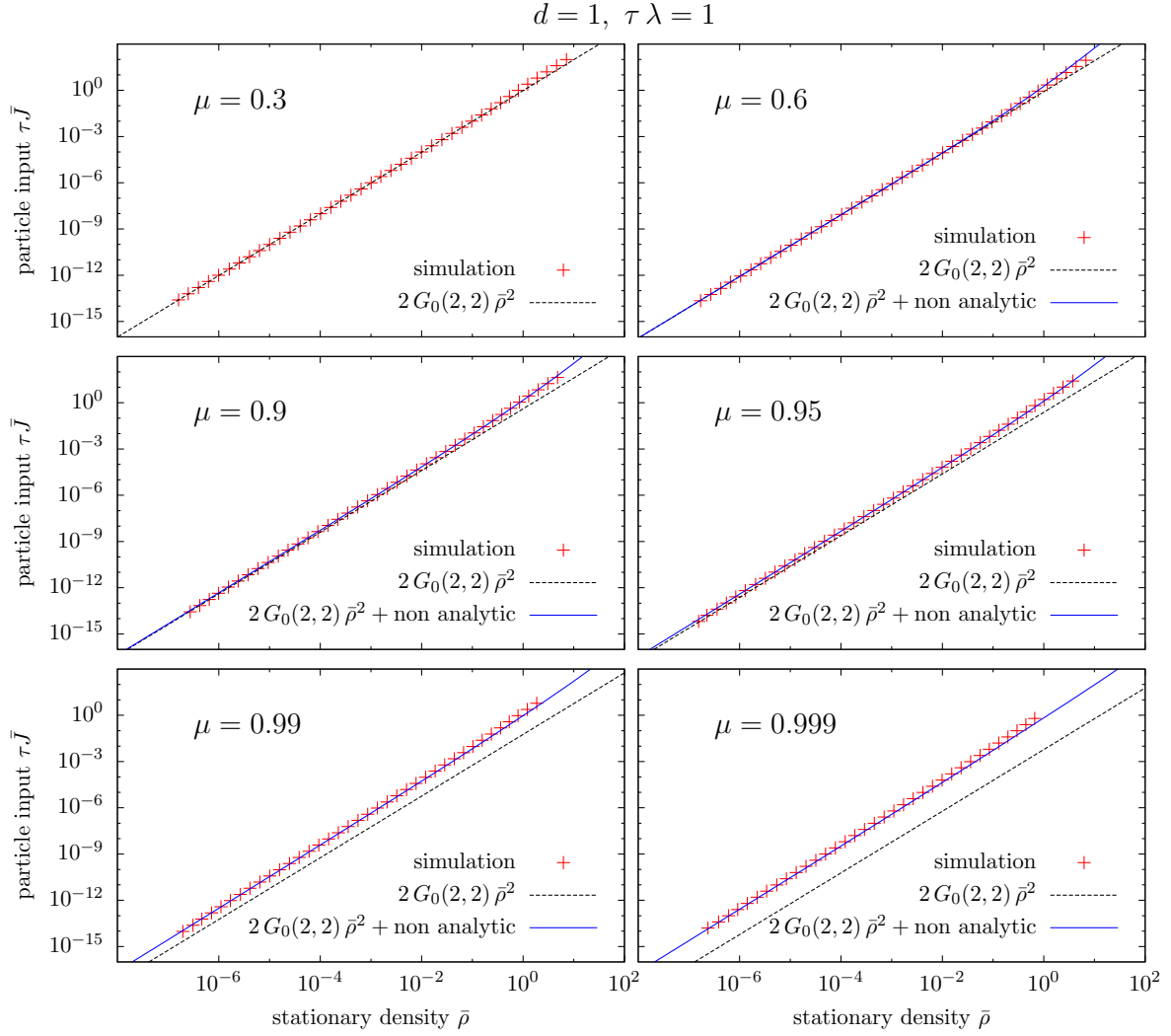


Figure 6.10: The validity of the law of mass action $\bar{J} \approx 2G_0(2,2)\bar{\rho}^2$ (dotted line) is tested for different Lévy flight exponents μ and initial reaction rate $\tau \lambda = 1$. In addition, for $\mu > d/2$, the non analytic corrections $\sum_{n=1}^N \mathcal{A}_n \bar{\rho}^{n(d/\mu-1)+2}$ are included in the blue graph. The number of non analytic correction terms N is chosen such that the exponents $n(d/\mu-1)+2$ are less than 3 for $n < N$. The deviation from the law of mass action for $\mu \gtrsim 0.9$ indicates the importance of corrections when the critical dimension μ is close to the spatial dimension $d = 1$. Figure 6.9 shows an analogous plot for infinite initial reaction rate.

Simulations in 2D

In contrast to the one dimensional case, we did not succeed to compute the macroscopic coupling $G_0(2, 2)$ with high accuracy as $\mu = d_c \rightarrow d = 2$. The reason is the lack of an expansion of $\epsilon(\mathbf{p})$ in powers of \mathbf{p} which makes the numerical integration of $\int_{\mathbf{p}} \epsilon(\mathbf{p})^{-1}$ difficult. Consequently, we were not able to test the validity of the non analytic correction terms in (6.55) close to the critical dimension. Figure 6.11 demonstrates the validity of the law of mass action for various Lévy exponents μ sufficiently less than 2 such that the numerical computation of $G_0(2, 2)$ is reliable. We performed the simulations on a cubic and on a hexagonal lattice. As the results for the two lattice geometries are barely distinguishable, figure 6.11 shows only the data for the cubic lattice $a\mathbb{Z}^2$.

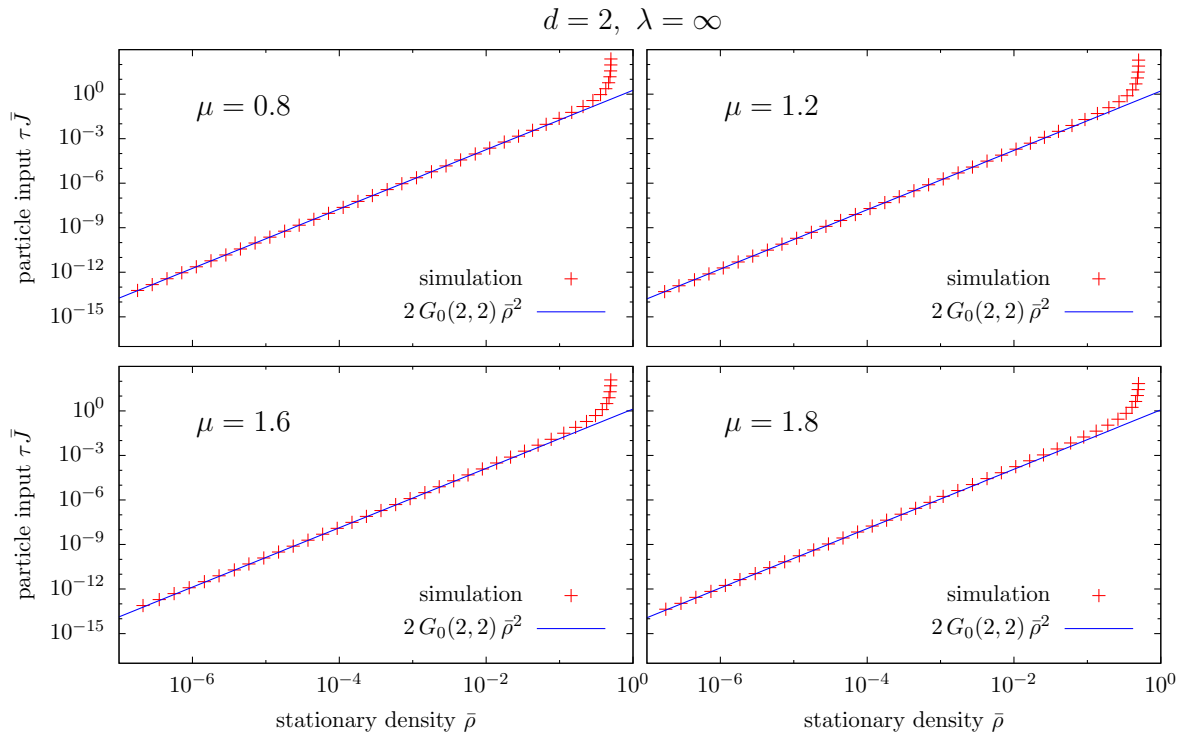


Figure 6.11: The validity of the law of mass action $\bar{J} \approx 2G_0(2, 2)\bar{\rho}^2$ is confirmed for different Lévy flight exponents μ and initial reaction rate $\lambda = \infty$ in $d = 2$ dimensions.

6.7 Summary

In this chapter we used the NPRG formalism in the simple local potential approximation to describe the pair annihilation process $A + A \rightarrow \emptyset$ above the critical dimension $d > d_c$. In the case where the A particles perform Lévy flights inside the lattice $a\mathbb{Z}^d$, the critical dimension is given by the Lévy flight exponent $d_c = \mu$ and becomes a manipulable bolt. The rate equation describing the decay of the particle density ρ was found to obey the law of mass action known from the mean field treatment. In contrast to mean field, the amplitude of the law of mass action gets renormalized and can be computed exactly. The amplitude is given by the

macroscopic reaction rate $G_0(2, 2)$ which depends *non universally* on the microscopic physics (such as the microscopic reaction rate, the particle dynamics and the lattice structure).

Corrections to the law of mass action are given by analytic and non analytic terms. The analytic corrections being *non universal*, are represented by vertices with more than two ingoing legs which are created along the renormalization flow. The analytic corrections lead to the concept of subordinate critical dimensions (see figure 6.5): As μ drops below the critical value d/n , the coupling $G_0(1, n+1)$ attains a finite value and the correction $\propto \rho^{n+1}$ is frozen out. Computer simulations suggest that these corrections play no significant role for small densities $\rho < 1$.

Close to the critical dimension, i.e. for $\mu \rightarrow d$, the fractional exponents of the non analytic correction terms are close to 2 and thus give important contributions to the law of mass action. These terms are created in the last part of the renormalization flow as $k \rightarrow 0$. The corrections originate from the most divergent Feynman diagrams which are build out of the $(*, 2)$ vertices. As a consequence, the correction amplitudes are *universal* functions of the *non universal* macroscopic rate $G_0(2, 2)$. The correction terms are interpreted as a hallmark of the breakdown of the law of mass action for $\mu \geq d$. The theoretical predictions match the simulations excellently.

The following chapter concentrates on the density decay below the critical dimension $d \leq d_c$.

7 The breakdown of the law of mass action in $d \leq d_c$

In chapter 6, the density decay was investigated for the pair annihilation process $A + A \rightarrow \emptyset$ above the critical dimension, $d > d_c$. Each A particle performs a Lévy flight and μ denotes the Lévy flight exponent (see chapter 3). The density decay was shown to fulfill the macroscopic law of mass action

$$\partial_t \rho(t) = -2 G_0(2, 2) \rho(t)^2 + \text{correction terms}, \quad \text{for } d > d_c = \mu, \quad (7.1)$$

where the macroscopic reaction rate $G_0(2, 2)$ is given by (6.15). The critical dimension $d_c = \mu$ separates the regime where $G_0(2, 2) > 0$ is finite from the regime where $G_0(2, 2) = 0$ and the law (7.1) breaks down. As derived in section 6.3, the vanishing of $G_0(2, 2)$ for $d < d_c$ is caused by the IR divergence of $\int_{\mathbf{p}} \epsilon(\mathbf{p})^{-1}$, and we have

$$G_k(2, 2) \sim k^{\mu-d} \xrightarrow{k \rightarrow 0} 0, \quad \text{for } d < d_c = \mu. \quad (7.2)$$

The other couplings behave as

$$G_k(*, m) \sim k^{\mu-(m-1)d} \xrightarrow{k \rightarrow 0} \infty, \quad \text{for } m \geq 3, d < d_c = \mu, \quad (7.3)$$

(note that $\mu - (m-1)d < 0$ because $d \geq 1$ and $\mu < 2$). Equation (7.3) is the analogon of (6.30) for $d < d_c$.

Equations (7.2) and (7.3) demonstrate that the values of the coupling constants $G_0(*, m)$ are solely determined by the macroscopic physics at $k \rightarrow 0$. This has two important consequences:

1. The microscopic lattice loses its influence on the macroscopic scale. The interpretation is that the long range fluctuations are strong enough to blur the lattice structure. Consequently, the pair annihilation should be described appropriately by a continuum model for $d < d_c$.
2. Related to the above mentioned is the implication that the macroscopic particle decay is universal for $d < d_c$. Mathematically, this universality is realized by a RG fixed point in the space of *dimensionless* coupling constants (see section 7.2).

This chapter is structured as follows. In section 7.1, the transition from the lattice model to the continuum model is performed. Subsequently, we prove the existence of the IR stable fixed point in the space of dimensionless coupling constants. Sections 7.3 and 7.4 deal with the rate equation for the density decay in $d < d_c$ and $d = d_c$, respectively. The chapter concludes with the comparison of the theoretical findings to the simulations.

7.1 The continuum model

Recall the Wetterich equation in the local potential approximation (6.11)

$$\begin{aligned} \partial_k U_k &= \frac{1}{2} \mathcal{V}(k) \frac{\frac{1}{\tau} \partial_k \epsilon_k \left(U_k^{(1,1)} + \frac{1}{\tau} \epsilon_k \right)}{\sqrt{\left(U_k^{(1,1)} + \frac{1}{\tau} \epsilon_k \right)^2 - U_k^{(2,0)} U_k^{(0,2)}}} \\ &\stackrel{(3.22)}{=} \frac{1}{2} \mathcal{V}(k) \frac{D_A \partial_k k^\mu \left(U_k^{(1,1)} + D_A k^\mu \right)}{\sqrt{\left(U_k^{(1,1)} + D_A k^\mu \right)^2 - U_k^{(2,0)} U_k^{(0,2)}}}. \end{aligned} \quad (7.4)$$

The only sign of the microscopic lattice $a\mathbb{Z}^d$ is hidden in the factor $\mathcal{V}(k) = \int_{\mathbf{p}} \Theta(\epsilon_k - \epsilon(\mathbf{p}))$, where the integration is performed over the Brillouin zone $[-\pi/a, \pi/a]^d$. The continuum model is obtained by approximating $a\mathbb{Z}^d$ by \mathbb{R}^d as the lattice spacing a vanishes. The Brillouin zone becomes \mathbb{R}^d and the Fourier series on the lattice is replaced by the Fourier transform on the continuum (see appendix A):

$$\begin{aligned} \int_{\mathbf{x}} &= \sum_{\mathbf{x} \in a\mathbb{Z}^d} \xrightarrow{a \rightarrow 0} \int_{\mathbf{x}} = \int_{\mathbb{R}^d} d^d x & \text{and} & \int_{\mathbf{p}} = \int_{\text{BZ}} \frac{d^d p}{\left(\frac{2\pi}{a}\right)^d} \xrightarrow{a \rightarrow 0} \int_{\mathbf{p}} = \int_{\mathbb{R}^d} d^d p \\ \left[\int_{\mathbf{x}} \right] &= 1 \xrightarrow{a \rightarrow 0} \left[\int_{\mathbf{x}} \right] = \text{length}^d & & \left[\int_{\mathbf{p}} \right] = 1 \xrightarrow{a \rightarrow 0} \left[\int_{\mathbf{p}} \right] = \text{length}^{-d}. \end{aligned}$$

Moreover, the dispersion relation $\epsilon(\mathbf{p})$ is replaced by (compare the discussion of the generalized central limit theorem in section 3.3)

$$\epsilon(\mathbf{p}) \xrightarrow{a \rightarrow 0} \epsilon(\mathbf{p}) = \tilde{D}_A (a|\mathbf{p}|)^\mu \quad (7.5)$$

and the discrete fractional derivative operator ∇^μ (3.16) becomes the continuous fractional derivative

$$-\nabla^\mu \equiv \tilde{D}_A^{-1} a^{-\mu} \mathcal{F}^{-1} \epsilon(\mathbf{p}) \mathcal{F} \xrightarrow{a \rightarrow 0} -\nabla^\mu \equiv \mathcal{F}^{-1} |\mathbf{p}|^\mu \mathcal{F}.$$

Using (7.5) and the new meaning of $\int_{\mathbf{p}}$ in $\mathcal{V}(k)$, yields

$$\mathcal{V}(k) \xrightarrow{a \rightarrow 0} \mathcal{V}(k) = \int_{\mathbf{p}} \Theta(\epsilon_k - \epsilon(\mathbf{p})) = \frac{V(B^d(1))}{(2\pi)^d} k^d, \quad [\mathcal{V}(k)] = \text{length}^{-d}, \quad (7.6)$$

which is used in the flow of the local potential (7.4). This gives the continuum flow equation.

A result of the continuum limit is the fact that the previously dimensionless Ψ field acquires the dimension $[\Psi] = \text{length}^{-d}$. The reason for this change is that Ψ measures ‘the number of particles per *lattice site*’ in the discrete case, whereas Ψ measures ‘the number of particles per *unit volume*’ in the continuous case. The $\bar{\Psi}$ field remains dimensionless. A formal way to see this, is to look at the *dimensionless* action functional

$$S[\bar{\Psi}, \Psi] = \int_x \bar{\Psi} (\partial_t - D_A \nabla^\mu) \Psi + U_\Lambda(\bar{\Psi}, \Psi),$$

and use $[\int_x] = \text{time} \cdot \text{length}^d$. In addition, $[U] = \text{time}^{-1} \cdot \text{length}^{-d}$ is observed. In order to find the advertised fixed point, the flow equation (7.4) is rephrased in the dimensionless form. The dimensionless fields and the dimensionless potential are defined by

$$\bar{\chi} \equiv \bar{\Psi}, \quad \chi \equiv k^{-d} \Psi \quad \text{and} \quad u_k(\bar{\chi}, \chi) \equiv (D_A k^\mu)^{-1} k^{-d} U_k(\bar{\Psi}, \Psi), \quad (7.7)$$

respectively. Equation (7.4) induces the flow

$$k \partial_k u_k(\bar{\chi}, \chi) = d \chi u_k^{(0,1)} - (\mu + d) u_k + \frac{\mu}{2} \frac{V(B^d(1))}{(2\pi)^d} \frac{u_k^{(1,1)} + 1}{\sqrt{(u_k^{(1,1)} + 1)^2 - u_k^{(2,0)} u_k^{(0,2)}}} \quad (7.8)$$

of the *dimensionless* potential u_k . The crux in the definition of the dimensionless quantities (7.7) is to use the *running* length scale k^{-1} and the *running* time scale $(D_A k^\mu)^{-1}$. This rescaling is chosen in order to ‘keep eye contact’ during the coarse graining procedure. The idea is related to Kardaroff’s block spin transformation [9] and it is essential to find fixed points [5].

7.2 The IR stable fixed point

The dimensionless coupling constants $g_k(n, m)$ are defined as the coefficients in the Taylor expansion of the dimensionless potential

$$u_k(\bar{\chi}, \chi) = \sum_{\substack{m \geq 2 \\ n \leq m}} g_k(n, m) \bar{\chi}^n \chi^m.$$

The definition (7.7) relates $g_k(n, m)$ to the dimensional couplings via

$$G_k(n, m) = D_A k^{\mu - (m-1)d} g_k(n, m). \quad (7.9)$$

Comparing (7.9) to equations (7.2) and (7.3) suggests that the dependence of $g_k(n, m)$ on k becomes weak as $k \rightarrow 0$. In other words the dimensional couplings $g_k(n, m)$ flow to the fixed point values $\lim_{k \rightarrow 0} g_k(n, m) \equiv g^*(n, m)$. The interpretation is the following: Even though the dimensional couplings $G_k(n, m)$ flow to trivial values (either zero or infinity), the scaling in (7.9) functions as a microscope and allows to extract the *nontrivial* information $g^*(n, m)$. Intriguingly, (7.9) is the result of simple dimensional considerations.

Let us calculate the nontrivial fixed point values $g^*(n, m)$. The PDE (7.8) imposes ODE’s for the dimensionless couplings $g_k(n, m)$. The flow equation of the $g_k(2, 2)$ is closed:

$$k \partial_k g_k(2, 2) = (d - \mu) g_k(2, 2) + \mu \frac{V(B^d(1))}{(2\pi)^d} g_k(2, 2)^2. \quad (7.10)$$

For the initial value $g_\Lambda(2, 2) = D_A^{-1} \Lambda^{d-\mu} \lambda > 0$, the coupling $g_k(2, 2)$ flows into the IR stable fixed point $g^*(2, 2) = \frac{\mu-d}{\mu} \frac{(2\pi)^d}{V(B^d(1))} > 0$ as $k \rightarrow 0$.

To compute the other fixed point values $g^*(n, m)$, we proceed inductively along the vertex hierarchy (see figure 5.4). Assume all $g^*(*, *)$ prior to $g^*(n, m)$ in the vertex hierarchy are known. The flow equation of the $g_k(n, m)$ coupling reads

$$k \partial_k g_k(n, m) = m d g_k(n, m) - (\mu + d) g_k(n, m) + F(g_k(*, *)), \quad (7.11)$$

where the term F stands for the terms resulting from the one loop Feynman diagrams. Due to the property (P8) on page 42, the expression F is linear in $g_k(n, m)$. We write $F = c_1 g_k(2, 2) g_k(n, m) + c_2$, where $c_1 > 0$ is a numerical constant and c_2 depends on the vertices prior to $g_k(n, m)$ in the hierarchy. Since the couplings $g_k(*, *)$ depend only weakly on k as $k \rightarrow 0$, we may replace the couplings in c_2 by its known fixed point values. Thus, (7.11) takes the simple linear form

$$k \partial_k g_k(n, m) = \tilde{c}_1 g_k(n, m) + c_2, \quad \text{where } \tilde{c}_1, c_2 \in \mathbb{R} \text{ constant.}$$

As the prefactor \tilde{c}_1 is positive, the fixed point $g^*(n, m) = -c_2/\tilde{c}_1$ is IR stable and the mathematical induction closes. The first couplings obtained in this manner (with the help of a computer algebra system) for $d = 1$ are summarized in the following table.

$g^*(n, m)$	$m = 2$	$m = 3$	$m = 4$	\dots
$n = 1$	$\frac{2\pi(\mu-1)}{\mu}$	$\frac{16\pi^2(\mu-1)^3}{(5\mu-4)\mu^2}$	$-\frac{12\pi^3(\mu-1)^4(192-704\mu+829\mu^2-309\mu^3)}{(5\mu-4)^2\mu^3(18-49\mu+33\mu^2)}$	\dots
$n = 2$	$\frac{\pi(\mu-1)}{\mu}$	$\frac{24\pi^2(\mu-1)^3}{(5\mu-4)\mu^2}$	$-\frac{18\pi^3(\mu-1)^4(384-1408\mu+1667\mu^2-629\mu^3)}{(5\mu-4)^2\mu^3(18-49\mu+33\mu^2)}$	\dots
$n = 3$	/	$\frac{8\pi^2(\mu-1)^3}{(5\mu-4)\mu^2}$	$\frac{12\pi^3(\mu-1)^4(240-520\mu+263\mu^2)}{(11\mu-9)(5\mu-4)^2\mu^3}$	\dots
$n = 4$	/	/	$\frac{3\pi^3(\mu-1)^4(240-520\mu+263\mu^2)}{(11\mu-9)(5\mu-4)^2\mu^3}$	\dots
\vdots	/	/	/	\ddots

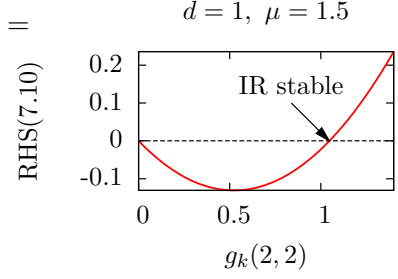
The analytic expressions quickly become complicated due to the nested nature of the vertex hierarchy.

The table suggests that

$$g^*(*, 2) \sim (\mu - d) \quad \text{and} \quad \text{as } (\mu - d) \rightarrow 0, \quad (7.12)$$

$$g^*(*, m) \sim (\mu - d)^m, \quad m \geq 3$$

We prove (7.12) by induction along the vertex hierarchy. Assume (7.12) holds for $\tilde{m} < m$. Let us look at the Feynman diagram contributing to $k \partial_k g(*, m)$, which consists of (n_i, m_i) , $i = 1, \dots, N$ vertices. The one loop structure forces $m = \sum_i m_i - N$. For the diagram which



contains only $(*, 2)$ vertices, we have $m_i = 2$ and $N = m$. By the induction hypothesis, this diagram scales as $(\mu - d)^m$. By the same argument, the diagram where only $M < N$ of the N vertices are $(*, 2)$ couplings, scales as $(\mu - d)^{N-M+m}$. In this sense, the diagram which is exclusively built out of $(*, 2)$ vertices, gives the leading contribution to the flow of $g(*, m)$ in the limit $(\mu - d) \rightarrow 0$. Using this finding in the flow equation (7.11), proves the claim (7.12). \square

7.3 The density decay in $d < d_c$

The previous section explained how the renormalization flow drives the *dimensionless* potential $u_k(\bar{\chi}, \chi)$ into the IR stable fixed point

$$u^*(\bar{\chi}, \chi) = \sum_{\substack{m \geq 2 \\ n \leq m}} g^*(n, m) \bar{\chi}^n \chi^m. \quad (7.13)$$

In principle, the fixed point couplings $g^*(n, m)$ can be computed exactly. Let us derive some implications of the fixed point for the density decay.

The exponent of the leading term

The macroscopic rate equation describing the density decay is

$$\partial_t \rho(t) = -U_0^{(1,0)}(0, \rho(t)).$$

The existence of the fixed point (7.13) has the consequence that the rate equation is universal, independent of microscopic details. We compute

$$\begin{aligned} \lim_{k \rightarrow 0} U_k^{(1,0)}(0, \rho) &\stackrel{(7.7)}{=} \lim_{k \rightarrow 0} D_A k^{d+\mu} u_k^{(1,0)}(0, k^{-d} \rho) \\ &\stackrel{(7.13)}{=} \lim_{k \rightarrow 0} D_A k^{d+\mu} \sum_{m=2} g^*(1, m) (k^{-d} \rho)^m = \lim_{k \rightarrow 0} D_A k^{d+\mu} f^*(k^{-d} \rho), \end{aligned}$$

where $f^*(\chi) \equiv \sum_{m=2} g^*(1, m) \chi^m$. In the last line, $g_k(1, m)$ is replaced by the fixed point value $g^*(1, m)$. This is valid, because the fixed point is reached sufficiently fast as $k \rightarrow 0$. In order to guarantee the existence of a *nontrivial* limit $k \rightarrow 0$ of $U_k^{(1,0)}$, the scaling form $f^*(\chi) \xrightarrow{\chi \rightarrow \infty} \mathcal{A} \chi^{1+\mu/d}$ is predicted. This leads to

$$\partial_t \rho(t) = -U_0^{(1,0)}(0, \rho) = -\mathcal{A} D_A \rho(t)^{1+\mu/d}, \quad \text{for } d < d_c = \mu. \quad (7.14)$$

The dimensionless amplitude \mathcal{A} is universal and can be calculated numerically by the requirement $f^*(\chi) = \sum_{m=2} g^*(1, m) \chi^m \xrightarrow{\chi \rightarrow \infty} \mathcal{A} \chi^{1+d/\mu}$. Interestingly, *all* couplings $g^*(1, *)$ are needed for \mathcal{A} . We did not find a way to compute \mathcal{A} analytically. An approximation of \mathcal{A} for $\mu \rightarrow d$ is given below.

The large time solution of (7.14) is

$$\rho(t) \xrightarrow{t \rightarrow \infty} [\mu \mathcal{A} D_A \cdot t]^{-1/\mu} \equiv \tilde{\mathcal{A}} (D_A t)^{-1/\mu}.$$

The exponent of this power law is known to be exact [15, 14].

There is a second, related, way to derive (7.14) by means of dimensional analysis: The only *macroscopic, dimensional* quantities that can possibly appear in the rate equation are D_A and ρ with $[D_A] = \text{length}^\mu \cdot \text{time}^{-1}$ and $[\rho] = \text{length}^{-d}$. Hence,

$$\partial_t \rho(t) = f(D_A, \rho).$$

Since $[f] \stackrel{!}{=} \text{length}^d \cdot \text{time}^{-1}$ and D_A is the only quantity containing units of time, we rewrite

$$\partial_t \rho(t) = D_A \rho^{\mu/d} g(\rho) \quad (7.15)$$

with some new unknown function g . The requirement $[g] \stackrel{!}{=} \text{length}^{-d}$ leads to $g(\rho) = -\mathcal{A} \rho$ and (7.14) is recovered. As \mathcal{A} is dimensionless, there is no way to determine \mathcal{A} by this kind of reasoning.

The dimensional consideration shows that (7.14) is the *only* dimensionally valid form. In particular, this excludes the possibility of correction terms. The physical reason for the absence of corrections to (7.14) can be pinned down to the fact that the particles are considered to be structureless point particles moving in the continuum. This assumption becomes incorrect if the particle density is large. For large particle densities, the particle's spatial extension becomes important and introduces a new microscopic length scale a (a can be thought of as the particle's radius). The new length has the important consequence, that (7.15) is replaced by

$$\partial_t \rho(t) = D_A \rho^{\mu/d} g(\rho, a) = D_A \rho^{1+\mu/d} \tilde{g}(a^d \rho),$$

where $\tilde{g}(0) = -\mathcal{A}$. This new form allows for the existence of correction terms as long as $a \neq 0$. Instead of interpreting the length scale a as the particle radius, the spatial extend of the particles can also be modeled by reintroducing the lattice $a \mathbb{Z}^d$ and sticking to point particles.

The upshot is: The *universal* leading term $\mathcal{A} D_A \rho^{1+\mu/d}$ in the rate equation (7.14) is computed in the continuum limit $a \mathbb{Z}^d \rightarrow \mathbb{R}^d$. The universal character guarantees that the microscopic lattice has no influence and the continuum limit is expected to lead to the exact result. The corrections to $\mathcal{A} D_A \rho^{1+\mu/d}$ are important for large densities ρ , where the continuum limit becomes unfaithful as it neglects the particle's extension. Hence, the correction terms still depend on the lattice structure and are non universal. The fixed point is blind for these correction terms.

The amplitude of the leading term

We derive an approximation for the universal amplitude \mathcal{A} in

$$U_0^{(1,0)}(0, \rho) = -\mathcal{A} D_A \rho^{1+\mu/d}. \quad (7.16)$$

The Wetterich equation (7.4) induces the flow equation for $U_k^{(1,0)}(0, \rho)$

$$\partial_k U_k^{(1,0)}(0, \rho) = \frac{1}{2} \mathcal{V}(k) D_A \partial_k k^\mu \frac{U_k^{(2,0)} U_k^{(0,2)}}{2 \left(U_k^{(1,1)} + D_A k^\mu \right)^2}$$

and hence,

$$U_0^{(1,0)}(0, \rho) = U_\Lambda^{(1,0)}(0, \rho) - \frac{1}{2} \int_0^\Lambda dk \mathcal{V}(k) D_A \partial_k k^\mu \frac{U_k^{(2,0)} U_k^{(0,2)}}{2 \left(U_k^{(1,1)} + D_A k^\mu \right)^2}, \quad (7.17)$$

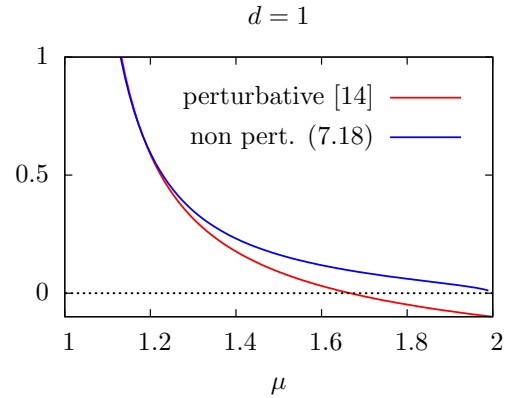
where $\mathcal{V}(k)$ is given by (7.6). As \mathcal{A} is universal, we may use the fixed point potential $U_k(\bar{\Psi}, \Psi) = D_A k^{\mu+d} u^*(\bar{\chi}, \chi)$ in the integrand of (7.17) and extract the term (7.16) after the integration. The integral is too difficult to be solved exactly and an approximation is needed. The approximation consists of using $U_k(\bar{\Psi}, \Psi) = D_A k^{d-\mu} (g^*(2, 2) \bar{\Psi}^2 \Psi^2 + 2g^*(2, 2) \bar{\Psi} \Psi^2)$ instead of the full fixed point potential. Consequently, only Feynman diagrams are taken into account which can be build out of $(*, 2)$ vertices. We may expect this approximation to be valid in the limit $(\mu - d) \rightarrow 0$, because the higher order couplings are suppressed as $g^*(*, m) \sim (\mu - d)^m$ (7.12) and become negligible. For $d = 1$, the approximation yields

$$\mathcal{A} \approx \frac{2^{2\mu}}{2\pi} \frac{\mu^2}{1+\mu} \Gamma(-\mu) \Gamma(2+\mu) g^*(2, 2)^{1+\mu}, \quad \text{where } g^*(2, 2) = \frac{\pi(\mu-1)}{\mu}. \quad (7.18)$$

For $\mu \rightarrow d = 1$, the dependence of the amplitude \mathcal{A} on μ is a simple power law:

$$\mathcal{A} = 2\pi (\mu - d)^1.$$

This is the analog of the power law $G_0(2, 2) \propto (d-\mu)^1$ (6.19) above the critical dimension. As $(d-\mu) \rightarrow 0$, the result (7.18) agrees with the perturbative $\epsilon \equiv (d - \mu)$ expansion to one loop order [14] (see figure). For large ϵ , (7.18) is slightly better than the perturbative result. The divergence of $\tilde{\mathcal{A}}$ for $\mu \rightarrow d$ indicates the breakdown of the universal behavior ruled by the fixed point (see chapter 6).



7.4 The density decay in $d = d_c$

Naively setting $d = d_c$ in (7.14), gives the law of mass action. However, at $d = d_c = \mu$ the fixed point becomes trivial, $g^*(*, *) = 0$ (compare the table on page 82), and the reasoning leading to (7.14) breaks down. This section demonstrates how the rate equation becomes the law of mass action dressed with a logarithmic corrections factor in $d = d_c$.

The starting point is the discrete lattice model¹ described in chapter 6. The solution (6.14) of the $(2, 2)$ vertex's flow equation is dominated by the logarithmic term as $k \rightarrow 0$:

$$G_k(2, 2) \xrightarrow{k \rightarrow 0} \left[\text{finite} - \frac{V(B^d(1))}{(2\pi)^d} \frac{a^d}{D_A} \mu \log(ak) \right]^{-1}, \quad d = \mu. \quad (7.19)$$

¹In principal, one could also start with the continuous model described in section 7.1. The lattice model has the advantage that it is not plagued by UV divergences due to the natural cutoff.

As a consequence, the finite, non universal terms in the square bracket are suppressed and universal behavior emerges. The rate equation is approximated by

$$\partial_t \rho = -U_0^{(1,0)}(0, \rho) = -\lim_{k \rightarrow 0} 2 G_k(2, 2) \rho^2. \quad (7.20)$$

Performing the limit $k \rightarrow 0$ in (7.20) leads to a coarse grained picture, which is too rough, as it gives the trivial result $G_0(2, 2) = 0$. Instead, we claim that the particle density ρ decreases in the limit $k \rightarrow 0$, such that

$$(ak)^{-d} \rho = 1/c = \text{const} \quad (7.21)$$

remains constant. The interpretation is the following. The coarse graining length scale k^{-1} induces a typical volume k^{-d} which contains $(ak)^{-d}$ lattice sites. As ρ measures particles per lattice site, $(ak)^{-d} \rho$ is the number of particles in a typical coarse grained box at the scale k . Using (7.19) and (7.21) in (7.20), yields the logarithmically corrected law of mass action

$$\partial_t \rho = -2 \frac{(2\pi)^d}{V(B^d(1))} \frac{D_A}{a^d} \frac{\rho^2}{\log(c\rho)}, \quad d = \mu. \quad (7.22)$$

The dependence of (7.22) on the arbitrary constant c vanishes in the limit $\rho \rightarrow 0$. In the one dimensional case $d = \mu = 1$, we have $\tilde{D}_A = 3/\pi$ (3.15) and (7.22) becomes

$$\partial_t \rho = -\frac{6}{\tau} \frac{\rho^2}{\log(\rho)}, \quad d = \mu = 1. \quad (7.23)$$

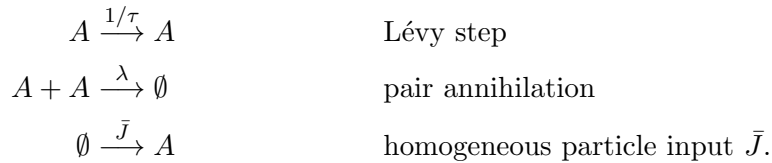
The rate equation (7.22) is solved by

$$\rho(t) \xrightarrow{t \rightarrow \infty} \frac{1}{2} \frac{V(B^d(1))}{(2\pi)^d} \frac{a^d}{D_A} \frac{\log t}{t}, \quad d = \mu. \quad (7.24)$$

For $d = \mu = 2$, (7.24) goes over into the diffusion result $\rho(t) = (8\pi)^{-1} \log t / (D_A t)$ [20, 69].

7.5 Comparison with simulations

We use the Gillespie algorithm [67] to simulate the process



As described in section 6.6, the stationary density $\bar{\rho}$ is measured for each particle input $\bar{J} > 0$. The associated pairs of \bar{J} and $\bar{\rho}$ fulfill

$$U_0^{(1,0)}(0, \bar{\rho}) = \bar{J}.$$

This relation is used to test the theoretical predictions. Figure 7.1 confirms the power law $U_0^{(1,0)}(0, \rho) = \mathcal{A} D_A \rho^{1+\mu/d}$ (7.14) for small densities ρ in $d = 1$ dimensions. For $\mu \lesssim 1.3$, the amplitude \mathcal{A} is accurately approximated by (7.18). For $\mu \gtrsim 1.3$ the approximation (7.18) of \mathcal{A} becomes unfaithful and higher vertices have to be included into the computation of \mathcal{A} .

In order to test the universality of the power law $U_0^{(1,0)}(0, \rho) = \mathcal{A} D_A \rho^{1+\mu/d}$, we performed the simulations for different microscopic reaction rates λ . For sufficiently small densities $\bar{\rho}$ the simulations are insensitive to λ due to the fixed point. The different microscopic details can only be observed by the non universal corrections for large $\bar{\rho}$. These corrections e.g. lead to a divergence of \bar{J} at $\bar{\rho} = 0.5$ for $\lambda = \infty$.

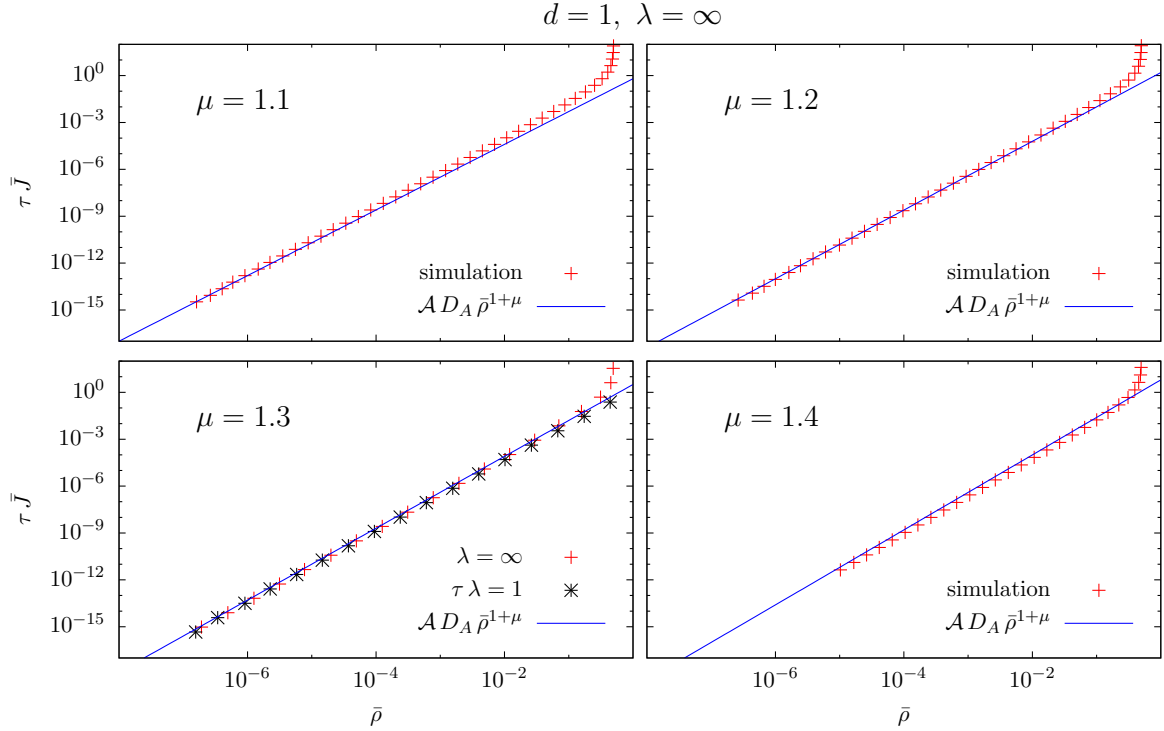


Figure 7.1: The validity of the power law $U^{(1,0)}(0, \rho) = \mathcal{A} D_A \rho^{1+\mu/d}$ (solid line) is examined in $d = 1$ for different Lévy flight exponents μ and initial reaction rate $\lambda = \infty$. The amplitude \mathcal{A} is approximated by (7.18). As long as the critical dimension μ is close to the spatial dimension, i.e. $\mu \lesssim 1.3$, the $(*, 2)$ vertices give the dominant contributions to \mathcal{A} and the approximation is valid. In the case of $\mu = 1.3$, we plot simulations with finite microscopic reaction rate $\tau \lambda = 1$ in addition to $\lambda = \infty$. The two cases coincide for sufficiently small densities due to the universal behavior at the fixed point.

Figure 7.2 shows the plot of $U^{(1,0)}(0, \rho)$ at the critical dimension $d = d_c = \mu = 1$. The plot supports the theoretically predicted form (7.23).

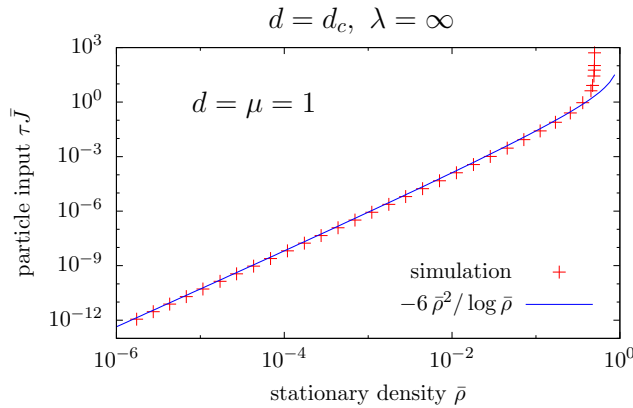


Figure 7.2: At the critical dimension the law of mass action $\bar{J} \propto \bar{\rho}^2$ is corrected by a logarithmic factor (see eq. (7.22)). The plot supports the correctness of $\partial_t \rho = -6/\tau \rho^2 / \log(\rho)$ in $d = \mu = 1$.

8 Trimolecular reaction kinetics

This chapter briefly discusses the case of the ternary annihilation reaction



In the case where the A particles perform diffusive motion in space, the critical dimension¹ is known to be $d_c = 1$ [69]. To the author's knowledge, the process (8.1) was only investigated for diffusion in $d = 1$ at the critical dimension [70, 71, 72, 73, 69]. The main result concerning the particle density decay in this case is given by

$$\rho(t) = \left(\frac{1}{4\pi\sqrt{3}} \right)^{1/2} \sqrt{\frac{\log t}{t}} \quad \text{at } d = d_c = 1 \quad (8.2)$$

for late times t . Equation (8.2) was derived by a perturbative field theory approach in [20] and can also be obtained by a Smoluchowski argument [69] similar to [11]. The amplitude of the logarithmically corrected power law (8.2) is known to be exact and universal [20].

Above the critical dimension, i.e. for $d > d_c$, the density is known to be described by the law of mass action

$$\partial_t \rho(t) = -\mathcal{A} \rho(t)^3 \quad (8.3)$$

for small densities ρ . Mean field predicts the amplitude $\mathcal{A} = 3\lambda$. No attempts have been made to calculate the renormalized amplitude $\mathcal{A} = 3G_0(3, 3)$ beyond mean field so far.

If the diffusive dynamics of the particles is replaced by Lévy flights with Lévy exponent $0 < \mu < 2$ (see chapter 3), the critical dimension is reduced and takes the value $d_c = \mu/2$. In the present chapter, we investigate the ternary reaction (8.1) for Lévy flights in $d \geq 1$ dimensions, i.e. above the critical dimension. In contrast to the pair annihilation process $A + A \rightarrow \emptyset$ (compare chapter 6), the NPRG formalism cannot be applied in the obvious way. We give a possible explanation for this instance and devise two alternative methods. One of this methods is inspired by the perturbative approach [60].

8.1 The problem of NPRG in $3A \rightarrow \emptyset$

The field theory for the ternary annihilation process (8.1) is obtained by the Doi Peliti procedure similar to the pair annihilation process (see chapter 2). The resulting microscopic action is given by

$$S[\bar{\Psi}, \Psi] = \int_x [\bar{\Psi}(x) (\partial_t - D_A \nabla^\mu) \Psi(x) + U_\Lambda(\bar{\Psi}(x), \Psi(x))], \quad (8.4)$$

¹More generally, the critical dimension of $kA \xrightarrow{\lambda} lA$ with $l < k$ is given by $d_c = 2/(k-1)$ [20]. This is obtained by using that the coupling constant λ (of the continuum model) is dimensionless at the critical dimension.

where

$$U_\Lambda(\bar{\Psi}, \Psi) = \lambda \cdot (\bar{\Psi}^3 + 3\bar{\Psi}^2 + 3\bar{\Psi}) \Psi^3 \quad (8.5)$$

is the microscopic local potential. The anomalous diffusion term $D_A \nabla^\mu$, defined by (3.16), encodes the Lévy flights on the lattice $L = a \mathbb{Z}^d$ (recall that $x = (t, \mathbf{x}) \in \mathbb{R} \times L$ and $\int_x = \int dt \sum_{\mathbf{x} \in L}$).

The Wetterich equation (4.10) imposes the flow equation (6.11) for the running local potential U_k . The only difference compared to the pair annihilation case is the different initial condition (8.5). A far reaching consequence of this initial condition is the absence of the $(*, 2)$ vertices on all scales k , as they cannot be created in one loop Feynman diagrams based on the $(*, 3)$ vertices. Moreover, a similar topological argument leads to the conclusion that the one loop Feynman diagrams cannot dress the $(*, 3)$ vertices. Therefore, the renormalization of the $(*, 3)$ vertices by means of the NPRG flow equation (6.11) is excluded:

$$G_0(3, 3) = G_k(3, 3) = \lambda. \quad (8.6)$$

The missing renormalization of the $(*, 3)$ vertices is obviously false as it contradicts the intuition of coarse graining. We suspect the error to be rooted in the Doi Peliti prescription. More concretely, as already noted in the footnote on page 2, a critical step in the Doi Peliti formalism is the path integral formulation: To arrive at (8.4) the sum of the operator $\exp(-\Delta t H) = \sum_n (\Delta t H)^n / n!$ is implicitly commuted with the integral arising from the coherent state unities. For the ternary process (8.1), the hamiltonian H contains an interaction term proportional to $\lambda a_{\mathbf{x}}^3$ (recall that $a_{\mathbf{x}}$ denotes the annihilation operator at site $\mathbf{x} \in L$). We sketch the problem, by looking at $\langle 0 | \exp(\lambda a^3) | 0 \rangle = 1$ for the lattice consisting of a single site [22]. Inserting the unity operator $1 = \int d^2 \Phi / \pi |\Phi\rangle \langle \Phi|$ (see eq. (2.9)), yields

$$1 = \langle 0 | \sum_{n=0} \frac{(\lambda a^3)^n}{n!} \int \frac{d^2 \Phi}{\pi} |\Phi\rangle \langle \Phi | 0 \rangle \cong \int \frac{d^2 \Phi}{\pi} \exp(-|\Phi|^2 + \lambda \Phi^3).$$

At the last ‘equality sign’ \cong , the sum and the integral are commuted and give an incorrect statement (the right hand side is diverging whereas the left hand side is 1). For binary reactions, such as the pair annihilation, the reaction term λa^3 is replaced by λa^2 and the commutation of sum and integral is allowed (at least for small λ). Despite the problem of interchanging sums and integrals in the Doi Peliti procedure, the resulting action gives valid results if the interaction are treated perturbatively [22].

The upshot is: If we want to study the ternary process $3A \rightarrow \emptyset$ by means of the action (8.4), the Doi Peliti formalism forces us to treat the interactions perturbatively. As we try to apply the Wetterich equation, we get the erroneous result (8.6).

One possibility to circumvent the problem is by introducing an auxiliary particle B that represents a pair of two A particles on the same lattice site. The process (8.1) is then rephrased by



The decay of the B particle accounts for the case that one of the A particles contained in a pair B performs a Lévy step and leaves its partner. This modified process consists of binary

reactions only and is therefore not plagued by the problem of interchanging sums and integrals. Consequently, the reaction rate λ becomes renormalized by the Wetterich equation as can be seen by looking at the new one loop Feynman diagrams. We do not follow this approach further as it is too complicated for concrete calculations. Instead, we use a perturbative approach in the following section.

8.2 The perturbative approach

Perturbation theory in (quantum) field theory is well established [26, 51]. The idea is to treat the reaction part $\lambda \cdot (\bar{\Psi}^3 + 3\bar{\Psi}^2 + 3\bar{\Psi})\Psi^3$ in (8.4) as a perturbation upon the ‘kinetic’ part $\bar{\Psi}(x)(\partial_t - D_A\nabla^\mu)\Psi(x)$. The use of perturbation theory for the reaction diffusion process $2A \rightarrow A$ *below* the critical dimension goes back to Peliti [60]. The approach was extended to $nA \rightarrow \emptyset$ by Lee [20]. We follow the reasoning of [20] to calculate the renormalized coupling $G_0(1, 3)$ for the process $3A \rightarrow \emptyset$ *above* the critical dimension. As $G_0(1, 3)$ is non universal, we use the action (8.4) defined on the discrete lattice space $L = a\mathbb{Z}^d$ and do not perform the continuum limit.

The (perturbative) propagator Δ_F is defined as the inverse of the operator $(\partial_t - D_A\nabla^\mu)$. The integral kernel is given by²

$$\Delta_F((t_2, \mathbf{p}_2), (t_1, \mathbf{p}_1)) = \Theta(t_2 - t_1) \exp\left[-\frac{1}{\tau}\epsilon(\mathbf{p}_2) \cdot (t_2 - t_1)\right] \widehat{\delta}(\mathbf{p}_2 - \mathbf{p}_1).$$

In contrast to [20], we keep contact to the microscopic lattice model by using the full dispersion function $\epsilon(\mathbf{p})$. Calculating the renormalized $(1, 3)$ vertex $G_R(1, 3)$ perturbatively leads to an expansion of $G_R(1, 3)$ in terms of the bare coupling λ . The result is given in a Feynman diagrammatic way:

$$\text{Diagrammatic expansion of } G_R(1, 3) \text{ as a series of Feynman diagrams.} \quad (8.7)$$

In contrast to the NPRG formalism, the Feynman diagrams in (8.7) are allowed to contain more than one loop. This avoids the topological constraint that forbids the renormalization in the Wetterich equation. Translating the diagrams (8.7) into algebraic expressions, yields [20]

$$\begin{aligned} G_R(1, 3)(t_2 - t_1) &= 3\lambda \delta(t_2 - t_1) + 3\lambda \cdot I(t_2 - t_1) + 3\lambda \cdot \int_{t_1}^{t_2} d\tau I(t_2 - \tau) I(\tau - t_1) + \\ &+ 3\lambda \cdot \int_{t_1}^{t_2} d\tau_1 \int_{t_1}^{\tau_1} d\tau_2 I(t_2 - \tau_1) I(\tau_1 - \tau_2) I(\tau_2 - t_1) + \dots, \end{aligned}$$

where

$$I(t) \equiv -3! \lambda \int \int \int_{\mathbf{p}_1 \mathbf{p}_2 \mathbf{p}_3} \widehat{\delta}(\mathbf{p}_1 + \mathbf{p}_2 + \mathbf{p}_3) \exp\left[-\frac{1}{\tau} \sum_{i=1}^3 \epsilon(\mathbf{p}_i) \cdot t\right]$$

²Recall the definition $D_A\nabla^\mu \equiv \tau^{-1} \mathcal{F}^{-1} \epsilon \mathcal{F}$ (3.16). The dispersion relation ϵ encodes the random dynamics on the lattice as was discussed in chapter 3.

represents one ‘bubble’ made out of three propagators, two loops and one (3, 3) vertex. The convolution structure of the consecutive bubble diagrams is converted into a geometric series by applying the Laplace transform $\tilde{f}(s) = \int_{t>0} dt f(t) \exp(-st)$:

$$\tilde{G}_R(1, 3)(s) \equiv \int_0^\infty dt G_R(1, 3)(t) e^{-st} = 3\lambda \cdot \left[1 + \tilde{I}(s) + \tilde{I}(s)^2 + \tilde{I}(s)^3 + \dots \right] = \frac{3\lambda}{1 - \tilde{I}(s)}.$$

(Strictly speaking, the sum does not converge for large λ . In the case where the sum does not converge, the last equality amounts to an analytic continuation.) The macroscopic limit is obtained as $s \rightarrow 0$:

$$G_0(1, 3) = \tilde{G}_R(1, 3)(s = 0) = 3 \left[\frac{1}{\lambda} + 3! \tau \int_{\mathbf{p}_1} \int_{\mathbf{p}_2} \frac{1}{\epsilon(\mathbf{p}_1) + \epsilon(\mathbf{p}_2) + \epsilon(\mathbf{p}_1 + \mathbf{p}_2)} \right]^{-1}. \quad (8.8)$$

This result is *exact*. It is one of the rare cases, where the perturbative series is resummed exactly and gives *non universal* results.

Equation (8.8) can easily be extended to the more general case of $nA \xrightarrow{\lambda} \emptyset$. The macroscopic coupling becomes

$$G_0(1, n) = n \left[\frac{1}{\lambda} + n! \tau \prod_{i=1}^n \int_{\mathbf{p}_i} \hat{\delta}(\sum_i \epsilon(\mathbf{p}_i)) \frac{1}{\sum_{i=1}^n \epsilon(\mathbf{p}_i)} \right]^{-1}. \quad (8.9)$$

For $n = 2$ we recover the result (6.15) obtained via the NPRG formalism. Using $\epsilon(p) \propto p^\mu$ for small momenta in (8.9) shows that $G_0(1, n)$ vanishes for $d \leq \mu/(n - 1)$. We conclude $d_c = \mu/(n - 1)$ in agreement with [20].

Figure 8.1 shows the dependence of the macroscopic reaction rate $G_0(3, 3) = G_0(1, 3)/3$ on the Lévy exponent μ in $d = 1$. The numerical calculation of (8.8) suggests that the coupling $G_0(3, 3)$ takes the asymptotic value

$$G_0(3, 3) \xrightarrow{\mu \rightarrow 2} 0.103\dots \quad (8.10)$$

as the critical dimension $d_c = \mu/2$ reaches the critical dimension $d = 1$. This result is surprising in the sense, that it is a new feature compared to the pair annihilation process $2A \rightarrow \emptyset$, where the macroscopic coupling goes to zero as the critical dimension reaches the spatial dimension (compare eq. (6.19) and figure 6.4). We did not find a physical explanation for (8.10). A consequence of (8.10) is that the law of mass action term of the rate equation

$$\partial_t \rho(t) = \underbrace{-3 G_0(3, 3) \rho^3}_{\text{law of mass action}} + \text{corrections}$$

does not become arbitrarily small in the limit $\mu \rightarrow 2$. Hence, we expect the corrections to the law of mass action to be less important, even close to the critical dimension (see figure 8.2).

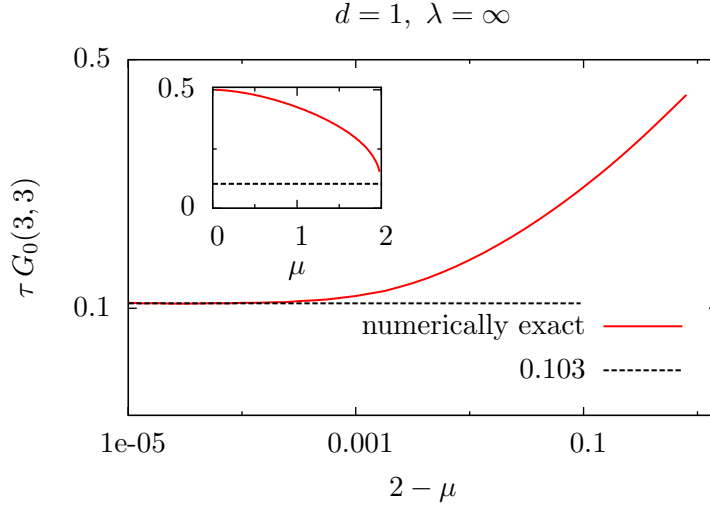
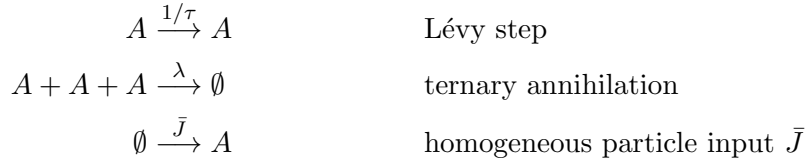


Figure 8.1: The macroscopic coupling $G_0(3, 3)$ of the ternary reaction $3A \rightarrow \emptyset$ with infinite microscopic rate is plotted against the Lévy exponent μ . As the critical dimension $d_c = \mu/2$ reaches the spatial dimension $d = 1$, the coupling obtains the asymptotic value $G_0(3, 3) = 0.103 \dots$. The numerical integration of (8.8) was performed by the GSL routine such that the absolute error of $G_0(3, 3) = 0.103$ is 10^{-5} . The dispersion function $\epsilon(p)$ was approximated by (3.18) up to the order $\mathcal{O}(p^6)$.

8.3 Comparison with simulations

Analogously to section 6.6, we used the Gillespie algorithm to simulate the process



for different Lévy exponents μ and different microscopic reaction rates λ . For every particle input \bar{J} the associated stationary density $\bar{\rho}$ is measured. The simulations are in good agreement with the theoretically predicted law of mass action

$$\bar{J} = G_0(1, 3) \bar{\rho}^3$$

where $G_0(1, 3)$ is given by (8.8). Figure 8.2 shows the exemplary case of $\lambda = \infty$ for different Lévy flight exponents μ . The theoretical result matches the simulations well, even for $\mu \rightarrow 2$. As explained in the previous section, the good agreement is due to the fact that $G_0(1, 3)$ approaches a finite value for $\mu \rightarrow 2$.

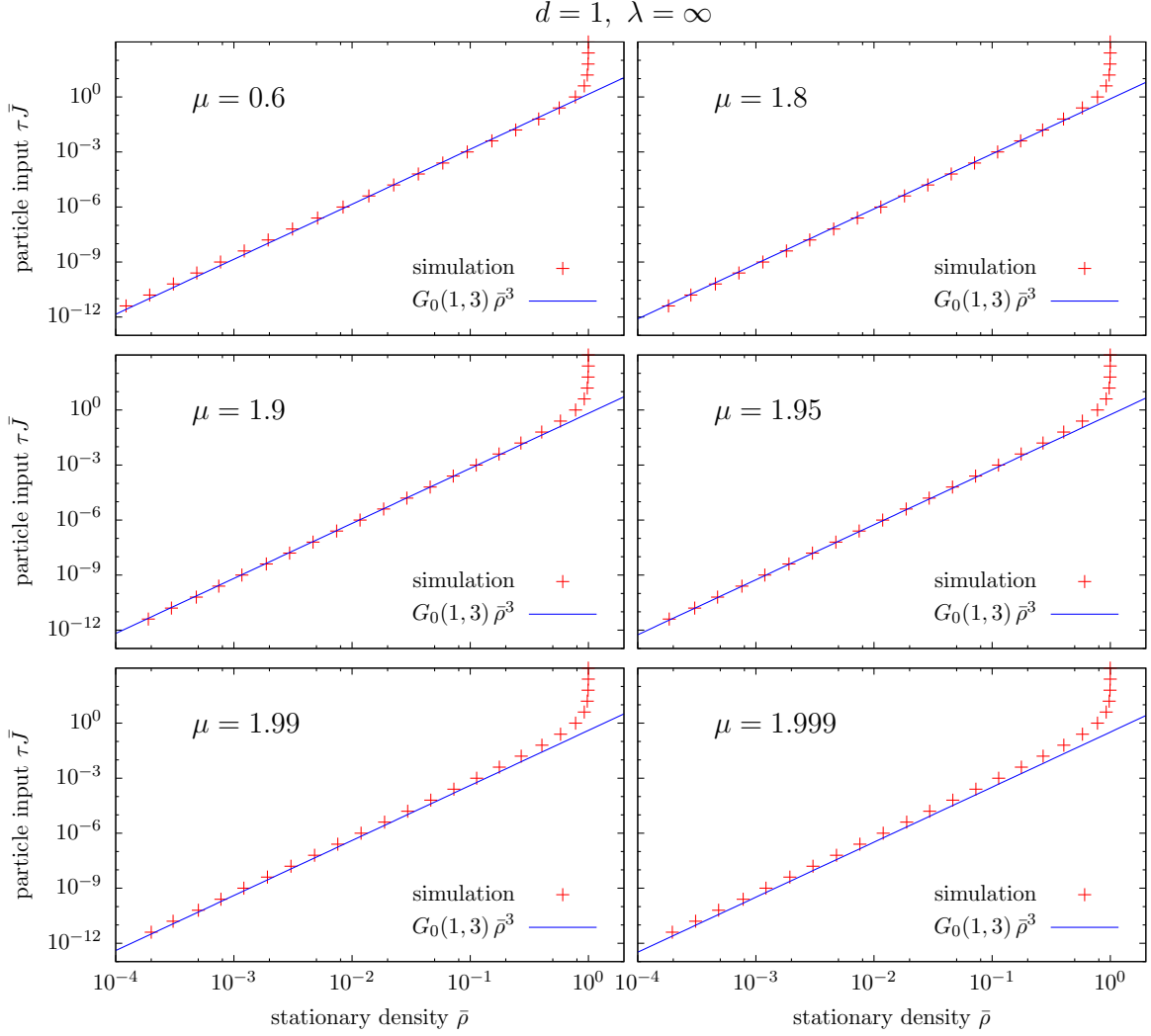


Figure 8.2: The macroscopic law of mass action $\bar{J} = G_0(1, 3) \bar{\rho}^3$ (blue line) is compared to the simulations (red points) for $\lambda = \infty$ in $d = 1$ dimensions and different Lévy flight exponents μ . The macroscopic coupling $G_0(1, 3)$ is given by (8.8). The good agreement with the simulations (even close to the critical dimension $d_c = \mu/2$) is a consequence of the fact that $G_0(1, 3)$ reaches a *finite* value as $\mu \rightarrow 2$ (see figure 8.1).

The divergence of \bar{J} at $\bar{\rho} = 1$ is an artifact of $\lambda = \infty$: For large inputs $\bar{J} \rightarrow \infty$ one third of all lattice sites will be empty (after a reaction occurred) another third will contain one particle and the last third will be occupied by two particles, viz. $\bar{\rho} \rightarrow 1/3 + 2/3 = 1$.

9 Conclusion

In this thesis we investigate the non equilibrium pair annihilation process $A + A \rightarrow \emptyset$ where the A particles perform Lévy flights inside the cubic lattice \mathbb{Z}^d . On the microscopic lattice scale, the system is defined by a master equation. As common to nontrivial many body problems, fluctuation effects have crucial implications on the macroscopic scale. The transition to macroscopics is performed in two steps. **First** the master equation is mapped onto a field theory by the Doi Peliti formalism. In a **second** step, the field theory is investigated by means of the non perturbative renormalization group (NPRG) flow equation. The Doi Peliti prescription, as well as the NPRG formalism are *exact* methods and go beyond phenomenology. This enables the computation of *non universal* quantities which depend on the details of the microscopic model.

Above the critical dimension ($d > d_c$) and for small particle densities, the pair annihilation process is known to obey the law of mass action, which states that the reaction rate is proportional to the product of the concentrations of the reacting particles. We compute the non universal proportionality factor and discuss its dependence on the particle dynamics, the microscopic reaction rate and the lattice shape.

If the system happens to be below or at the critical dimension ($d \leq d_c$), long range fluctuations are influential enough to blur the underlying microscopic model. As a consequence, the law of mass action breaks down and the system is described by a universal rate equation, independently of the microscopic details. The mathematical reason for the universality is the existence of an IR stable fixed point. We rediscover the known results of perturbation theory within the formalism of NPRG.

In order to examine the transition from the non universal law of mass action in $d > d_c$ to the universal fixed point driven law in $d \leq d_c$, we adjust the Lévy flight parameter such that the critical dimension becomes close to the spatial dimension. We found that the law of mass action is corrected by additional non analytic power law terms. Since these correction terms are created in the very last part of the renormalization flow, they have universal character. As the number and influence of these corrections grows close to the critical dimension they are interpreted as a hallmark of the breakdown of the law of mass action. Although the necessity of the non analytic correction terms is confirmed by computer simulations in $d = 1$, it remains questionable why the number of relevant correction terms increases unboundedly as the critical dimension approaches the spatial dimension.

A brief discussion on the ternary annihilation process $3A \rightarrow \emptyset$ demonstrates that the naive application of NPRG leads to the erroneous impression that the mean field result is not renormalized above the critical dimension. We propose an explanation for the failure of NPRG and devise an alternative strategy to determine the quantitatively correct law of mass action. Computer simulations confirm the result.

We conclude that the pair annihilation model with Lévy flights constitutes an accessible model to study the transition from $d > d_c$ to $d \leq d_c$ by analytic methods. We gained new insight into the physics of universal and non universal quantities above the critical dimension. To further elaborate in this direction we propose to study extended particles by means of reaction kernels [74].

The example of the ternary process shows that it is expected to be difficult to apply the reasoning to other processes. More work has to be done in this respect.

A Fourier transform

Inter alia, Fourier transform is used to diagonalize operators. In this appendix the conventions are set. The Fourier transform communicates between some position space X and the corresponding momentum space \widehat{X} . In the following, the two cases of a d dimensional continuous position space $X = \mathbb{R}^d$ and a d dimensional discrete lattice $X = L$ are distinguished.

Fourier transform on $X = \mathbb{R}^d$

Given some¹ function $f: \mathbb{R}^d \rightarrow \mathbb{C}$, its Fourier transform $\mathcal{F}(f) \equiv \widehat{f}$ is defined as

$$\widehat{f}: \mathbb{R}^d \longrightarrow \mathbb{C}, p \mapsto \int_{\mathbb{R}^d} d^d x f(\mathbf{x}) e^{-i\mathbf{x} \cdot \mathbf{p}} \equiv \int_{\mathbf{x}} f(\mathbf{x}) e^{-i\mathbf{x} \cdot \mathbf{p}} \quad (\text{A.1})$$

and the inverse transform $\mathcal{F}^{-1}(\widehat{f}) \equiv f$ is given by

$$f: \mathbb{R}^d \longrightarrow \mathbb{C}, x \mapsto \int_{\mathbb{R}^d} \frac{d^d p}{(2\pi)^d} \widehat{f}(\mathbf{p}) e^{i\mathbf{x} \cdot \mathbf{p}} \equiv \int_{\mathbf{p}} \widehat{f}(\mathbf{p}) e^{i\mathbf{x} \cdot \mathbf{p}}. \quad (\text{A.2})$$

The abbreviations $\int_{\mathbb{R}^d} d^d x \equiv \int_{\mathbf{x}}$ and $\int_{\mathbb{R}^d} \frac{d^d p}{(2\pi)^d} \equiv \int_{\mathbf{p}}$ are introduced. The consistency of (A.1) with (A.2) (and vice versa) is expressed via

$$\int_{\mathbf{x}} e^{-i\mathbf{x} \cdot \mathbf{p}} = (2\pi)^d \delta^d(\mathbf{p}) \equiv \widehat{\delta}^d(\mathbf{p}) \quad \text{and} \quad \int_{\mathbf{p}} e^{i\mathbf{x} \cdot \mathbf{p}} = \delta^d(\mathbf{x}). \quad (\text{A.3})$$

Fourier transform on a lattice $X = L$

Let

$$L = \left\{ \sum_{i=1}^d c_i \mathbf{a}_i \mid c_i \in \mathbb{Z}, i = 1 \dots d \right\} \equiv \text{span}_{\mathbb{Z}}(\mathbf{a}_1, \dots, \mathbf{a}_d) \subset \mathbb{R}^d$$

be the d dimensional lattice spanned by the d linear independent lattice vectors $\mathbf{a}_i \in \mathbb{R}^d$. The corresponding reciprocal lattice

$$L^* = \text{span}_{\mathbb{Z}}(\mathbf{b}_1, \dots, \mathbf{b}_d) \subset \mathbb{R}^d$$

is spanned by the reciprocal lattice vectors $\mathbf{b}_i \in \mathbb{R}^d$ which fulfill

$$\mathbf{a}_i \cdot \mathbf{b}_j = 2\pi \delta_{ij}. \quad (\text{A.4})$$

¹Although necessary for a mathematically rigorous definition, the function space is not specified any further.

Thinking of L as the position space, the momentum space cannot contain arbitrarily large momenta. Momenta that correspond to rapidly fluctuating modes in position space with a wavelength smaller than the lattice spacing are not allowed. The correctly truncated momentum space for L turns out to be, what is called the *first Brillouin zone*

$$1^{\text{st}}\text{B.Z.} \equiv \mathbb{R}^d/L^* \equiv \mathbb{R}^d/\sim \quad \text{where } \mathbf{p} \sim \mathbf{q} \Leftrightarrow \mathbf{p} - \mathbf{q} \in L^*.$$

The volume of the first Brillouin zone $V(L^*)$ is the volume of the parallelepiped spanned by the basis vectors $\{\mathbf{b}_i\}_{i=1,\dots,d}$

$$\text{Volume}(1.\text{B.Z.}) \equiv V(L^*) \equiv \mu(\mathbb{R}^d/L^*)$$

(here μ denotes the Lebesgue measure inherited from \mathbb{R}^d). Similarly, $V(L) \stackrel{(A.4)}{=} \frac{(2\pi)^d}{V(L^*)}$ denotes the volume of one unit cell in L .

Given some function $f: L \rightarrow \mathbb{C}$ on the lattice, its Fourier transform $\mathcal{F}(f) \equiv \hat{f}$ becomes the Fourier series

$$\hat{f}: \mathbb{R}^d/L^* \longrightarrow \mathbb{C}, \quad p \mapsto \sum_{\mathbf{x} \in L} f(\mathbf{x}) e^{-i\mathbf{x} \cdot \mathbf{p}} \equiv \int_{\mathbf{x}} f(\mathbf{x}) e^{-i\mathbf{x} \cdot \mathbf{p}} \quad (\text{A.5})$$

and the inverse transform $\mathcal{F}^{-1}(\hat{f})$ reads

$$f: L \longrightarrow \mathbb{C}, \quad x \mapsto \int_{\mathbb{R}^d/L^*} \frac{d^d p}{V(L^*)} \hat{f}(\mathbf{p}) e^{i\mathbf{x} \cdot \mathbf{p}} \equiv \int_{\mathbf{p}} \hat{f}(\mathbf{p}) e^{i\mathbf{x} \cdot \mathbf{p}}. \quad (\text{A.6})$$

Note that \hat{f} is well defined since $\hat{f}(\mathbf{p}) = \hat{f}(\mathbf{p} + \mathbf{q})$ for $\mathbf{q} \in L^*$ using (A.4). With the abbreviations $\sum_{\mathbf{x} \in L} \equiv \int_{\mathbf{x}}$ and $\int_{\mathbb{R}^d/L^*} \frac{d^d p}{V(L^*)} \equiv \int_{\mathbf{p}}$, the discrete Fourier transform (A.5) and (A.6) is formally identical to the continuous case (A.1) and (A.2), respectively. Analogously to (A.3) the identities

$$\int_{\mathbf{x}} e^{-i\mathbf{x} \cdot \mathbf{p}} = \frac{(2\pi)^d}{V(L)} \delta^d(\mathbf{p}) \equiv \hat{\delta}^d(\mathbf{p}), \quad \mathbf{p} \in \mathbb{R}^d/L^* \quad \text{and} \quad \int_{\mathbf{p}} e^{i\mathbf{x} \cdot \mathbf{p}} = \delta^d(\mathbf{x}), \quad \mathbf{x} \in L \quad (\text{A.7})$$

ensure the consistency of (A.5) and (A.6) (the second δ should not be confused with the Dirac delta in continuous space, but should rather be understood as a Kronecker delta in discrete space L).

Fourier transform in spacetime

We add a continuous temporal direction to the space X and look at functions $f: \mathbb{R} \times X \rightarrow \mathbb{C}$ defined the spacetime $\mathbb{R} \times X$. Defining the $(d+1)$ vectors

$$x \equiv (t, \mathbf{x}) \in \mathbb{R} \times X \quad \text{and} \quad p \equiv (\omega, \mathbf{p}) \in \mathbb{R} \times \hat{X} \quad \text{with} \quad x \cdot p \equiv t\omega - \mathbf{x} \cdot \mathbf{p}, \quad (\text{A.8})$$

the Fourier transform $\mathcal{F}(f) = \hat{f}: \mathbb{R} \times \hat{X} \rightarrow \mathbb{C}$ (where $\hat{X} \equiv \mathbb{R}^d$ in the continuous case and $\hat{X} \equiv \mathbb{R}^d/L^*$ in the lattice case) reads

$$\begin{aligned}\hat{f}(p) &= \int_{\mathbb{R}} dt \int_{\mathbf{x}} f(t, \mathbf{x}) e^{it\omega - i\mathbf{x}\cdot\mathbf{p}} \equiv \int_x f(x) e^{ix\cdot p} \\ f(x) &= \int_{\mathbb{R}} d\omega \int_{\mathbf{p}} \hat{f}(\omega, \mathbf{p}) e^{-it\omega + i\mathbf{x}\cdot\mathbf{p}} \equiv \int_p \hat{f}(p) e^{-ix\cdot p}.\end{aligned}\tag{A.9}$$

The notation is chosen to covers the spatially continuous case as well as the discrete case:

$$\int_x = \int_t \int_{\mathbf{x}} = \begin{cases} \int_{\mathbb{R}} dt \int_{\mathbb{R}^d} d^d x & \text{for } X = \mathbb{R}^d \text{ continuous} \\ \int_{\mathbb{R}} dt \sum_{\mathbf{x} \in L} & \text{for } X = L \text{ discrete,} \end{cases}\tag{A.10}$$

$$\int_p = \int_{\omega} \int_{\mathbf{p}} = \begin{cases} \int_{\mathbb{R}} d\omega \int_{\mathbb{R}^d} d^d p / (2\pi)^d & \text{for } \hat{X} = \mathbb{R}^d \text{ continuous} \\ \int_{\mathbb{R}} d\omega \int_{\mathbb{R}^d/L^*} d^d p / V(L^*) & \text{for } \hat{X} = \mathbb{R}^d/L^* \text{ discrete.} \end{cases}\tag{A.11}$$

Likewise,

$$\int_x e^{ix\cdot p} = \hat{\delta}^{d+1}(p) = \begin{cases} (2\pi)^{d+1} \delta^{d+1}(p) & \text{for } X = \mathbb{R}^d \text{ continuous} \\ (2\pi)^{d+1} / V(L) \delta^{d+1}(p) & \text{for } X = L \text{ discrete.} \end{cases}\tag{A.12}$$

The convention (A.8) is borrowed from special relativity, although the whole thesis deals with non relativistic physics.

B Operators and Integral Kernels

From a mathematical viewpoint this section is rather sloppy. When talking about operators, one needs to specify the domain in an appropriately equipped space on which the operator is defined. This issue is completely ignored. We merely set the notational convention.

Given an operator O acting on a function $f: \mathbb{R} \times X \rightarrow \mathbb{C}$ (see appendix A for the notation), denote $K(O)$ to be its integral kernel¹

$$(O f)(x) = \int_y K(O)(x, y) f(y).$$

(Note that the integral \int_y may actually contain a sum, whenever $X = L$ is a discrete lattice, as defined in eq. (A.10). In the discrete case the operator acts as a common matrix multiplication.)

We call $\widehat{O} \equiv \mathcal{F}O\mathcal{F}^{-1}$ the Fourier transform of O with kernel $K(\widehat{O})$

$$(\widehat{O} \widehat{f})(p) = \int_q K(\widehat{O})(p, q) \widehat{f}(q).$$

Surprisingly, $K(\widehat{O})$ is not the Fourier transform of $K(O)$, but

$$K(\widehat{O})(p_1, p_2) = \widehat{K(O)}(p_1, -p_2) \tag{B.1}$$

(notice the minus sign in the argument on the right hand side). A quick argument, ignoring mathematical rigor, goes like this

$$\begin{aligned} (\widehat{O} \widehat{f})(p) &= (\mathcal{F}O\mathcal{F}^{-1} \widehat{f})(p) = \mathcal{F} \left(\int_y K(O)(\cdot, y) f(y) \right) (p) = \int_{x,y} K(O)(x, y) f(y) e^{ix \cdot p} \\ &= \int_{x,y} \int_q K(O)(x, y) \widehat{f}(q) e^{-iy \cdot q + ix \cdot p} = \int_q \widehat{K(O)}(p, -q) \widehat{f}(q). \end{aligned}$$

The position space analogon of (B.1) is

$$K(O)(x_1, x_2) = (\mathcal{F}^{-1}K(\widehat{O})) (x_1, -x_2). \tag{B.2}$$

¹When confusion is excluded, the integral kernel is usually denoted by the same letters as the operator, i.e. just $K(O)(x, y) = O(x, y)$.

Multiplication versus convolution operators

One of the simplest operators are multiplication (diagonal) operators. Let O be a multiplication operator in position space

$$(Of)(x) = O(x) \cdot f(x)$$

with the formal integral kernel

$$K(O)(x_1, x_2) = O(x_1) \delta(x_1 - x_2).$$

Then (B.1) yields

$$K(O)(x_1, x_2) = O(x_1) \delta(x_1 - x_2) \iff K(\widehat{O})(p_1, p_2) = \widehat{O}(p_1 - p_2) \quad (\text{B.3})$$

for the integral kernel of \widehat{O} . This shows that the Fourier transform of an multiplication operator acts as a convolution

$$(\widehat{O}\widehat{f})(p) = \int_q \widehat{O}(p - q) \widehat{f}(q).$$

Analogously, if an operator is multiplicative in momentum space, it acts as a convolution in position space

$$K(\widehat{O})(p_1, p_2) = \widehat{O}(p_1) \widehat{\delta}(p_1 - p_2) \iff K(O)(x_1, x_2) = O(x_1 - x_2). \quad (\text{B.4})$$

Inverse operators

The kernel $K(O^{-1})$ of the inverse operator O^{-1} fulfills

$$\int_y K(O)(x_1, y) K(O^{-1})(y, x_2) = \delta(x_1 - x_2)$$

or in momentum space

$$\int_q K(\widehat{O})(p_1, q) K(\widehat{O}^{-1})(q, p_2) = \widehat{\delta}(p_1 - p_2).$$

Determining the kernel of the inverse operator is easy for multiplication (diagonal) operators

$$K(O)(x_1, x_2) = O(x_1) \delta(x_1 - x_2) \implies K(O^{-1})(x_1, x_2) = O(x_1)^{-1} \delta(x_1 - x_2) \quad (\text{B.5})$$

$$K(\widehat{O})(p_1, p_2) = \widehat{O}(p_1) \widehat{\delta}(p_1 - p_2) \implies K(\widehat{O}^{-1})(p_1, p_2) = \widehat{O}(p_1)^{-1} \widehat{\delta}(p_1 - p_2) \quad (\text{B.6})$$

in position and momentum space respectively. The symmetry between position and momentum space is due to the notation of \int_x , \int_p and $\widehat{\delta}(\cdot)$ (see eq. A.10, A.11 and A.12).

Trace

The trace of an operator O with integral kernel $K(O)$ is

$$\text{tr}(O) = \int_x K(O)(x, x) = \int_p K(\widehat{O})(p, p). \quad (\text{B.7})$$

Bibliography

- [1] F H Combley. (g-2) factors for muon and electron and the consequences for qed. *Rep. Prog. Phys.*, 42, 1979.
- [2] Sidney Coleman. Notes from sidney coleman's physics 253a. *arXiv*, physics.ed-ph, Oct 2011.
- [3] L. D. Landau and E. M. Lifshitz. *Fluid Mechanics*. Butterworth-Heinemann, second edition, 1987.
- [4] Nigel Goldenfeld. *Lectures on Phase Transitions and Renormalization Group*, chapter 10. Addison-Wesley Publishing Company, 1992.
- [5] Bertrand Delamotte. An introduction to the nonperturbative renormalization group. *arXiv*, cond-mat.stat-mech, Feb 2007.
- [6] C Bagnuls and C Bervillier. Exact renormalization group equations: an introductory review. *Physics Reports*, 2001.
- [7] C Bagnuls and C Bervillier. Exact renormalization group equations and the field theoretical approach to critical phenomena. *Arxiv preprint hep-th*, 2001.
- [8] C Wetterich. Average action and the renormalization group equations. *Nuclear Physics B*, 1991.
- [9] Leo Kadanoff. *Physics 2*, 263, 1966.
- [10] Leo Kadanoff. *Statistical Physics*. World Scientific, 2000.
- [11] M Smoluchowski. Versuch einer mathematischen theorie der koagulationskinetik kolloider lösungen. *Z. phys. Chem*, 1917.
- [12] A Lushnikov. Binary reaction $1 + 1 \rightarrow 0$ in one dimension. *Physics Letters A*, 1987.
- [13] M Bramson and D Griffeath. Asymptotics for interacting particle systems on \mathbb{Z}^d . *Probability Theory and Related Fields*, 1980.
- [14] D Vernon. Long range hops and the pair annihilation reaction $a + a \rightarrow 0$: Renormalization group and simulation. *Physical Review E*, Jan 2003.
- [15] H. Hinrichsen and M. Howard. A model for anomalous directed percolation. *The European Physical Journal B*, 1999.
- [16] P C Martin, E D Siggia, and H A Rose. Statistical dynamics of classical systems. *Physical Review A*, 8, 1973.

-
- [17] Masao Doi. Second quantization representation for classical many-particle system. *Journal of Physics A: Mathematical and General*, 9(9):1465–1477, Oct 1976.
- [18] Masao Doi. Stochastic theory of diffusion-controlled reaction. *Journal of Physics A: Mathematical and General*, 9(9):1479–1495, 1976.
- [19] L Peliti. Path integral approach to birth-death processes on a lattice. *Journal de Physique*, 46(9):1469–1483, 1985.
- [20] B Lee. Renormalization group calculation for the reaction $ka \rightarrow oe$. *Journal of Physics A: Mathematical and General*, 1994.
- [21] J Cardy and U Täuber. Field theory of branching and annihilating random walks. *Journal of statistical physics*, 90:1–56, Nov 1997.
- [22] UC Täuber, M Howard, and BP Vollmayr-Lee. Applications of field-theoretic renormalization group methods to reaction-diffusion problems. *Journal of Physics A: Mathematical and General*, 38:R79, 2005.
- [23] D Mattis and M Glasser. The uses of quantum field theory in diffusion-limited reactions. *Reviews of Modern Physics*, 1998.
- [24] J Cardy. Quantum hamiltonians and self-organised criticality. *Perspectives on solvable models*, 1994.
- [25] Lewis H. Ryder. *Quantum Field Theory*, chapter 5. Cambridge University Press, second edition, 1996.
- [26] John Negele and Henri Orland. *Quantum Many-Particle Systems*. Westview Press, 1998.
- [27] Léonie Canet, Hugues Chaté, and Bertrand Delamotte. General framework of the non-perturbative renormalization group for non-equilibrium steady states. *arXiv*, cond-mat.stat-mech, Jun 2011.
- [28] Lewis H. Ryder. *Quantum Field Theory*, chapter 6. Cambridge University Press, second edition, 1996.
- [29] B Delamotte L Canet, O Deloubrière, and N Wschebor. Nonperturbative renormalization-group study of reaction-diffusion processes. *Physical Review Letters*, 2004.
- [30] Léonie Canet, Hugues Chaté, and Bertrand Delamotte. Quantitative phase diagrams of branching and annihilating random walks. *Physical Review Letters*, 92(25):255703, 2004.
- [31] L Canet. Reaction–diffusion processes and non-perturbative renormalization group. *Journal of Physics A: Mathematical and General*, 2006.
- [32] Robert Brown. *Mikroskopische Beobachtungen, welche in den Monaten Juni, Juli und August 1927 gemacht wurden*. Bei Riegel und Wiessner, 1829.
- [33] A Einstein. Über die von der molekularkinetischen theorie der wärme geforderte bewegung von in ruhenden flüssigkeiten suspendierten teilchen. *Annalen der physik*, 1905.

- [34] A Einstein. Zur theorie der brownischen bewegung. *Annalen der physik*, 1906.
- [35] M von Smoluchowski. Zur kinetischen theorie der brownischen molekularbewegung und der suspensionen. *Annalen der physik*, 1906.
- [36] Jean Perrin. Wie wägt man ein atom? *Zeitschrift für Elektrochemie und angewandte physikalische Chemie*, 15(9):269–277, 1909.
- [37] Ralf Metzler and Joseph Klafter. The random walk’s guide to anomalous diffusion: a fractional dynamics approach. *Physics Reports*, 2000.
- [38] Ralf Metzler, Aleksei V Chechkin, and Joseph Klafter. Lévy statistics and anomalous transport: Lévy flights and subdiffusion. *arXiv*, cond-mat.stat-mech, Jun 2007.
- [39] Kenneth Falconer. *Fractal Geometry*, chapter 16. Wiley, second edition, 2003.
- [40] G Viswanathan, S Buldyrev, S Havlin, et al. Optimizing the success of random searches. *Nature*, 1999.
- [41] Benoit Mandelbrot. *The fractal geometry of nature*. W.H. Freeman and Company, 1983.
- [42] J Adamek, M Keller, A Senftleben, and H Hinrichsen. Epidemic spreading with long-range infections and incubation times. *Journal of Statistical Mechanics: Theory and Experiment*, 2005.
- [43] G Ramos-Fernández et al. Lévy walk patterns in the foraging movements of spider monkeys (*ateles geoffroyi*). *Behavioral Ecology and Sociobiology*, 2004.
- [44] G Zumofen and J Klafter. Spectral random walk of a single molecule. *Chemical physics letters*, 1994.
- [45] H Katori, S Schlipf, and H Walther. Anomalous dynamics of a single ion in an optical lattice. *Physical Review Letters*, 1997.
- [46] K Sengupta and N Dupuis. Non-perturbative renormalization-group approach to lattice models. *The European Physical Journal B*, 2008.
- [47] Laszlo Erdos. Lecture notes on quantum brownian motion. *arXiv*, math-ph, Sep 2010.
- [48] Detlef Dürr and Stefan Teufel. *Bohmian Mechanics*, chapter 5. Springer, 2009.
- [49] Vladimir V. Uchaikin and Vladimir M. Zolotarev. *Chance and Stability, Stable Distributions and Their Applications*, chapter 12.3. V.S.P. Intl Science, 1999.
- [50] I. S. Gradshteyn, I. M. Ryzhik, Alan Jeffrey, and Daniel Zwillinger. *Table of Integrals, Series, and Products*. Academic Press, sixth edition, 2000.
- [51] Lewis H. Ryder. *Quantum Field Theory*. Cambridge University Press, second edition, 1996.
- [52] J Berges, N Tetradis, and C Wetterich. Non-perturbative renormalization flow in quantum field theory and statistical physics. *arXiv*, hep-ph, May 2000.

- [53] L Canet, H Chaté, B Delamotte, I Dornic, and A Munoz. Nonperturbative fixed point in a nonequilibrium phase transition. *Physical Review Letters*, 2005.
- [54] L Canet, B Delamotte, D Mouhanna, and J Vidal. Optimization of the derivative expansion in the nonperturbative renormalization group. *Physical Review D*, 2003.
- [55] R Méndez-Galain and N Wschebor. Non-perturbative renormalization group calculation of the scalar self-energy. *The European Physical Journal B*, 2007.
- [56] Michael Fisher. Scaling, universality and renormalization group theory. In F. Hahne, editor, *Critical Phenomena*, volume 186 of *Lecture Notes in Physics*, pages 1–139. Springer Berlin / Heidelberg, 1983.
- [57] Haye Hinrichsen. Nonequilibrium critical phenomena and phase transitions into absorbing states. *arXiv*, cond-mat.stat-mech, 2000.
- [58] B Delamotte and L Canet. What can be learnt from the nonperturbative renormalization group? *Arxiv preprint cond-mat*, 2004.
- [59] S Coleman and E Weinberg. Radiative corrections as the origin of spontaneous symmetry breaking. *Physical Review D*, 1973.
- [60] L Peliti. Renormalisation of fluctuation effects in the $a + a$ to a reaction. *Journal of Physics A: Mathematical and General*, Jan 1986.
- [61] A Turing. The chemical basis of morphogenesis. *Philosophical Transactions of the Royal Society*, 1952.
- [62] Raoul Kopelman. Fractal reaction kinetics. *Science*, 241:1620–1626, 1988.
- [63] M. Howard and U. Täuber. ‘real’ vs ‘imaginary’ noise in diffusion-limited reactions. [arXiv:cond-mat/9701069v3](https://arxiv.org/abs/cond-mat/9701069v3), 1997.
- [64] D Litim. Optimized renormalization group flows. *Physical Review D*, 2001.
- [65] Léonie Canet. Optimization of field-dependent nonperturbative renormalization group flows. *arXiv*, hep-th, Sep 2004.
- [66] Grigory Isaakovich Barenblatt. *Scaling, Self-similarity, and Intermediate Asymptotics*. Cambridge University Press, 1996.
- [67] D Gillespie. A general method for numerically simulating the stochastic time evolution of coupled chemical reactions. *Journal of computational physics*, Jan 1976.
- [68] William Pugh. Skip lists: A probabilistic alternative to balanced trees. In F. Dehne, J. Sack, and N. Santoro, editors, *Algorithms and Data Structures*, volume 382 of *Lecture Notes in Computer Science*, pages 437–449. Springer Berlin / Heidelberg, 1989.
- [69] Benjamin P Vollmayr-Lee and Melinda M Gildner. Single-species three-particle reactions in one dimension. *arXiv*, cond-mat.stat-mech, Feb 2006.
- [70] D Ben-Avraham. Diffusion-limited three-body reactions in one dimension. *Physical Review Letters*, Jan 1993.

-
- [71] P Krapivsky. Diffusion-limited-aggregation processes with three-particle elementary reactions. *Physical Review E*, 1994.
- [72] G Oshanin, A Stemmer, S Luding, and A Blumen. Smoluchowski approach for three-body reactions in one dimension. *Physical Review E*, 52, 1995.
- [73] Ranjiva M Munasinghe, R Rajesh, and Oleg V Zaboronski. Multiscaling of correlation functions in single species reaction-diffusion systems. *Physical Review E*, 73, 2006.
- [74] Anton Winkler and Erwin Frey. Validity of the law of mass action in three-dimensional coagulation processes. *Phys. Rev. Lett.*, 108:108301, Mar 2012.

Danksagung

Mein Dank gilt zunächst Prof. Erwin Frey für das interessante Thema meiner Masterarbeit, die ich in seiner Arbeitsgruppe schreiben durfte. Ich habe die Betreuung als sehr freundlich und motivierend empfunden.

Prof. Ulrich Schollwöck danke ich für die Übernahme des Zweitgutachtens.

Ich danke meinem Betreuer Anton Winkler für die zahlreichen interessanten Diskussionen. Die Gespräche waren oft wegweisend und haben diese Masterarbeit maßgeblich geformt.

Kathrin Stähler danke ich für sorgfältiges Korrekturlesen. Fehler, die in dieser Arbeit verblieben sind, gehen allein auf mich zurück.

Meinen lieben Eltern danke ich für die kontinuierliche und bedingungslose Unterstützung während meines Physik Studiums und weit darüber hinaus.

Ich versichere, die Arbeit selbstständig angefertigt und dazu nur die im Literaturverzeichnis angegebenen Quellen benutzt zu haben.

München, den 15. März 2012